DESIGN AND FABRICATION OF DIFFERENT TEXTURED SURFACES WITH IMPROVED HYDROPHOBICITY FOR PHOTOVOLTAIC CELLS' APPLICATIONS

BY

Ahmed Owais Mohamed Ahmed

A Thesis Presented to the
DEANSHIP OF GRADUATE STUDIES

KING FAHD UNIVERSITY OF PETROLEUM & MINERALS

DHAHRAN, SAUDI ARABIA

In Partial Fulfillment of the
Requirements for the Degree of

MASTER OF SCIENCE

In

CHEMISTRY

May 2014

KING FAHD UNIVERSITY OF PETROLEUM & MINERALS

DHAHRAN- 31261, SAUDI ARABIA

DEANSHIP OF GRADUATE STUDIES

This thesis, written by **Ahmed Owais Mohamed Ahmed** under the direction of his thesis advisor and approved by his thesis committee, has been presented and accepted by the Dean of Graduate Studies, in partial fulfillment of the requirements for the degree of **MASTER OF SCIENCE IN CHEMISTRY.**

Dr. Mazen Mohamad Khaled
(Advisor)

Dr. Abdullah Al-Hamdan
Department Chairman

Prof. Bekir Sami Yilbas
(Member)

Dr. Salam A. Zummo
Dean of Graduate Studies

Prof. Abdullah AbulKibash
(Member)

27/5/14
Date

عمادة الدراسات العليا
DEANSHIP OF GRADUATE STUDIES

Dedication

I dedicate my dissertation work to the soul of my mother, Nadia Taha – may mercy be upon her – and to my wife, Dr. Nourhan Sayed.

ACKNOWLEDGEMENT

I wish to thank my committee members for their guidance. Special thanks to Dr. Mazen Khaled, my thesis committee chairman for his countless hours of reflecting, helping, encouraging, and most of all patience throughout the entire process. Thank you Prof. Bekir Yilbas, my committee member, for your readings, sincere help and generousity in information supplication. Special thanks to Prof. Abdullah Abulkibash for agreeing to serve on my committee and for giving scientific advices in writing up my proposal and thesis.

I would like to thank Dr. Kripa Varanasi and Dr. Gisele Azimi at Massachusetts Institute of Technology (MIT) for the hospitality and time, they gave to me. Thanks to Adam Paxson who saved no effort in training and helping me during my research at MIT. Thanks to Prof. Kamal Toumi for his hospitality and scientific advices. Thanks to the center or excellence for collaboration with MIT, which offered me the chance to travel, train and work at MIT.

I would like to acknowledge and thank the Chemistry department chairman for his kindness and help. Thanks to all my professors who directed me to be a good researcher. Special thanks to the department technicians and staff members for their continued help and support. Thanks to KFUPM for allowing me to conduct my research and providing any assistance requested.

TABLE OF CONTENTS

LIST OF FIGURES

LIST OF TABLES

ABSTRACT

Full Name: Ahmed Owais Mohamed Ahmed

Thesis Title: Design and fabrication of different textured surfaces with improved hydrophobicity for photovoltaic cells' applications

Major Field: Physical Chemistry

Date of Degree: Feb. 27, 2014

Acetone induced-recrystallization of polycarbonate was studied thoroughly in order to design hydrophobic and transparent surfaces for photovoltaic panels. Solvent-induced recrystallization of a thermoplastic substrate, composed of polycarbonate, is investigated to create a hierarchically-structured surface. The effects of the times of treating the surface texture with either acetone liquid or its vapor are studied at different solvent temperatures. The size of the generated spherules and gaps are studied using AFM, Goniometer, Optical Microscope, UV-Vis and FT-IR spectrophotometers. The results showed that the liquid acetone-induced recrystallization of polycarbonate surface lead to a hydrophobic surface with a contact angle of 144^{o} and 4.7% transmittance. AFM and optical microscope scans showed the formation of 13 μm-in width spherules (crystals) and 1750 nm-in depth gaps over the surface, after the treatment process, which are responsible for the high CA, Cassie-Baxter state, and low transmittance, Rayleigh scattering. The acetone vapor recrystallization has resulted in the production of hydrophilic surfaces with high transmittance, a CA of 78^{o} and transmittance of 86.8%. This research has deduced that 5 μm-in width crystals and 360 nm-in depth gaps formation lead to decreasing the hydrophobicity, however increasing transmittance of the surface, is in agreement with Wenzel wettability state and Rayleigh scattering theory.

ملخص الرساله

الإسم الكامل: احمد عويس محمد احمد

عنوان الرساله: تصميم وإنتاج أسطح بارزه بطرق مختلفه، ذات خصائص أفضل ضد التبلل بالماء، لإستخدامها كأسطح واقيه للخلايا الشمسيه

التخصص: الكيمياء الفيزيائيه

تاريخ الدرجه العلميه: 27 فبراير 2014

لقد تم إستحداث وتجربة طرق متعدده لتصميم أسطح بارزه ليتم إستخدامها كغطاء للخلايا الشمسيه. فبإستخدام طريقة البلمرة المستحثه بالمذيب العضوى للبلاستيكات الحراريه، التى تتكون من عديد الكاربونات، قد تم تخليق سطح غير مستوى. والمذيب العضوى الذى تم إستخدامه فى عملية البلمره هو الأسيتون. لقد تم استخدام الأسيتون فى حالتين فيزيائيتين، الأولى هى الحاله السائله، وقد تم إستخدام تركيزات مختلفه من الأسيتون السائل؛ أما الحاله الثانيه فهى الحاله الغازيه، وقد تم استخدامها عند درجتى حراره مختلفتين. لقد تمت دراسة تأثير التغير فى الحاله الفيزيائيه للمذيب العضوى، وتركيزات المذيب العضوى السائل، والفترات الزمنيه المستغرقه فى معالجة عديد الكربون بالأسيتون، وأخيراً درجات الحراره على أحجام الكريات والفجوات المخلقه على سطح عديد الكاربونات نتيجة عملية البلمره. لتوصيف الأسطح المعالجه وإتمام دراسة النتائج العديده والناشئه عن إستخدام طرق مختلفه فى عملية البلمره، فقد تم استخدام تقنيات مختلفه وعديده فى التوصيف لرسم صوره كامله عن السطح الناشئ وللمساعده فى تحسين عوامل التجربه لإنتاج الأسطح المرغوبه

CHAPTER 1

THE INTRODUCTION

An approach is proposed to develop dry hydrophobic surfaces with optimal optical properties. The work includes developing hierarchical superhydrophobic surfaces to significantly improve the hydrophobicity as well as the transparency, of the solar panels cover, thereby conserving cleaning water and reducing the operational costs. Novel characterization methods are developed to comprehend these characteristics at nanoscale.

1.1. The effect of dust accumulation on the PV cell efficiency:

About 5% of the solar light is reflected at the interface between the photovoltaic panel's surface and the air owing to the refractive-index difference. During the period of eight months from the date of the PV cells installation in the dessert, dust accumulation, furthermore, was found to reduce the efficiency of the cells' efficiency by 36% due to the surface-transmittance drop. This efficiency reduction extends to be by about 72% after 15 years of exposure to the dusty, dry environment of the dessert [1]. Thereby, for the PV panels, installed in dry environments, the dust particles should not stick over the surfaces of the cells. This may be achievable by texturing the surface to have a nano-pattern in order to mimic the lotus leaf phenomenon.

Figure1.1: A solar cells-field in Saudi Arabia dessert.

1.2. History of work:

Along the last decade, several studies have been performed in order to discuss the different techniques which are used to design hydrophobic surfaces by controlling the surface topography and chemistry [2]. In fact, the idea of developing hydrophobic surfaces is inspired from nature. Lotus leaf has gained the main the focus of the scientists who are interested in that field of research because its surface is rough and hydrophobic. Several crop plants also have the same characteristics like the Lotus leave, for example, *Brassica*, *Alchemellia* and *Lupinus* [3, 4].

Figure1.2: *Alchemellia* and *Lupinus* hydrophobic leaves

1.3. Polycarbonates: properties and synthesis:

Polycarbonates are considered as an organic polymeric material with two subclasses, aliphatic and aromatic. The bisphenol A [2,2-bis(p-hydroxyphenyl) propane]-based polycarbonates has interesting characteristics like high toughness, high transparency, high heat capability, low water absorbability, low synthesis cost and ease of decoration; therefore, industrially, they are considered the most important polymers. Synthesis of polycarbonates includes four different methods: **i**) Interfacial synthesis, **ii**) Transesterification, **iii**) Oxidative carboxylation and **iv**) Synthesis using CO_2 [5].

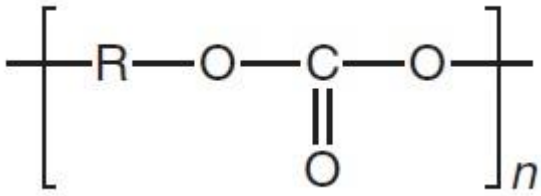

Figure1.3: General chemical structure of polycarbonate [5].

1.4. Crystallization process of Polycarbonates:

The interaction between the polycarbonate and acetone is utilized so as to texture the polycarbonate surface and form a hierarchical structure [6]. This is a crystallization reaction, where physical changes occur at the surface of the polycarbonate due to the phase-phase interaction between the polycarbonate surface and the acetone. This physical change leads to creating the hierarchical surface pattern with a certain roughness. The semi-crystalline polymers have higher chemical resistance, while amorphous polymers have a lower one. One more characteristic for the amorphous polymers is the high chain mobility which induces its crystallization [7]. The crystallization of polycarbonates is a very slow process [7, 8]. Polymer crystallization process can be induced either thermally or by using organic or inorganic solvents [9, 10]. Liang et al. [11] used diallyl-orthophtalate as a solvent to induce the polycarbonate crystallization process, in the presence of plasticizers. Turska et al. [12] treated the polycarbonate samples thermally, by heating till 190^{o}C for about seven days, in order to get a low degree of crystallization, which is 23% on average. Scientists found that the best organic solvent which can induce the polycarbonate crystallization process efficiently is the acetone [13, 14].

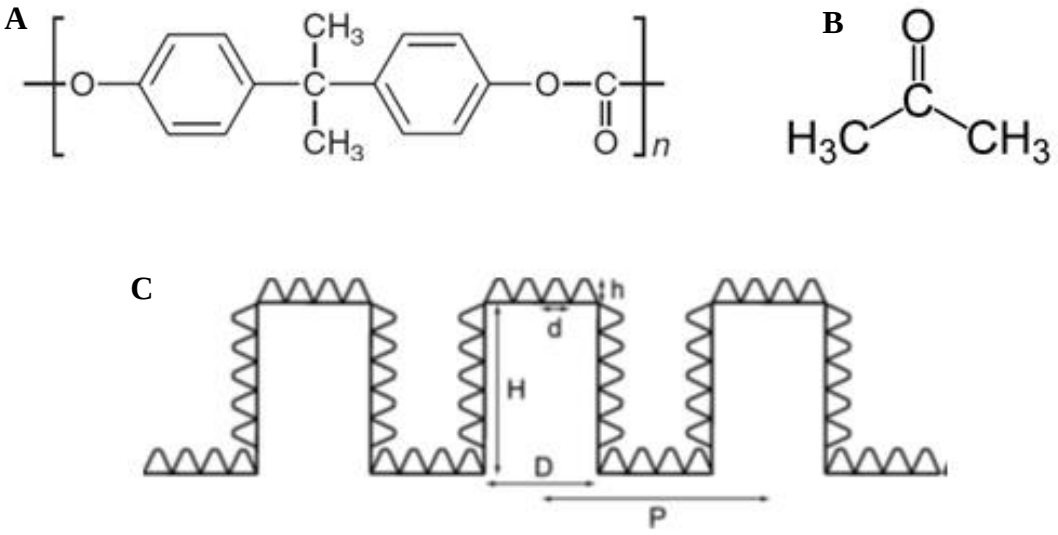

Figure1.4: A: Chemical structures of Polycarbonate, B: Chemical structures of acetone, and C: Schematic form of the hierarchical surface; D: diameter, H: height and P: pitch of the circular spherules; h: height and d: diameter of the pyramidal nano-asperities [6].

1.5. The proposed experimental work:

The proposed work involves designing and creating new textured surfaces which, mainly, possess the high transparency. With these two challenging characteristics, these types of surfaces can be utilized in many applications; the most important application, which we are concerned with, the photovoltaic panels in desert areas. The approach includes texturing polycarbonate surfaces with a suitable solvent, acetone via the solvent-induced crystallization mechanism. Hierarchical structure appears at the polycarbonate sheet's surface due to the crystallization process, caused by the treatment with the organic solvent. The exposure of the polycarbonate surface to the solvent can be performed by either treating the sheet with the liquid solvent or allowing the solvent in its vapor state to condense and diffuse through the sheet's surface layers. Promising data are expected, which allow choosing the most suitable technique for being used as a surface for the solar panels in the dry environments.

CHAPTER 2

THE LITERATURE REVIEW

2.1. Fabrication methods and technologies of superhydrophobic rough surfaces:

The designation of a superhydrophobic surface requires the generation of a rough and low-energy surface. The critical problem of increasing roughness is the light reflectance from the rough-surface and, as a consequence, the decrease of the rough-surface light-transmittance; therefore controlling the surface roughing process should be taken into consideration [15]. Several types of superhydrophobic rough surfaces can be designed by many techniques; every technique has its own characteristics, advantages and disadvantages [16]:

i) **Photolithography:** it is highly controlled and favored in academic studies (to study the effect of varying r and ϕ_s values), however it is very expensive.

ii) **Colloidal micro- and nano-particles:** these types of particles accumulate by self-assembly, can pattern wide surface-areas with multiple scales and the deposition process is controllable.

iii) **Template method:** A rough surface can be utilized as a negative template and filled up with a material in the liquid state, waiting for its hardening and getting it out. The method is simple and the template can be used for several runs.

iv) **Etching:** Several methods of etching, for example, acid, laser or plasma etching, are investigated to create textured surfaces.

2.2. Different methods of self-cleaning:

For the self-cleaning surfaces, scientists are spending significant efforts to design an optimized surface, which repels dust particles. In literature, a variety of methods for performing such a task are reported [17]:

i) **Superhydrophilic surfaces:** Over this surface, water droplet flattens, diffuses and rinses the accumulated dust. These surfaces are non-favorable for the solar cells because of the lack of rains in the desert and this method requires the utilization of large amounts of water.

ii) **Superhydrophobic surfaces:** Over this surface, water droplet, instead, rolls off and holds the accumulated dust with it. These surfaces are favorable in rainless areas.

iii) **Electrostatic removal of dust:** This is a relatively more complex method, in which electrodes are used to charge the dust particles that are present over the photovoltaic cell surface, so a repulsion force is established between the dust and the solar panel.

This technique is too difficult to be applied in the PV cells because they are exposed to rains and humid atmospheres, as a result the electrodes can be damaged.

2.3. Enhancing the transmittance of the rough surfaces:

Bruynooghe et al. [18] have enhanced the light transmittance of the glass surface by coating it with an antireflective material which uses the light destructive interference phenomenon to reduce the percentage of the scattered light. The coated substrate can be further coated with another coating material, which is hydrophobic (water repelling) and oleophobic (oil repelling) for making it durable and has a self-cleaning property. This top-layer coating includes MgF_2 (expensive material) in order to make the surface non-reflective. They achieved a CA of 110° after coating with 0.14% reflectance at incident angle of 78° in the spectral region 400-680 nm.

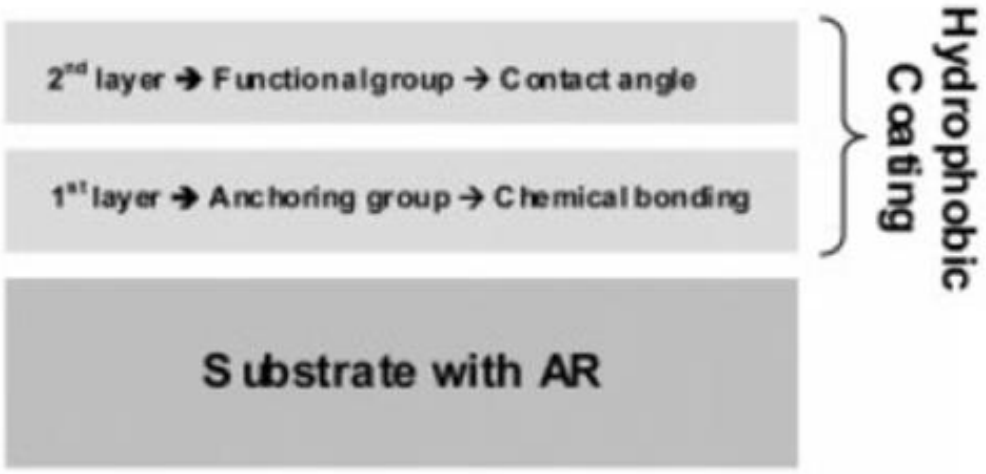

Figure2.1: Scheme of the designed, coated AR, hydrophobic surface [18].

2.4. Creating superhydrophobic and self-cleaning surfaces, using different coating materials:

Nakajima et al. [15] have designed boehmite-TiO_2 films, with varied TiO_2 compositions, and a following (heptadecafluorodecyl) trimethoxysilane (FAS-17) coating to be used as superhydrophobic coating materials. Both roughness and CA are studied with different TiO_2 wt% values. It was noticed that the roughness and CA increase with increasing the TiO_2 wt%. However, TiO_2-based coatings are affected by UV light, especially at higher TiO_2 compositions, leading to hydrophobicity drop due to the photocatalytic effect (strong oxidation power under UV light) of the TiO_2**.**

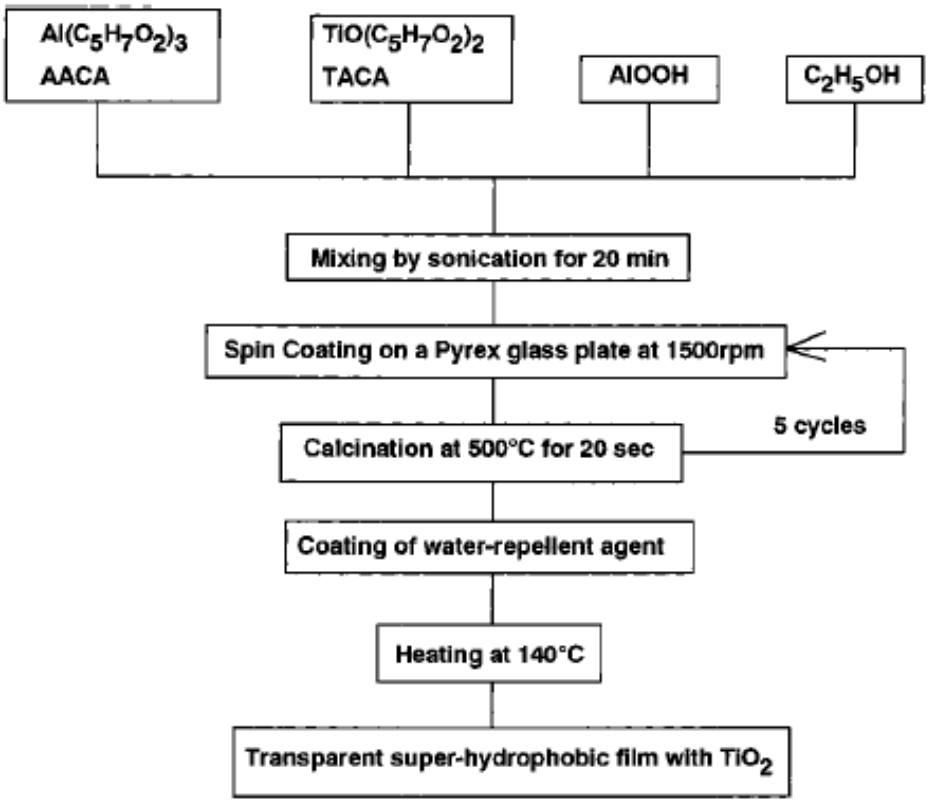

Figure2.2: Schematic diagram of the superhydrophobic film synthesis mechanism[15]
.

Ganbavle et al. [19] have used the sol-gel technique of a single step with a view to design a hydrophobic, self-cleaning silica coating material over a glass surface. The coating is tetraethoxysilane (TEOS) based with methyltrimethoxysilane (MTMS) as a co-precursor. The MTMS/TEOS ratio variation, by changing the MTMS concentration, versus the hydrophobicity and self-cleaning property is studied; it was found that at the ratio between 0.78-1.57, the water droplet sticks over the surface due to the Cassie impregnated state, in which a water-film is formed on the pillars causing the strong adhesion of the water droplet to the surface, this phenomenon is illustrated in figure 2.3**.** While at the ratio of 7.84, the coating showed a CA of 135°, but with a reduced light transmittance (80%)**.** Lai et al. [20], also, designed TiO_2-fluoroalkylsilane thin films, using an electrophoretic deposition method, demonstrating both superhydrophobicity and good transparency**.** By Stober method**,** Chen et al. [21] grew hollow-silica particles over carbon cores, using Chemical Vapor Deposition (CVD), in order to synthesize a superhydrophobic coating. The achieved a CA is 152° with transmittance of 90%, after one coating cycle, and 75%, after five coating cycles.

A

B

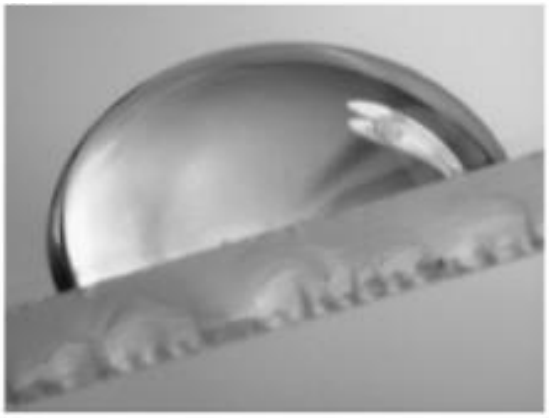

Figure2.3: A: surface with ratio = 1.57 (Cassie-impregnated state), B: surface with ratio = 7.84 [19]

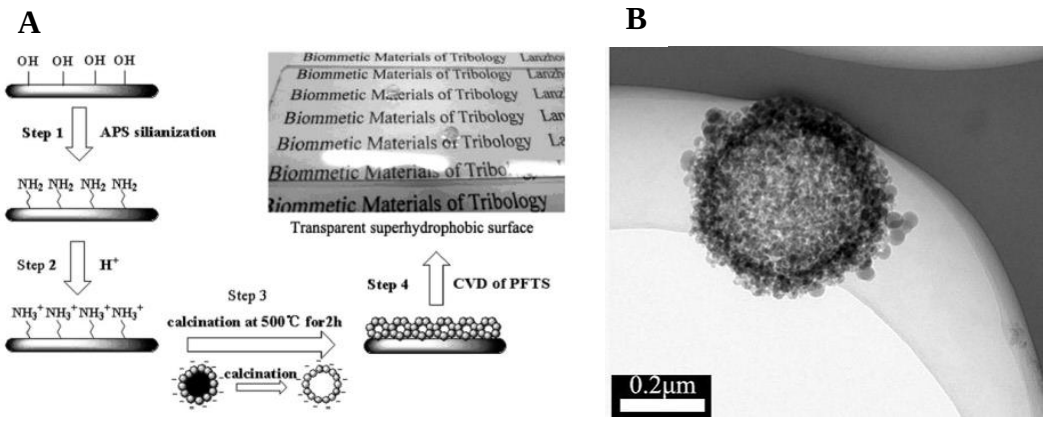

Figure2.4: A: Scheme for the preparation method. B: hollow silica particles [21].

2.5. Dust Mitigation Approaches:

One of the effective ways to reduce dust accumulation effect on the performance of PV modules is creating micro/nano textured surfaces with low adhesion and non-wetting properties .Such surfaces are called hydrophobic surfaces. It can enhance the cleaning efficiency and reduce the frequency of cleaning, hence less water usage. The chemistry and morphology of such surfaces can reduce adhesion forces between the particles and the surface, make high contact angle between water droplets and the surface, prevents water droplets sticking and promote its mobility along the surface. Hence, light air blowing or small amount of water would be enough to clean the surface. The wetting behavior of the surface is described by contact angle and contact angle hysteresis which mainly depend on surface morphologies and chemistry.

2.6. Wetting on Surface:

Wetting is one of the surface properties. It describes the behavior of deposited liquid droplets on a surface [22]. Wetting is characterized by contact angle between liquid droplets and a surface. Young [23] introduced equation (2.1) which relates liquid drops contact angle on homogenous and smooth surface with the specific interfacial energies of solid-gas, solid-liquid and liquid-gas.

$$\cos\theta_{flat} = \frac{\gamma_{sv} - \gamma_{sl}}{\gamma_{lv}}$$

Based on equation (2.1), it can be concluded that the solid-air interfacial energy is the key factor that determines surface wetting properties. In other words, decreasing the surface energy (i.e. solid-air energy) leads to enhance the surface hydrophobicity.

Another fundamental process to enhance the hydrophobicity is the surface texturing. According to Wenzel relation [24], increasing the roughness of hydrophobic surface tends to improve its non-wetting properties and vice versa. The following Wenzel equation relates contact angle with surface roughness [24]:

$$\cos\theta_{\mathrm{Rough}} = \mathrm{r}\cos\theta_{\mathrm{Flat}}$$

, where θ_{Rough} is the contact angle of a rough surface, θ_{Flat} is the contact angle of a flat surface, and r is the roughness factor of the rough surface. The roughness factor is defined as the ratio of the total surface area of the rough surface to the projected area of the rough surface [25].

Cassie Baxter assumes that liquid droplet do not completely wet the surface texture due to the presence of trapped air between posts of the surface texture. Consequently, the surface has two interfaces, solid-liquid and air-liquid as shown in figure 2.5 and described in the following relation [26]:

$$\cos\theta_{\mathrm{Rough}} = \varphi_{\mathrm{s}}\cos\theta_{\mathrm{Flat}} + \varphi_{\mathrm{v}}\cos\theta_{\mathrm{LV}} = \varphi_{\mathrm{s}}\cos\theta_{\mathrm{Flat}} - (1 - \varphi_{\mathrm{s}})$$

, where $\emptyset_s$ and $\emptyset_v$ are the fractions of solid and air contacting the liquid. The contact angle between air and water equals 180°. Based on equation (2.3), solid fraction is the key parameter that can control the wetting properties of the surface.

The substitution of equations (2.2) into (2.3) leads to introducing a definition of critical contact angle given by [27]:

$$\cos\theta_c = \frac{1-\varphi_s}{r-\varphi_s}$$

Equation (2.4) indicates that liquid contact angle on a flat surface is more than the critical angle; the liquid tends to partially wet the surface (i.e. Cassie Baxter). Otherwise the surface is completely wetted as shown in (i.e. Wenzel state).

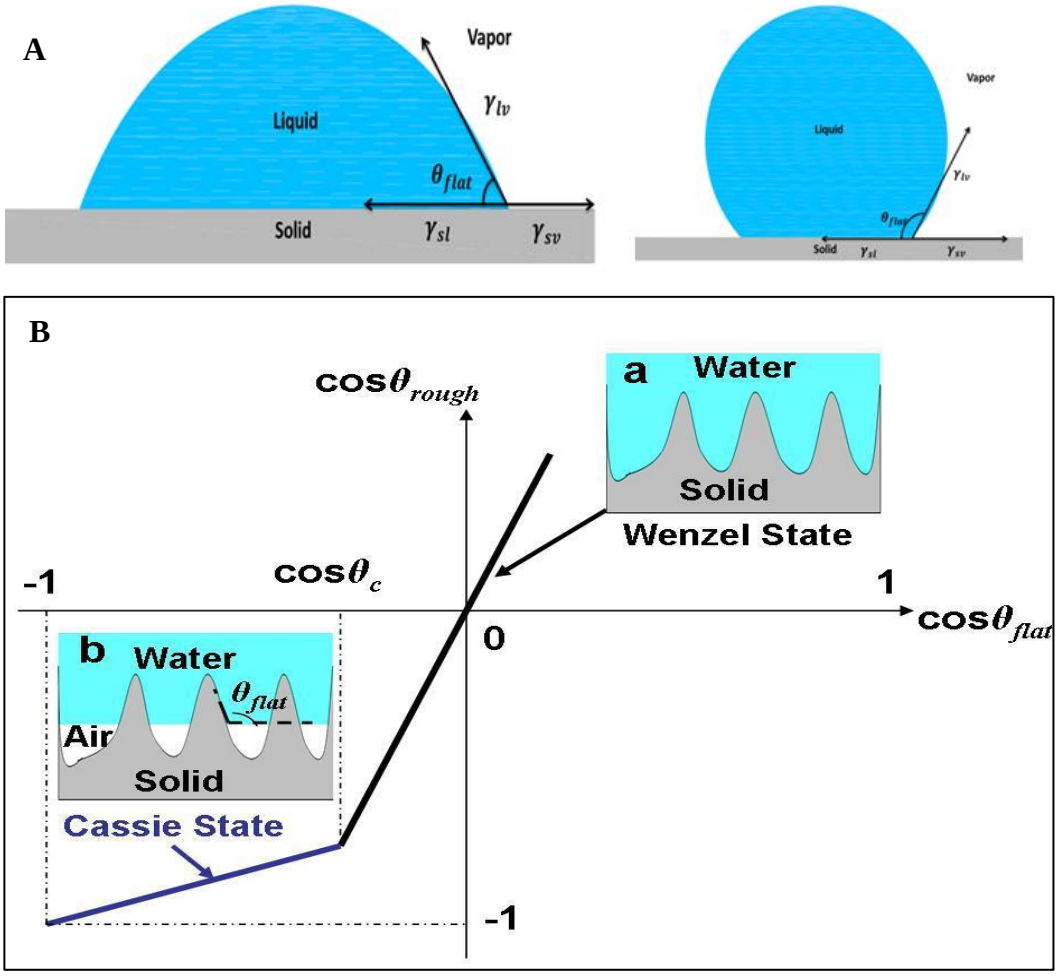

Figure2.5: A: Water contact angle on hydrophobic and hydrophilic surfaces, and B: Wenzel and Cassie Baxter wetting states [26].

2.7. Contact Angle Hysteresis:

Contact angle hysteresis (CAH) determines the sliding and rolling properties of liquid droplets along the surface. It is a type of dynamic contact angles. When inflating a droplet, there is a threshold value of contact angle beyond which the line of contact start move (i.e. increase in area of contact) which is implied with advancing angle. Likewise, when deflating a droplet, there is as a threshold value of contact angle beyond which the line of contact start move (i.e. decrease in area of contact) which is implied with receding angle [22]**.** CAH equals the difference between advancing and receding contact angles. CAH depends on the type of deposited liquid [28], surface texture posts spaces and morphologies[29-32] and the type of impregnated liquid in case of lubricant impregnated surfaces [33, 34].

Hydrophobic surfaces can be categorized into two categories based on the type of fluid being trapped between the posts of surface texture: dry hydrophobic surface which traps air inside its textures, and wet hydrophobic where the spaces between the texture posts are filled with lubricant.

2.8. Dry Hydrophobic Surface:

Mimicking the morphologies of natural superhydrophobic surface like the lotus leaf structure is the first step to come up with hydrophobicity properties. Template-based

techniques, plasma treatment, self-assembly and self-organization, chemical deposition, layer-by-layer (LBL) deposition, colloidal assembly, phase separation and electrospinning are some of the main methods to develop hydrophobic surfaces [35-37]. A number of studies on developing self-cleaning solar module glass cover surface with high optical properties are reported in the literature. Park et al. [38] developed superhydrophobic surface with contact angle higher than 150° and a hysteresis of lower than 20° by fabricating an ordered microshell array on transparent and flexible polydimethylsiloxane (PDMS) elastomer surface without a need to a low surface energy chemical coating. Verma et al. [1] created superhydrophilic nano-structured glass with contact angle less than 5° by deposition of thin film of nickel on glass substrates, followed by annealing to create nickel nanoparticles. Their result showed an improvement in the solar cell performance, since net optical transmission increased and the surface is proven to be self-cleaning. Hee et al. [39] using a simple method deposited different thicknesses of TiO_2 film on glass surface. They observed that dust accumulation is decreased due to the deposition effect and this effect became more significant when increasing the film thickness.

However, such dry hydrophobic surfaces do have their limitations for example. It cannot sustain high impact pressure. During the vapor condensation, surface loses its non-wetting properties. In addition micro-textures can enhance the light reflection. Lubricant impregnated surfaces do overcome limitations. In addition, wet hydrophobic

surface exhibit extremely low contact angle hysteresis thus provides better self-cleaning and slippery properties.

2.9. Wet Hydrophobic Surfaces:

Texturing the hydrophobic surfaces enhances the non-wetting properties by increasing the surface geometry while the trapped air between the surface texture posts leads to a superhydrophobic behavior, because the droplets sit partially on air [32]. However, there is a challenge in keeping the air pockets stable between the texture posts. But in case of humid conditions like KSA environment, the air pockets can collapse due to dew condensation or evaporation. This occurs at a nanoscale throughout the texture and in turn leads to a highly wetted textured surface [32]. Such effect drew the attention to develop non-wetting surfaces with self-healing properties are maintained by creating pockets of liquid instead of air by impregnating the texture with lubricant. The lubricant is stabilized by capillary wicking arises from the Micro or Nano texture [34]. **Lui et al.** [40] fabricated lubricant-impregnated surfaces (LIS) by filling organogel-based film on substrate with oil. The surface showed low contact angle hysteresis and self-cleaning efficiency. Wong et al. [28] prepared LIS through impregnating ordered epoxy-resin-based nanostructured surfaces and a random network of Teflon nano fibrous membranes with lubricant perfluorinated fluids. It has been showed that LIS has the ability to repel different types of low and high surface tension liquids such as water, Glycerol, and

Ethylene glycol. Furthermore, matching the refractive indexes of lubricant fluid and substrate leads to render the micro-texture high transparent [28, 33]. Also, LIS demonstrated self-healing properties .In case of any surface physical damage, the oil can flow and fill cracks and retain its surface properties [28]. On the other hand, LIS can sustain high drop impact pressure [28], reduce ice accretion [28, 41, 42] and enhances condensation and heat transfer dissipation [43, 44].

The lowest total interface energy state of water droplet represents the thermodynamics stable configuration. It depends on surface texture and impregnated liquid properties such as viscosity, spreading coefficient and density [22]. Viscosity of oil plays a role in droplet sliding angle and velocity. High viscous oil leads to reduce the droplet rolling speed and increases the sliding angle [22, 40, 45]. On the other side, using high viscous oil can enhance the shearing sustainability of the surface [43].

2.10. Polymer crystallization:

De Oliveira et al. [7] casted a bisphenol-A polycarbonate film, with different molar mass, and exposed it to acetone vapor-saturated environment for one and two days. The setup is not discussed in the published work. The study deduced that there is a direct relationship between the polymer molar mass, the melting enthalpy, the size of the formed spherules and the degree of crystallization. Liu et al. [46] studied the effect of polycarbonate thickness on the acetone transport kinetics within the polymer sheets.

Varanasi group [6, 47, 48] has used of liquid acetone-induced polycarbonate crystallization to create superhydrophobic surfaces. They achieved a high contact angle with low contact angle hysteresis between the textured, crystallized polycarbonate surface and a water droplet. They deduced that the polymeric nano-fibers, secondary texture over the spherule, have a great effect on the surface hydrophobicity. However, they did not study the effect of the texturing process on the surface transmittance. In addition, their study has only focused on solid-liquid interface and they did not refer to using the acetone in its vapor state.

CHAPTER 3

THE THEORETICAL MODELS

3.1. Fundamental knowledge:

Surface tension (γ_{LV}); is defined as the force which is responsible for reducing the free liquid's surface area; the unit of this force is N m^{-1} or J m^{-2} [49]. Two forces affect the status of the water droplet over the solid surface, i) gravitational force and ii) surface tension. The volume of the droplet is the main factor, by which the effecting force is determined. For a water droplet present over a solid surface, interfacial tension forces γ_{SL}, γ_{SV} and γ_{LV} are established, the status of the water droplet, either flattened over the surface or remained as a sphere, depends upon the balance between these forces [3].

$$S = \gamma_{SL} + \gamma_{LV} - \gamma_{SV} > 0$$

-where S: the power of spreading, γ_{SL}: the solid-liquid surface tension, γ_{LV}: the liquid-vapor surface tension, and γ_{SV}: the solid-vapor surface tension.

3.2. Young's equation (for flat surfaces):

The hydrophobicity of a surface can be identified as the incapability of the surface to interact with water, therefore leading to create a high contact angle, θ (i.e. the angle between the surface and the tangent of the water droplet which is found over it) so as to minimize the contact area between the droplet and the surface. In contrast, the hydrophilic surface likes water; it makes a small contact angle, θ, with the water droplet in order to maximize the contact area, thereby leading to droplet-flattening over the surface. The surface is described as hydrophilic if $\gamma SV < \gamma SL$, the contact angle is lower than 90°, while, the hydrophobic surface possesses a contact angle higher than 90° if $\boldsymbol{\gamma}_{SV} > \boldsymbol{\gamma}_{SL}$ [3].

For flat surfaces, there is a mathematical model which illustrates the behavior of a water droplet on such surfaces. Young's equation shows the relation of the three-phase contact line between the droplet and the flat surface [23]:

$$\cos \boldsymbol{\theta}_{\boldsymbol{y}} = \frac{\gamma_{SV} - \gamma_{SL}}{\gamma_{LV}}$$

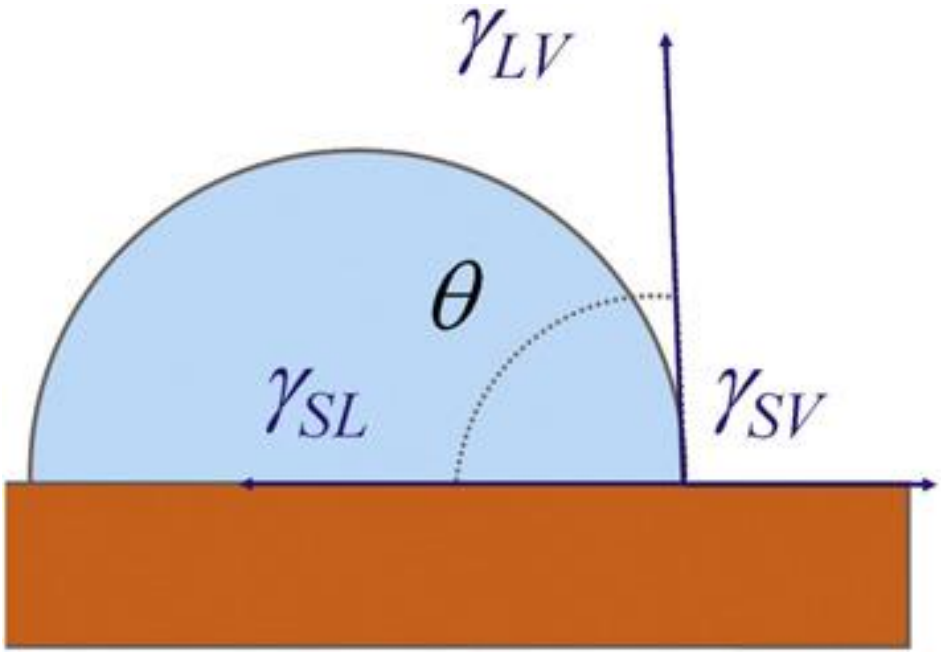

Figure3.1: Three-phase contact line diagram of a water droplet on a solid surface [23].

3.3. Wenzel and Cassie-Baxter states (for rough surfaces):

However, not all the surfaces are flat, there are rough surfaces. The water droplet behavior on the rough surface is totally different from the smooth one because, in this case, surface texture plays a major role in **i**) the degree of the hydrophilicity or the hydrophobicity of the surface and **ii**) the droplet mobility over the surface. In order to identify the rough surface, basically, it is the surface that has a lower surface energy than the corresponding flat surface of the same material. The energy of the rough surface is lower because if a square with a certain area is taken from a flat surface of a certain material and compared with another square with the same area, which is taken from a rough surface of the same material, more surface area can be found in the rough square because it is a three-dimensional one, while the flat square is only two-dimensional.

Two mathematical models are utilized to study the behavior of the water droplet on the rough surface, Wenzel model and Cassie-Baxter model. In Wenzel model, upon the landing of the water droplet over the rough surface, a water film is produced over the texture because water replaces the trapped air and fills the air-pockets. According to this case, the water droplet sticks over the surface and does not move, even under the effect of the gravitational force. Wenzel's formula can be formulated as in (**Eqn. 3 & 4**) [24]:

$$\cos\theta_w = \mathrm{r}\cos\theta_y$$

$$\mathbf{r} = \frac{\mathbf{actual\ surface}}{\mathbf{geometric\ surface}}$$

, where θ_w: apparent contact angle (i.e. contact angle over the rough surface or Wenzel's contact angle), θ: actual contact angle (i.e. contact angle over the corresponding smooth surface or Young's contact angle) and r: roughness factor. This state is non-favorable because it causes stickiness of the water droplet over the surface, so this is against the idea of water droplet rolling which is favorable for self-cleaning surfaces.

In Cassie-Baxter state, there is no water film formation because there is no water-diffusion in the air-pockets. However, instead, the water droplet still touches only the tops of the surface-pillars, leaving the areas between them filled with air (**Eqn. 5**). In Cassie-Baxter state, the droplet-curvature is smaller than the gaps due to the weight of the droplet [3].

$$\mathbf{cos}\ \boldsymbol{\theta_{cb}} = \mathbf{fs}\left(\mathbf{cos}\ \boldsymbol{\theta_y} + \mathbf{1}\right) - \mathbf{1}$$

, where θ_{cb}: apparent contact angle (i.e. contact angle over the rough surface or Wenzel's contact angle), θ: actual contact angle (i.e. contact angle over the corresponding smooth surface or Young's contact angle), f_s: the total area of the liquid-air interface [26].

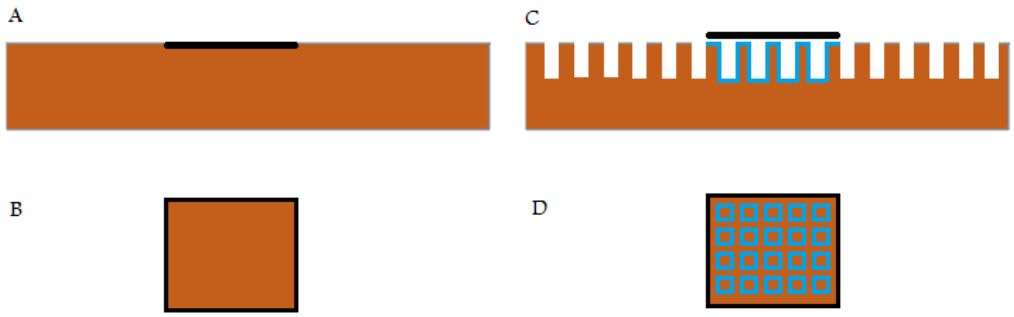

Figure3.2: A & B: diagrams illustrate the flat surface and a cross-section in it, and C & D: diagrams illustrate the rough surface and a cross section in it. From the diagrams, you can see that the rough square has a higher surface area, so a lower surface energy, than the flat square.

3.4. The effect of the chemical treatment and the roughness on the surface hydrophobicity:

The roughness cannot alter the nature of the surface, in other words, it cannot transform the hydrophobic surface to be a hydrophilic one or vice versa. The chemical structure and the terminal groups at the materials' surfaces are the only factors that control if the material is hydrophobic or hydrophilic. The chemical composition or treatment of the surfaces, by coating, etching … etc., can only increase the contact angle over the smooth, hydrophobic surfaces up to 120°, while for the smooth, hydrophilic surfaces, chemical treatment cannot reach a contact angle of 5°. The purpose of texturing the surface is to increase its hydrophobicity or hydrophilicity [50]. Thereby for the hydrophobic and rough surface, the contact angle can reach more than 160° and, in this case, the surface is called superhydrophobic, whereas for the hydrophilic rough surface, the contact angle can reach less than 5° and the surface is known as superhydrophilic surface. The contact angles for both the superhydrophobic and the superhydrophilic surfaces are apparent angles, and they are referred back to Cassie-Baxter (θ_{cb}) and Wenzel (θ_w) states, respectively [51].

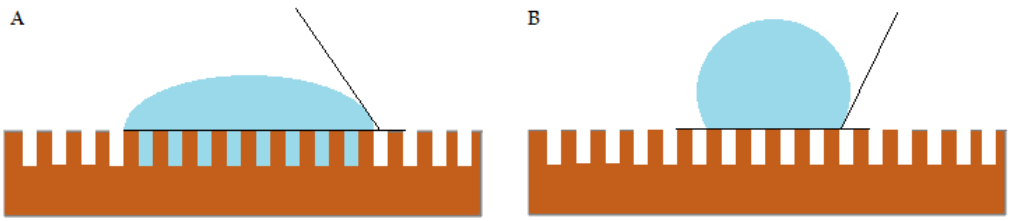

Figure3.3: A: Wenzel state, or commonly known as Wenzel impregnated state. The water replaced the air in the gaps and the water droplet flattened, forming an acute angle between its tangent and the surface. B: Cassie-Baxter state. The water droplet is in a semi-sphere shape, forming an obtuse angle between its tangent and the surface.

3.5. Classification of rough surfaces:

Designation of rough surfaces can result in three forms of the surface texture: **i**) regular, **ii**) hierarchical and **iii**) random textured surface. For the regular rough surfaces, the etching can be done by using photolithography; and this type has a single-scaled roughness; and it is helpful in investigating the droplet behavior over the rough surfaces. The hierarchical rough surfaces, designed by chemical etching, possesses complex structure, include roughness are of two-scales. However, the random rough surfaces, fabricated by plasma-etching, are of multiple-scaled roughness [52].

3.6. Self-cleaning surfaces:

Acquiring the self-cleaning property is one of the surface characteristics that are favorable to be present. The self-cleaning feature requires uniformed, smooth mobility of the water droplet over the hydrophobic surface. The regular rolling of the water droplet over the hydrophobic surface allows the removal of the accumulated dust particles and contaminants, like in the Lotus leave. The degree of easiness and smoothness, in which the water droplet can move over the hydrophobic surface can be measured by measuring **i**) the advancing contact angle (i.e. the contact angle at the front of the moving water droplet, θ_A; at this point, the volume of the water droplet increases with its motion) and

ii) the receding contact angle (i.e. the contact angle at the back of the moving water droplet, θ_B; at this point, the volume of the water droplet shrinks with its motion).

The difference between the advancing and receding contact angles results in a new term, called contact angle hysteresis, θ_h, which is a measurement of the surface homogeneity (**Eqn. 6**). Both, the advancing and receding contact angles are measured at a surface-tilt angle of 1° to 30°, for example.

$$\boldsymbol{\theta_h = \theta_A - \theta_B}$$

Three cases can be found in the values of the contact angle hysteresis: **i**) zero or approaching zero value; in this case, the surface is homogeneous and the water droplet rolls smoothly over it, **ii**) positive value; in this case, the surface is heterogeneous and the water droplet rolls slowly or slides over it and **iii**) negative value; in this case the water droplet sticks over the surface.

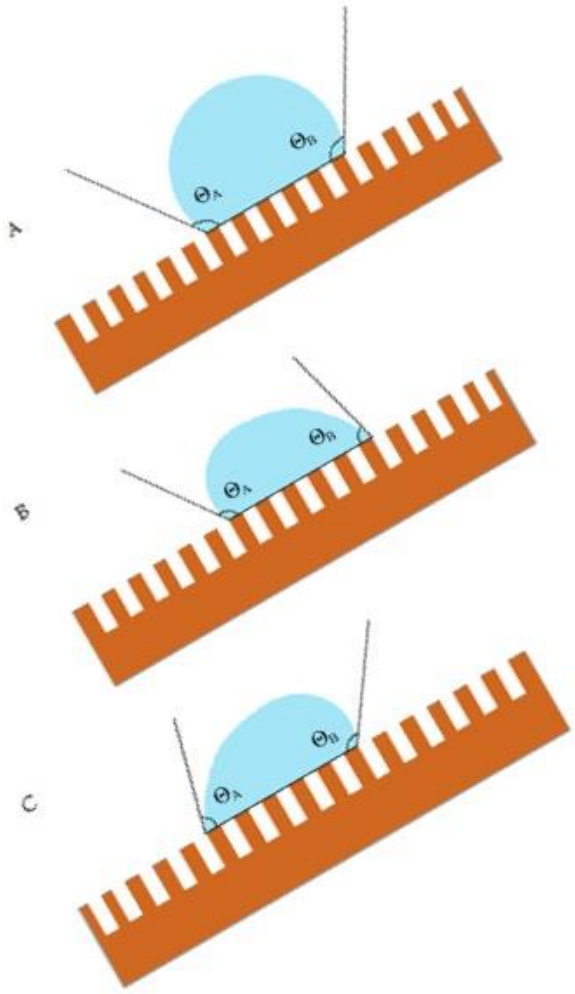

Figure3.4: A: Uniformed (contact angle hysteresis = zero), B: Non-uniformed (hysteresis contact angle = positive value) and C: Non-uniformed (contact angle hysteresis = negative value) water droplet movement over the rough hydrophobic surface.

CHAPTER 4

THE EXPERIMENTAL WORK

4.1. Introduction:

The performed experiments included the usage of various lab tools and characterizing techniques. The tools helped in handling the chemicals safely and accurately in a simple way in order to perform the different experiments smoothly, with a high reproducibility. The characterizing techniques allowed the group to study the outcomes of the experiments; so that, a well-studied decisions and, as a result, a scientifically arranged steps are taken during the development of the work. This chapter includes the recitation of all the used tools, instruments and techniques within the experiments. This part of the thesis, also, exposes to the various procedures and protocols of the work in discuss.

4.2. The equipment:

The experimental work included the usage of 10 mL- and 25 mL-graduated cylinders, 50 mL-, 100 mL-, 150 mL- and 400 mL-beakers, a 250 mL-conical flask and rounded-

glass dishes for liquid chemicals handling. Distilled water is used for the glassware washing and cleaning purposes. Deionized water is utilized for dilution purposes. For drying purposes, an air pump is investigated. Polycarbonates sheets, of thickness 1.6 mm and produced by Bayer Company, were obtained from Sheffield Plastics (Sheffield, MA). Liquid acetone, from Sigma Aldrich with boiling point 56^{o}C and molecular weight 58.08, is investigated.

Several characterization techniques are used in order to study the different effects of changing the experimental parameters within the investigated work on the chemical and physical properties of the textured surfaces. A balance is utilized to follow up the rate of acetone vaporization from the polycarbonate sheet after the treatment process by taking the weight change with time. An optical microscope is used for a first-phase study of the different textured surfaces. Atomic Force Microscope (AFM) - Molecular imaging, PicoSPM LE 5100, Agilent technologies – used to determine surface topography, and roughness profile Fourier-Transform Infrared (FTIR), model 6700 from Thermo Electron Corporation, was utilized in the identification of different functional groups that are present on the surface before and after the texturing process. UV-Vis spectrophotometer, Lambda EZ 210 from PerkinElmer Company, is utilized to measure the transmittance of the polycarbonate sheet before and after the patterning process. A Goniometer is used to determine the degree of both the hydrophilicity and the hydrophobicity of the surface by measuring the static contact angles between a deionized water droplet (of 0.4-5µL volume) and the surface.

4.3. Experimental procedures:

This study includes two main branches, which are: **i**) The Solid-liquid interface method for polycarbonate surface crystallization and **ii**) The Solid-vapor interface method for polycarbonate surface crystallization. In the former method, the acetone is used in its liquid state, while, in the other one, the acetone is used in its vapor state. The solid-vapor interface method was carried out under the following conditions: **i**) Vaporization of acetone at 18^{o}C, and **ii**) Vaporization of acetone at 33^{o}C.

4.3.1. The solid-liquid interface method for polycarbonate surface crystallization:

Polycarbonate sheets are immersed in liquid acetone. Two factors are varied during the study: i) Acetone concentration, and ii) immersion duration.

Several concentrations of acetone were investigated, pure, 75% and 50% acetone. When acetone was diluted by distilled water with different percentages, it is noticed that there is a film formed, which covered the immersed polycarbonate sheet. This film acted as a barrier which prevents the acetone molecules from reaching the polycarbonate sheet's surface, and this was deduced because polycarbonates sheets were treated with distilled water-diluted acetone for hours without being textured. The distilled water contains dissolved ions, these ions precipitates over the polycarbonate surface and

forming a thin film, which can be easily mechanically removed; however the deionized water is ions-free. So, deionized water is used for diluting the acetone liquid. The aim of using the deionized water is to avoid the water-dissolved ions, in case of using either the distilled or the tap water.

The immersion duration plays a key factor in the polycarbonate crystallization process [6, 8]. Polycarbonate sheets are immersed in the liquid acetone for different durations in order to study the effect of immersion duration on the surface texture. Immersion durations are varied according to the concentration of the acetone liquid used. Upon using pure liquid acetone, immersion durations were 1, 1.5, 2, 3, 4, 5 and 10 min. For the 75% acetone liquid, immersion durations were 2, 4, 6, 8 and 10 min. However, for 50% acetone liquid, immersion durations were 5, 10, 15, 20 and 25 min. The immersion durations and liquid acetone concentrations were chosen for establishing a regular study. The study took in consideration that due to the acetone dilution process, the rate of the crystallization reaction decreased accordingly with decreasing the acetone concentration; therefore, the immersion durations were increased with increasing the deionized water/acetone ratio. Table 3.1 illustrates the varied parameters within the solid-liquid interface method.

Table4.1: The table illustrates the solid-liquid interface method's parameters

Solid-Liquid method of crystallization		
serial	acetone conc.	immersion time
i1	100%	1 min
i2		2 min
i3		3 min
i4		4 min
i5		5 min
i6		10 min
i7	75%	2 min
i8		4 min
i9		6 min
i10		8 min
i11		10 min
i12	50%	5 min
i13		10 min
i14		15 min
i15		20 min
i16		25 min

4.3.2. The solid-vapor interface method for polycarbonate surface crystallization:

Polycarbonate sheets exposed to the acetone which is in its vapor state. Acetone is readily vaporizable, i.e. it has both a low boiling point and a low molecular weight. Therefore, acetone can convert from the liquid state to the vapor state in the ambient temperature, i.e. the room temperature and atmospheric pressure. This phenomenon allowed studying the effect of exposing the polycarbonate sheet's surface to the acetone vapor at **i**) 18^{o}C, and **ii**) 33^{o}C.

The treatment duration plays a key factor in the polycarbonate crystallization process [6, 8]. The polycarbonate sheets are treated with pure acetone vapor for different durations in order to study the effect of exposure duration on the surface texture. A designed setup is used in order to expose the polycarbonate surface to the acetone vapor, which evolves in down-up direction, figure 3.1. When the system temperature was 18^{o}C, the polycarbonate surface was exposed to acetone vapor for 5, 15, 20, 25 and 30 minutes.

However, when the system temperature was 33^{o}C, two different vapor-outlets shapes are chosen for the acetone vapor: **i**) 1 cm x 1cm squared out let, figure 3.2-A, and **ii**) holed vapor-outlet, figure 3.2-B. The aim of using different vapor-outlets is trying to control the surface patterning process, by using regularly-holed vapor-outlet with equal-sized holes. At 33^{o}C, polycarbonate surface exposed to acetone vapor, passing through a 1 cm x 1cm squared out let, for 1, 2, 3, 4, 6, 7, 8 and 9 minutes. However, for the setup

with the holed vapor-outlet, treatment durations are 2, 4, 6, 8 and 10 min. The treatment durations are chosen for establishing a regular study. Table 3.2 illustrates the varied parameters within the solid-liquid interface method.

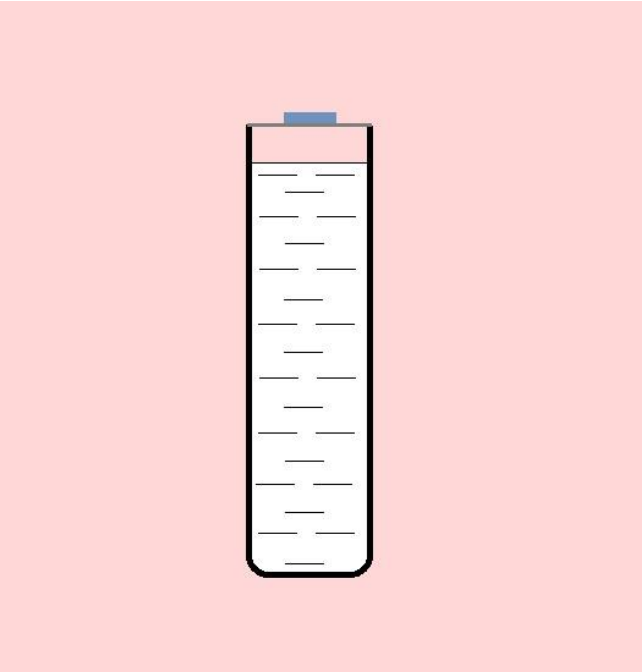

Figure4.1: The designed setup for the liquid-vapor interface method (lateral view).

Table4.2: The tables illustrate the solid-vapor interface method's parameters

Solid-Vapor method at 18°C	
serial	exposure time
s1	5 min
s2	15 min
s4	20 min
s5	25 min
s3	30 min

Solid-Vapor method at 33°C	
serial	exposure time
c4	1 min
c5	2 min
c6	3 min
c7	4 min
c8	6 min
c9	7 min
c10	8 min
c11	9 min

Solid-Vapor method at 33°C, holed outlet	
serial	exposure time
cr2	2 min
cr4	4 min
cr6	6 min
cr8	8 min
cr10	10 min

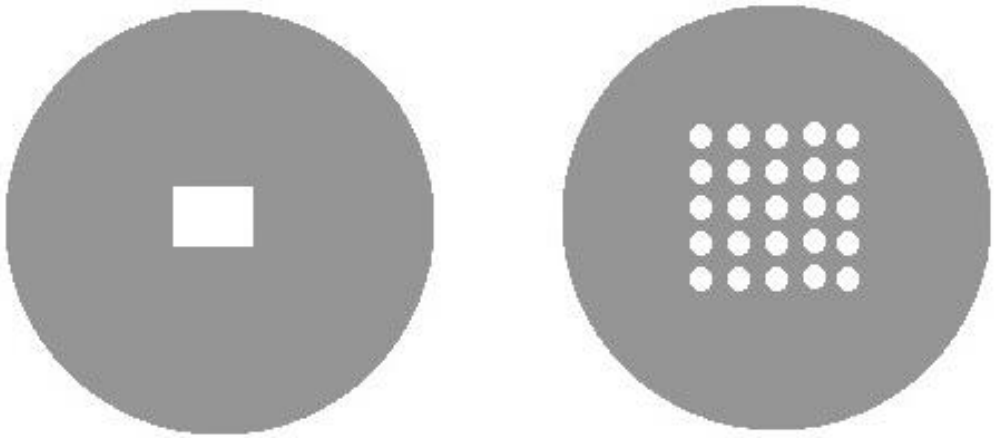

Figure4.2: A: 1cm x 1cm-squared vapor-outlet. B: holed vapor-outlet

CHAPTER 5

RESULTS

In this chapter, the data and outcomes of the characterization of the experimental work are discussed. Atomic Force Microscope micrographs, surface profiles, transmittance data, contact angle measurements, optical microscope images and FT-IR data are presented. The discussions are provided in line with the resulted data under the following sub-headings.

5.1. Smooth, untreated Polycarbonate surface:

5.1.1. Atomic force microscope (AFM) micrographs:

5.1.1.1. Surface topography:

Several AFM scans are taken for different areas on the textured polycarbonate surface, at different scales (500 nm, 1, 5, 10, 20 and 40 μm). The micrographs ascertain the absence of any kind of texture over the surface of the polycarbonate sheet, figure 5.1-A with a scanning scale of 40 μm. There is an elevation appears at the top-right of the micrograph, this is due to the sample's surface general morphology due to manufacturing process. Figures 5.1-B to 5.1-F, at lower scales, further demonstrate the smoothness of the surface.

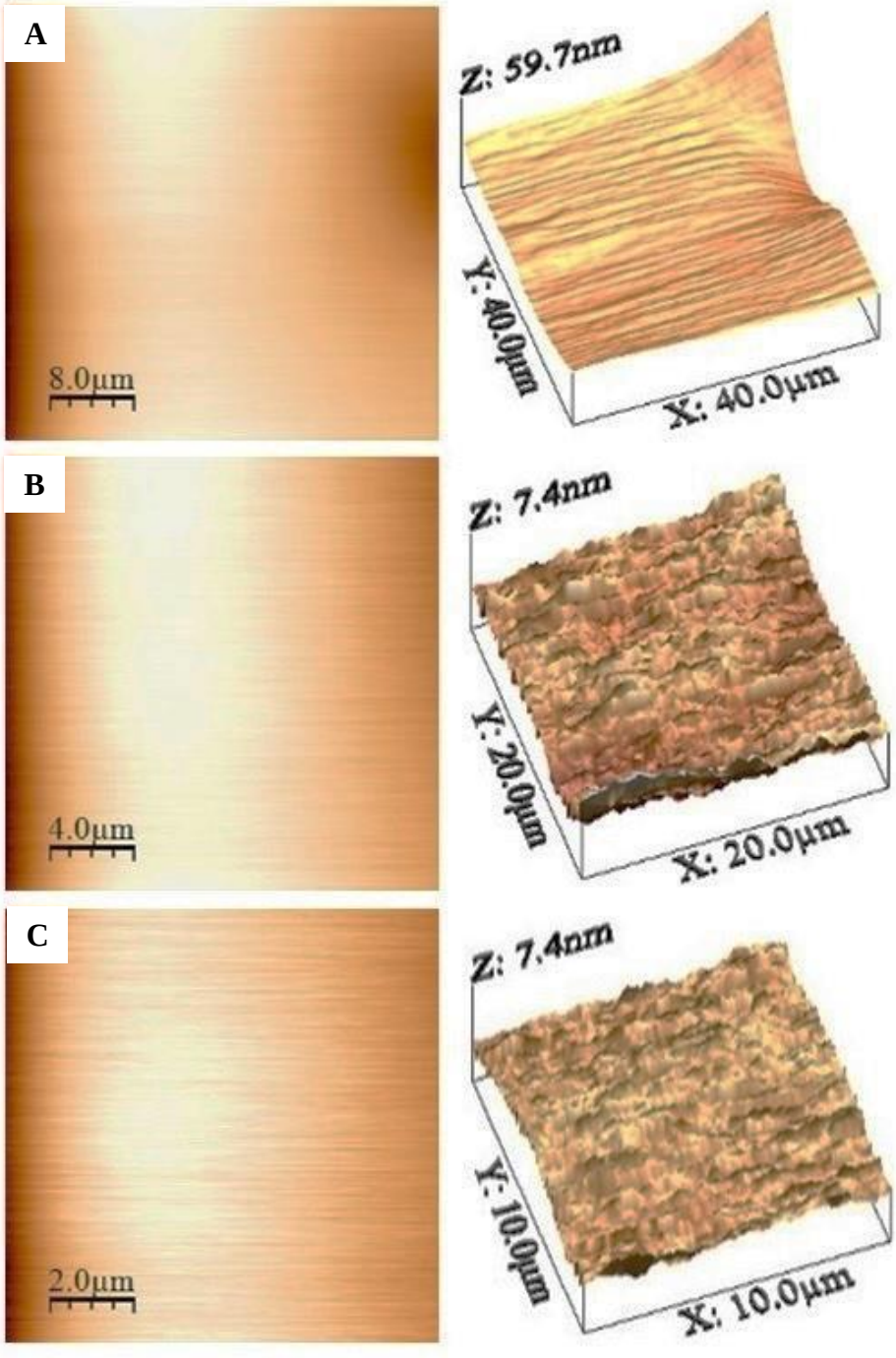
A
8.0µm
Z: 59.7nm
Y: 40.0µm
X: 40.0µm
B
4.0µm
Z: 7.4nm
Y: 20.0µm
X: 20.0µm
C
2.0µm
Z: 7.4nm
Y: 10.0µm
X: 10.0µm

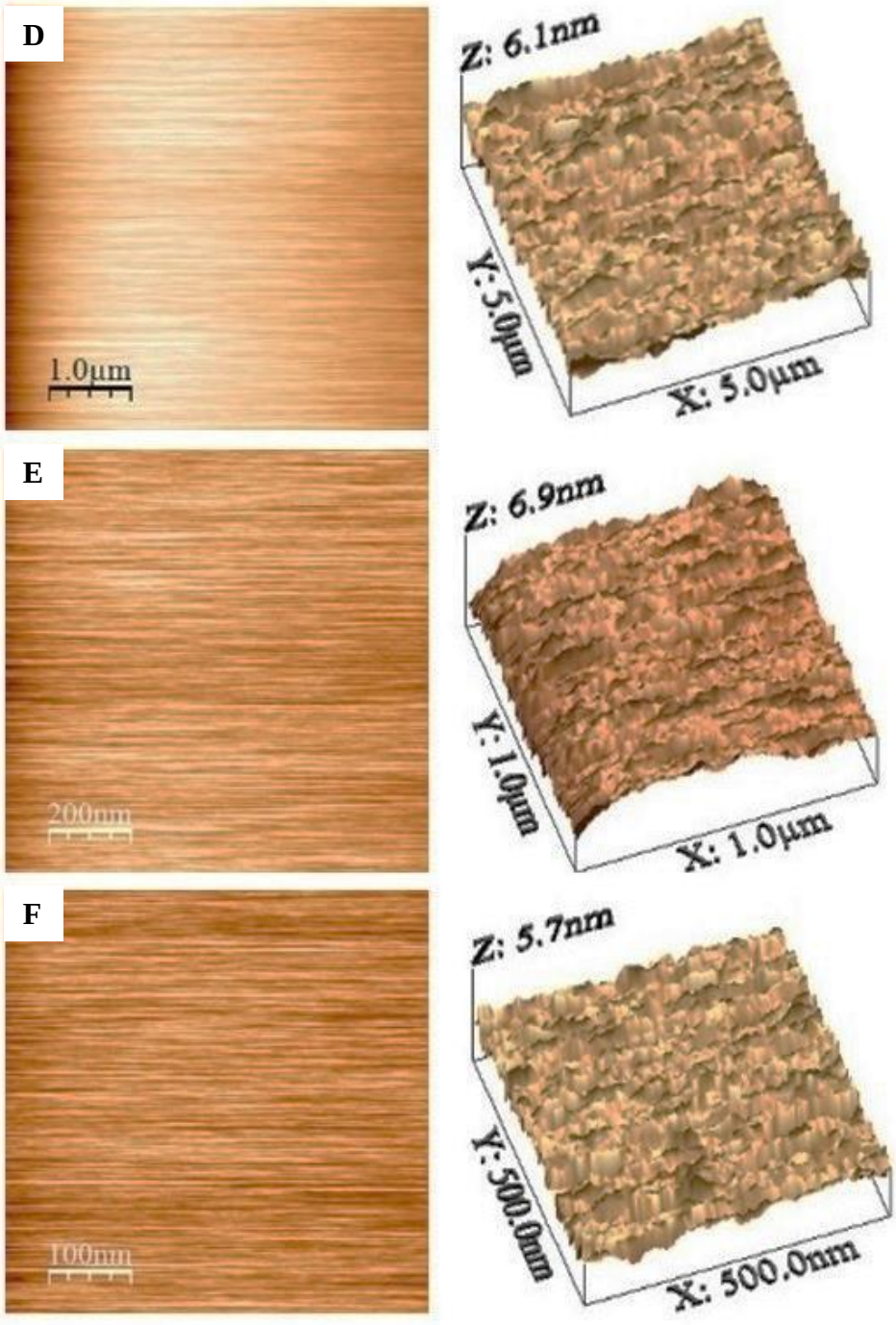

Figure5.1: A: 2D and 3D AFM micrographs at 40 µm scale. B: 2D and 3D AFM micrographs at 20 µm scale. C: 2D and 3D AFM micrographs at 10 µm scale. D: 2D and 3D AFM micrographs at 5 µm scale. E: 2D and 3D AFM micrographs at 1 µm scale. F: 2D and 3D AFM micrographs at 500 nm scale.

5.1.1.2. Texture profile micrographs:

A line profile is drawn on the AFM micrograph and shows the morphology of the surface. It can be noticed that through the various scales, from 40 μm to 500 nm through the figures from 5.2-A to 5.2-F, that the surface texture does not exceed 2.75 nm in height. This indicates the degree of smoothness of the non-textured polycarbonate surface.

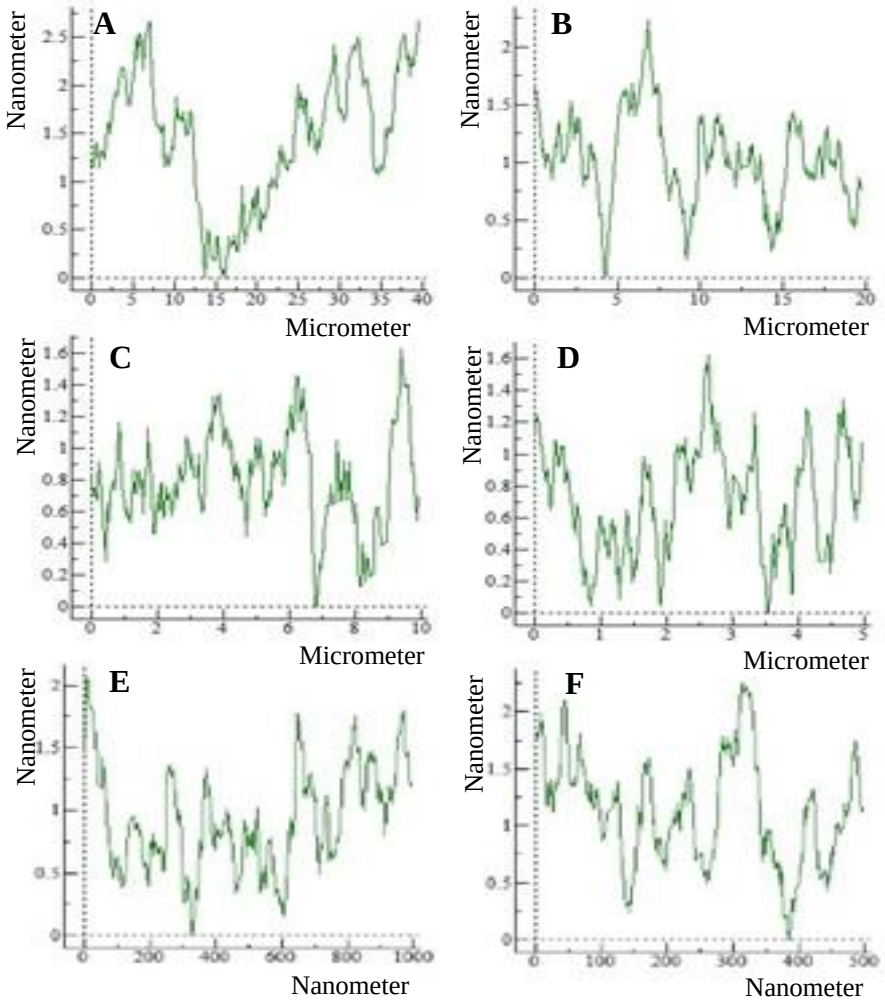

Figure5.2: A: AFM texture profile micrographs at 40 μm scale. B: AFM texture profile micrographs at 20 μm scale. C: AFM texture profile micrographs at 10 μm scale. D: AFM texture profile micrographs at 5 μm scale. E: AFM texture profile micrographs at 1 μm scale. F: AFM texture profile micrographs at 500 nm scale.

5.1.2. Transmittance:

Bare polycarbonate sheets as received are scanned between 400 nm to 800 nm to measure their transmittances. This study is focused on the visible spectrum; consequently a transmittance is plotted versus the visible spectrum region, figure 5.3. The average transmittance of the untreated polycarbonate glass in the visible area is 89.6%.

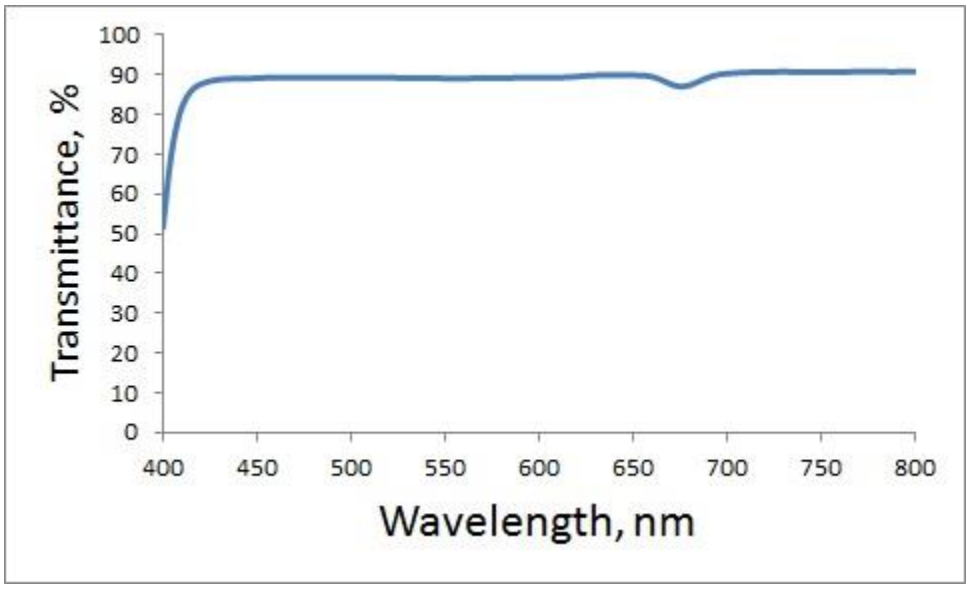

Figure5.3: Visible spectrum of smooth, untreated polycarbonate glass.

5.1.3. Contact angle measurements:

CA of the untreated polycarbonate surface is measured by dropping a deionized water droplet over the surface and measured, using a goniometer. Different areas of the surface are taken into consideration during the measurements. It is found that the average contact angle is 84.3^{o}; indicating the slight hydrophilicity of the smooth polycarbonate surface, figure 5.4.

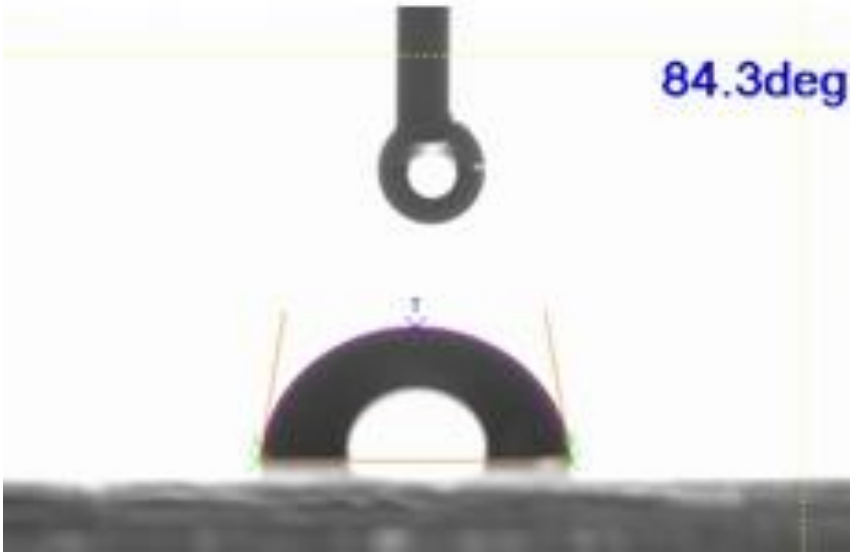

Figure5.4: Contact angle of smooth, untreated polycarbonate surface.

5.1.4. FT-IR spectra:

Fourier-transform Infrared technique is applied for determining the presence of chemical groups, functional, side and terminal groups, within a certain chemical compound through the detection of the different stretching and bending modes of the bonds, present in these groups. A special tool is used to detect the chemical groups, present on the surface of the smooth polycarbonate glass.

In figure 5.5, FT-IR spectrum of smooth, untreated polycarbonates surface is illustrated. The study focuses on the wavelength at which the peak of carbonyl, C=O, stretching mode appears. Before the exposure to acetone, the peak of carbonyl stretching mode appears at 1764 cm^{-1}, with absorbance value of 0.34. The peak of the phenyl stretching mode appears at 1499 cm^{-1}, with absorbance value of 0.25.

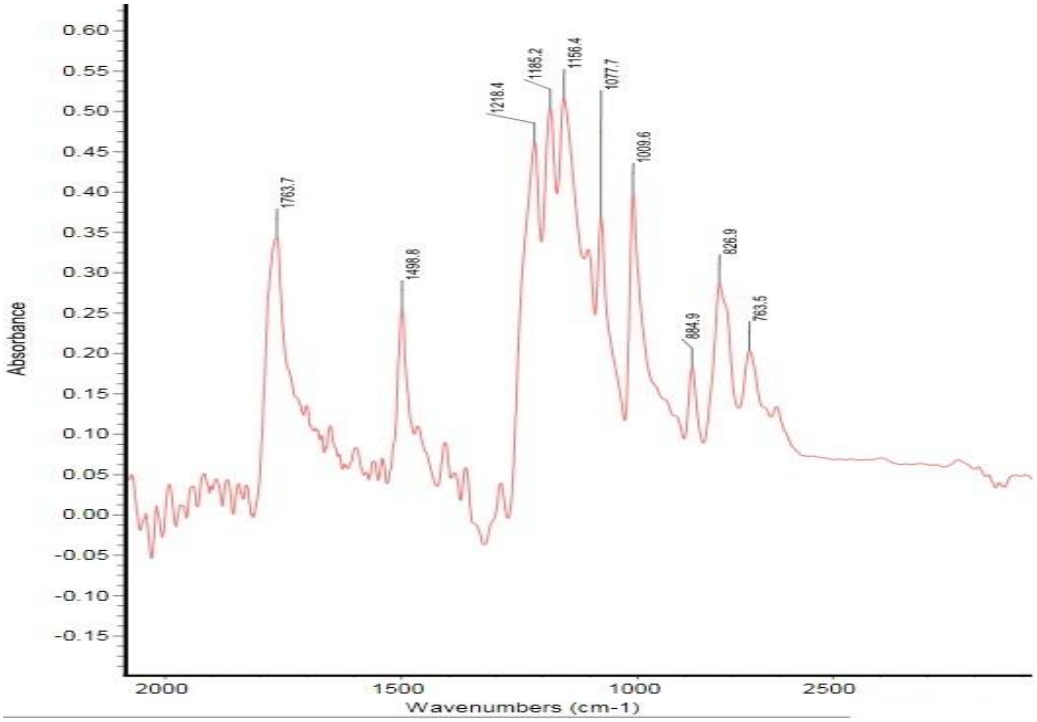

Figure5.5: FTIR of smooth, untreated polycarbonate glass.

5.2. The solid-liquid interface, polycarbonate-liquid acetone:

Polycarbonate sheets are immersed in liquid acetone of different concentrations (pure acetone, 75% and 50% acetone) for different durations. In this arrangement, the effect of the acetone concentration and the dipping duration on the developed texture is studied. Texture profile micrographs, from Atomic Force Microscope, give detailed images which illustrate the distances between the pillars within the textured surfaces. Roughness mean square and roughness average values, from AFM, are the parameters which give insight into the surface texture and provide information to enhance the hydrophobicity of the surface. All the former characterizations flew in the direction of measuring the contact angles of water droplets over the different textured surfaces as a tool for deducing the surfaces hydrophobicities.

5.2.1. Drying rate of the surface

After immersion in liquid acetone, the polycarbonate sheet is allowed to dry in the ambient atmosphere. The drying step is of high importance, because the diffused acetone through the layers of the sheet can evaporate, and during the evaporation process, crystallization of polycarbonate surface occurs. The crystallization process is the base of forming the surface texture and structure. In the current work, the rate of drying at the extracted polycarbonate sheet from the acetone medium is measured as the immersed sheet represents mass loss over time appears to be 15 min. The drying curve is smooth, indicating a uniformed evaporation of the acetone from the surface, figure 5.6. During the first minute of the drying period, ~7.6 mg/min of acetone evaporates; then, the rate of acetone evaporation decreases down to 5 mg/min during the following next 3 minutes; and finally, from the 5^{th} to the 15^{th} minutes the evaporation rate decreases from being 2.9 mg/min down to 0.8 mg/min.

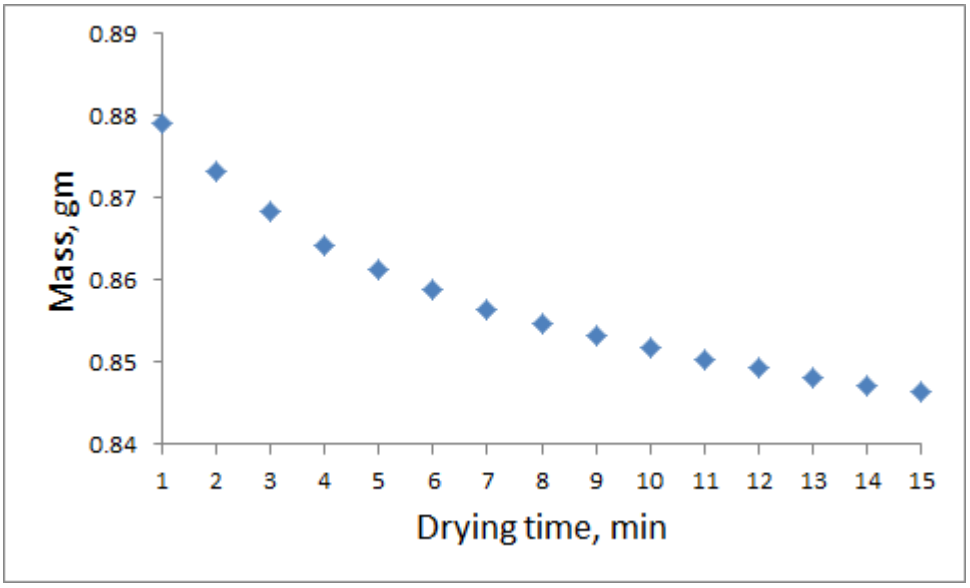

Figure5.6: Drying rate curve of a polycarbonate sample, after immersion in pure liquid acetone.

5.2.2. Atomic force microscope (AFM) micrographs for a textured polycarbonate glass sample, immersed in liquid acetone for 10 minutes:

5.2.2.1. Surface topography micrographs:

Several AFM scans are taken for different areas on the textured polycarbonate glass surface, at different scales (500 nm, 1, 5, 10, 20 and 40 μm). The micrographs illustrate clearly the appearance of a new surface texture after the immersion process. In figure 5.7-A, with a scanning scale of 40 μm, large spherules appear over the surface after immersing the sample for 10 minutes. The average size of the spherules, appearing in the figure, is nearly 12 μm in width. The lines appearing as tails to the spherules are present due to AFM-tip slipping during the scanning process. In figure 5.7-B and at a scale of about 20 μm, the spherule appears more obviously and it can be noticed that the middle spherule is about 10 μm in width. By zooming in and reducing the scanning scale, the surface of the spherule shows more details. Figure 5.7-C illustrates that there is texture over the spherule's surface, which is clear also in the three-dimensional micrograph. At lower scales, the surface of the spherule becomes more obvious and the texture over it can be obviously detected. It can be noticed that the surface of the spherule is not homogenous, in other words, the spherule's surface becomes hilly, this hilly surface is full of a grass-like texture one, and this can be inferred from the three-dimensional micrograph, figure 5.7-D. In both figures 5.7-E and 5.7-F, the scales are 1 μm and about 500 nm, respectively.

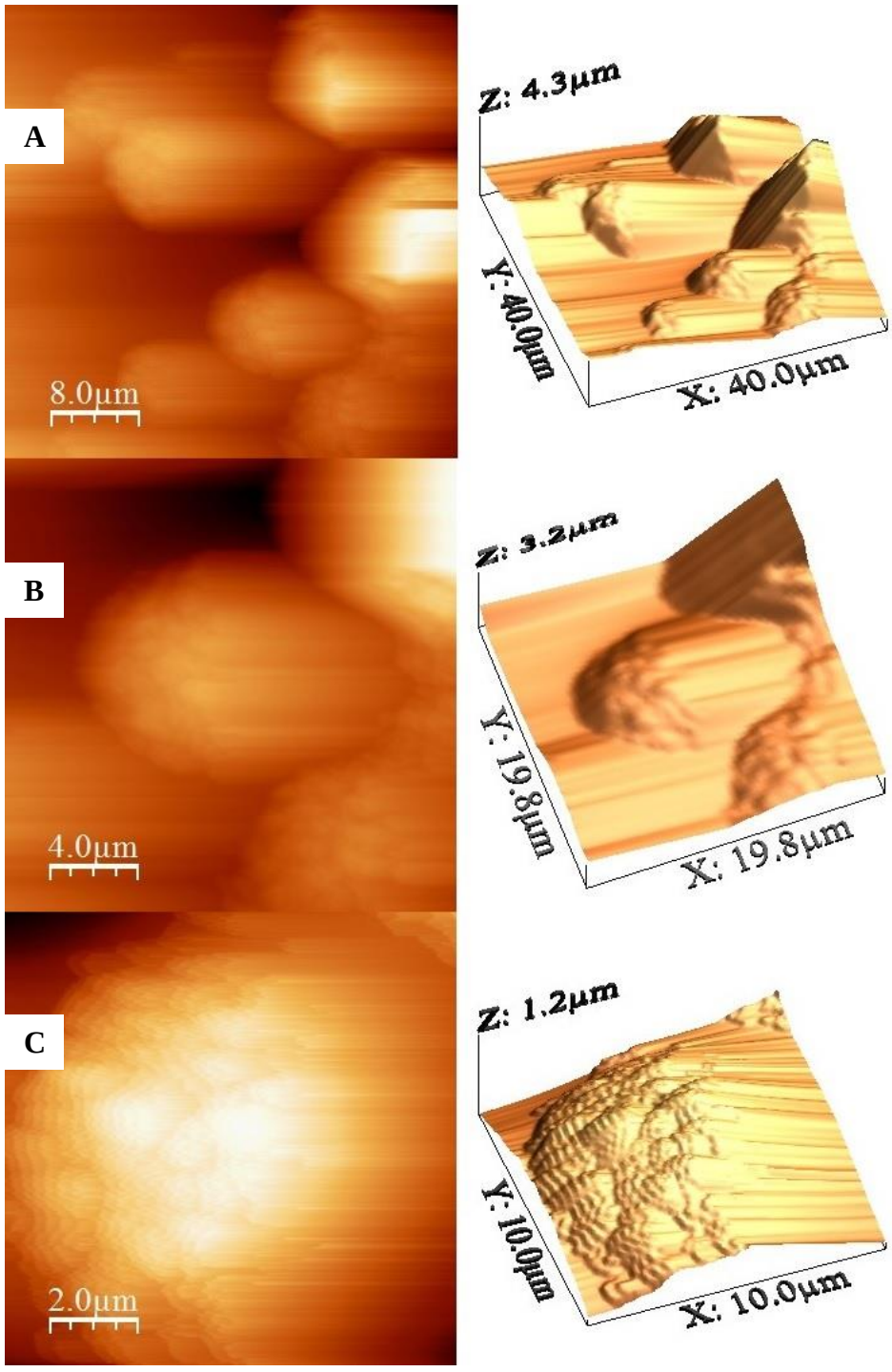
A
8.0µm
Z: 4.3µm
Y: 40.0µm
X: 40.0µm
B
4.0µm
Z: 3.2µm
Y: 19.8µm
X: 19.8µm
C
2.0µm
Z: 1.2µm
Y: 10.0µm
X: 10.0µm

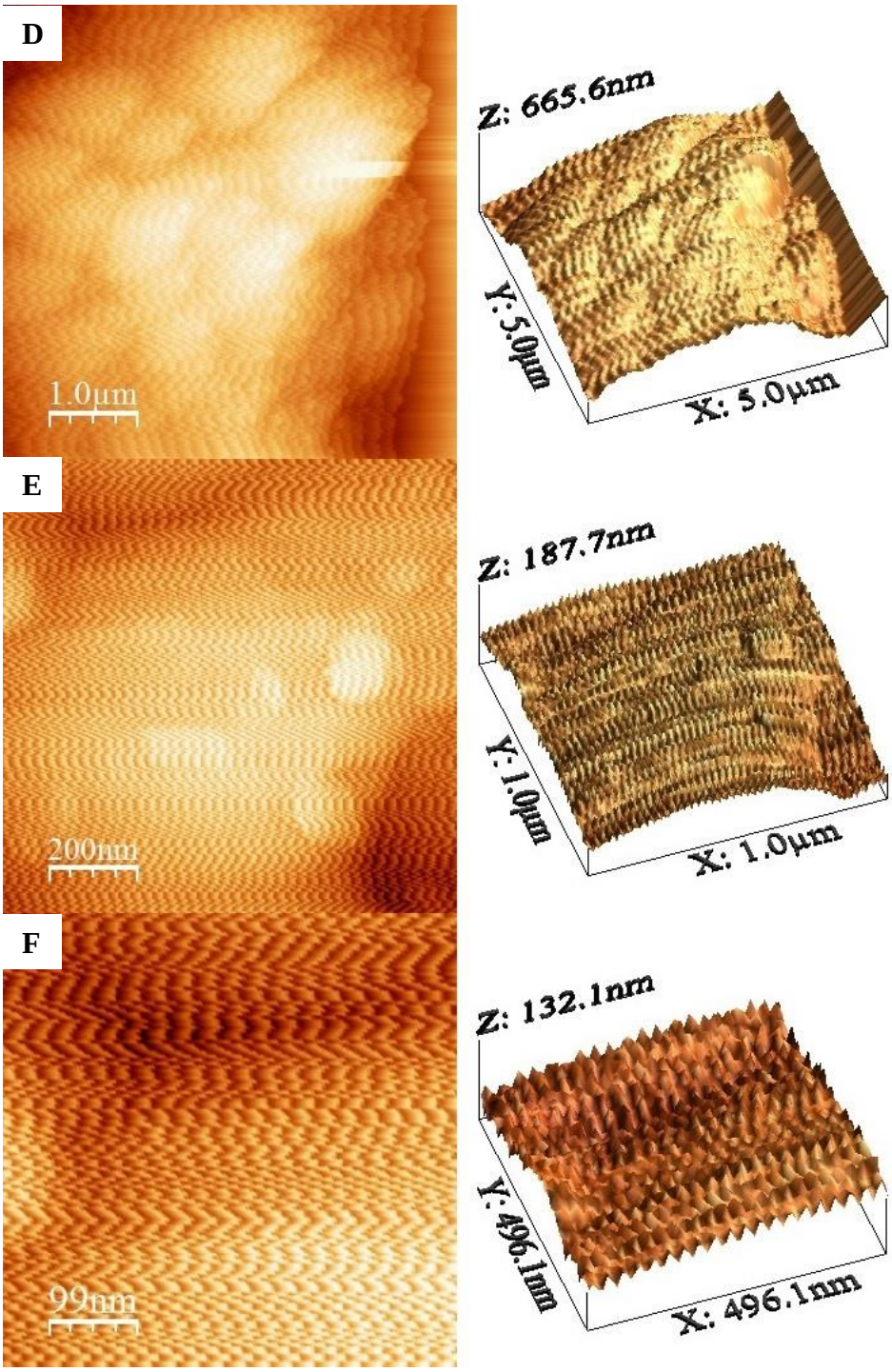

Figure5.7: 2D and 3D AFM micrographs at: A: 40 µm scale. B: 20 µm scale. C: 10 µm scale. D: 5 µm scale. E: 1 µm scale. F: 500 nm scale, for a textured polycarbonate surface by immersion in pure liquid acetone for 10 minutes.

5.2.2.2. Texture profile micrographs:

The study involves investigating the topology of the textured surface by using surface profile micrographs from AFM in order to follow up the effect of acetone on the polycarbonate surface. It is obvious that through the various scales, from 40 μm to 500 nm, that the surface texture height is in the range of 1.75 μm. In figure 5.8-A, the height of the spherules can be measured, it is about 1.8 μm. The width of the middle spherule is about 13 μm. Figure 5.8-B illustrates a single and small spherule of 600 nm in height and nearly 12 μm in width. The texture over the spherule is shown in the figure. For further examination of the surface of the spherule, scanning scale is reduced and the texture over the spherule's surface starts to appear in figure 5.8-C. In figure 5.8-D, a distinctive profile micrograph of the single spherule appears. The spherule contains three small elevations over its surface, each elevation is textured. This promotes the observation of the hilly surface and the grass-like hills, which is pointed out within the description of figure 5.7-D. In figure 5.8-E, the elevation (hilly surface) appears clearly, including the texture (noise-like) over its surface. The width of the hill is 1 μm and its height is 100 nm. For further investigation to the texture, the scanning scale is reduced down to 500 nm, figure 5.8-F. In this figure, the texture (noise-like) is very apparent; it's regular in height, which is about 48 nm in average. The average width of the texture is about 25 nm.

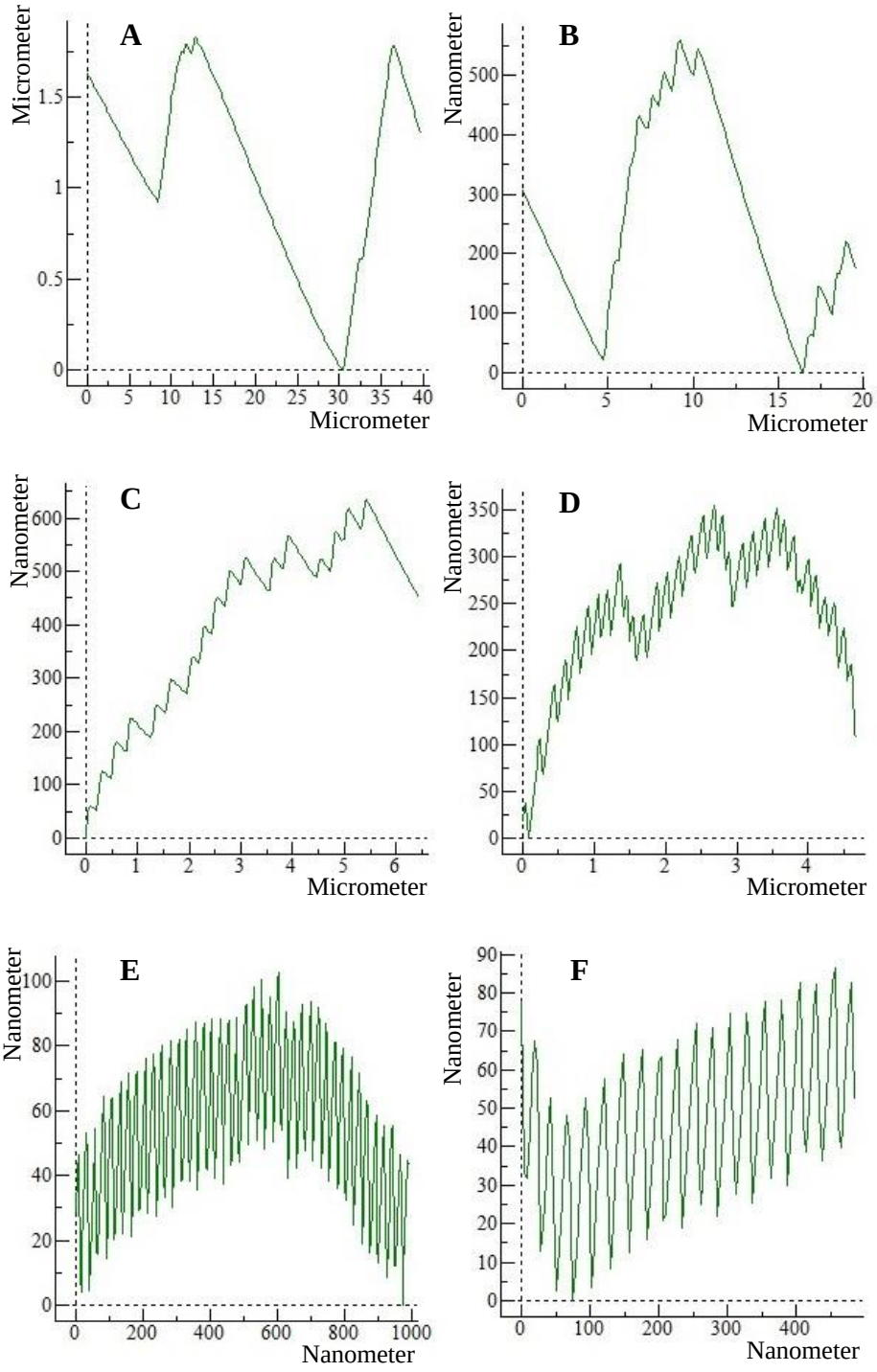

Figure5.8: AFM texture profile micrographs at: A: 40 µm scale. B: 20 µm scale. C: 10 µm scale. D: 5 µm scale. E: 1 µm scale. F: 500 nm scale, for a textured polycarbonate surface by immersion in pure liquid acetone for 10 minutes.

5.2.3. Transmittance:

Textured, rough polycarbonate sheets, due to immersion in liquid acetone, exposed to a spectrum, starting from 400 nm to 800 nm to measure their transmittance values. The research's focus is on the visible spectrum, so the transmittance is plotted versus the visible spectrum region (400 nm to 800 nm). The transmittance values of the different samples under investigation are examined by placing each sample, alone and vertically to cut the light path from the light source to the detector inside the chamber of UV-Vis spectrophotometer. The instrument is set to give readings every 4 nm, with medium scan speed and scanning rate of 100 nm/ min.

In figure 5.9-A, the sample, denoted i1, is immersed in pure liquid acetone for 1 min. The average transmittance in the visible region is 7.24%. In figure 5.9-B, the sample i2 is immersed in pure liquid acetone for 2 min. The average transmittance of this sample is 4.97%. In figure 5.9-C, the sample i3 is immersed in pure liquid acetone for 3 min. The average transmittance of this sample is 3.85%. The sample i4, figure 5.9-D, is immersed in pure liquid acetone for 4 min. The average transmittance of this sample is 3.56%. The sample i5, figure 5.9-E, is immersed in pure liquid acetone for 5 min. The average transmittance of this sample is 4.73%. The sample i6, figure 5.9-F, is immersed in pure liquid acetone for 10 min. The average transmittance of this sample is 0.85%.

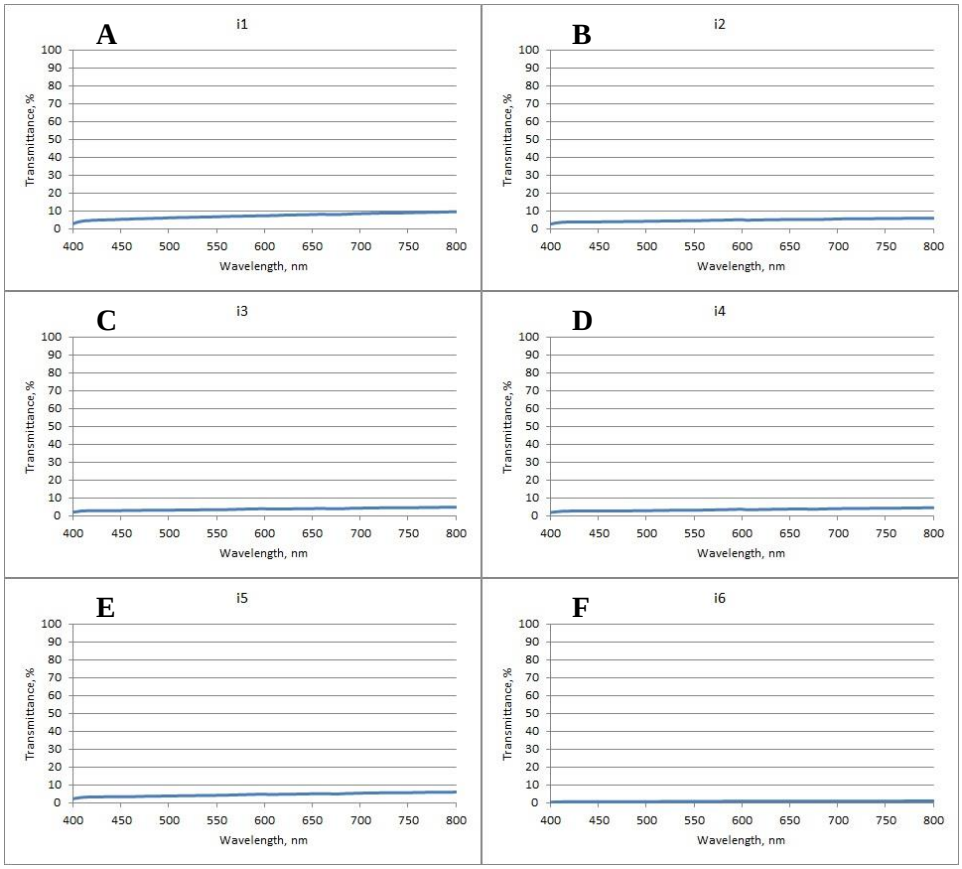

Figure5.9: Visible spectrum of a textured polycarbonate sample by immersion in pure liquid acetone for: A: 1 minute. B: 2 minutes. C: 3 minutes. D: 4 minutes. E: 5 minutes. F: 10 minutes.

Figure 5.10 shows all the transmittance curves for the 6 samples. The descending arrangement of the samples according to immersion duration is i6 > i5 > i4 > i3 > i2 > i1. The descending arrangement of the transmittance values for the samples are i1 > i2 > i3 > i4 > i5 > i6. It can be inferred that the transmittance value is inversely proportional to the immersion duration. Hence, by increasing the immersion duration, at a fixed acetone concentration, the transmittance of the patterned surface decreases. Figure 5.11 illustrates the relation between the immersion duration and the average transmittance of each sample.

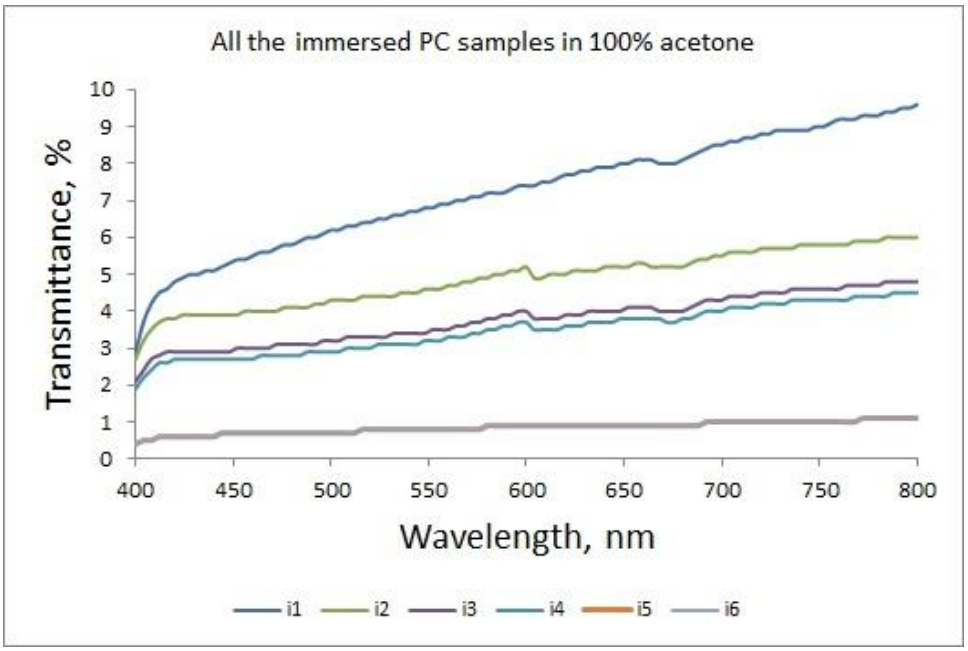

Figure5.10: Visible spectra of all the textured polycarbonate by immersion in pure liquid acetone for different durations.

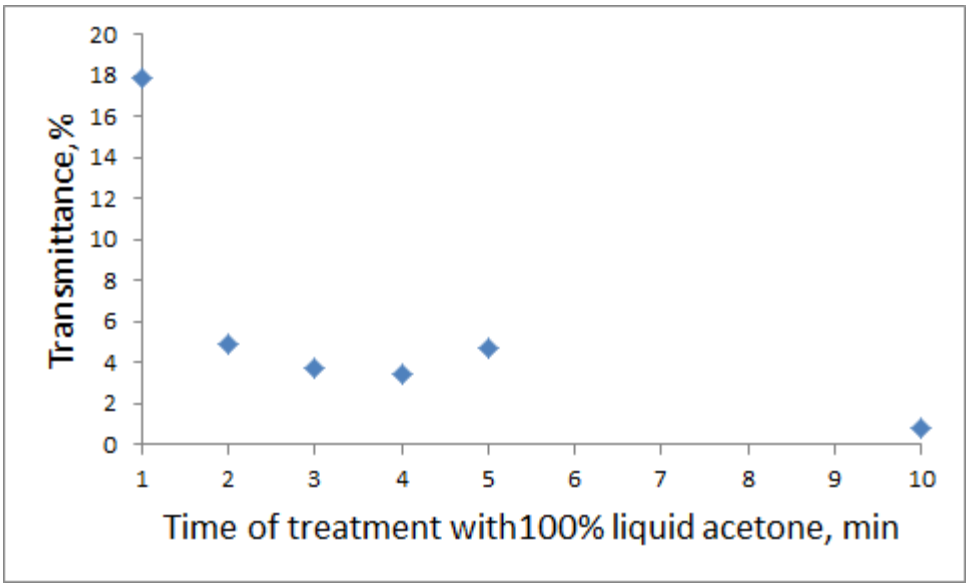

Figure5.11: The effect of the immersion duration of polycarbonate in acetone on the average transmittance value.

In figure 5.12-A, the sample, denoted i9, is immersed in 75% liquid acetone (with 25% deionized water) for 6 minutes. The average transmittance in the visible region is 57.77%. In figure 5.12-B, the sample i10 is immersed in 75% liquid acetone for 8 minutes. The average transmittance of this sample is 58.97%. In figure 5.11-C, the sample i11 immersed in 75% liquid acetone for 10 minutes. The average transmittance of this sample is 16.84%.

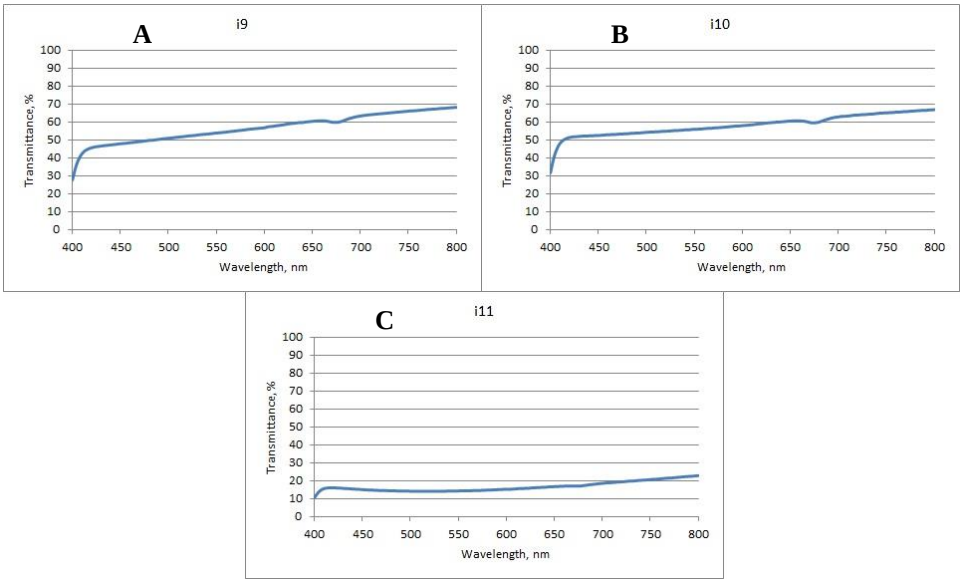

Figure5.12: Visible spectrum of a textured polycarbonate sample by immersion in pure liquid acetone for: A: 1 minute. B: 2 minutes. C: 3 minutes.

Figure 5.13 includes all the transmittance curves for the 3 samples. The descending arrangement of the samples according to immersion duration is i11 > i10 > i9. The descending arrangement of the transmittance values for the samples are i9 > i10 > i11. This further proves that the transmittance value is inversely proportional to the immersion duration. Figure 5.14 illustrates the relation between the immersion duration and the average transmittance of each sample. Furthermore, a comparison can be made polycarbonate sheet in pure liquid acetone for 10 min, 0.85%, and that immersed in 75% liquid acetone for 10 min, 16.84%. Therefore, it's clear that there is an inverse proportionality between the acetone concentration and the transmittance value, so by increasing the acetone concentration, at constant immersion duration, the transmittance of the textured surface decreases.

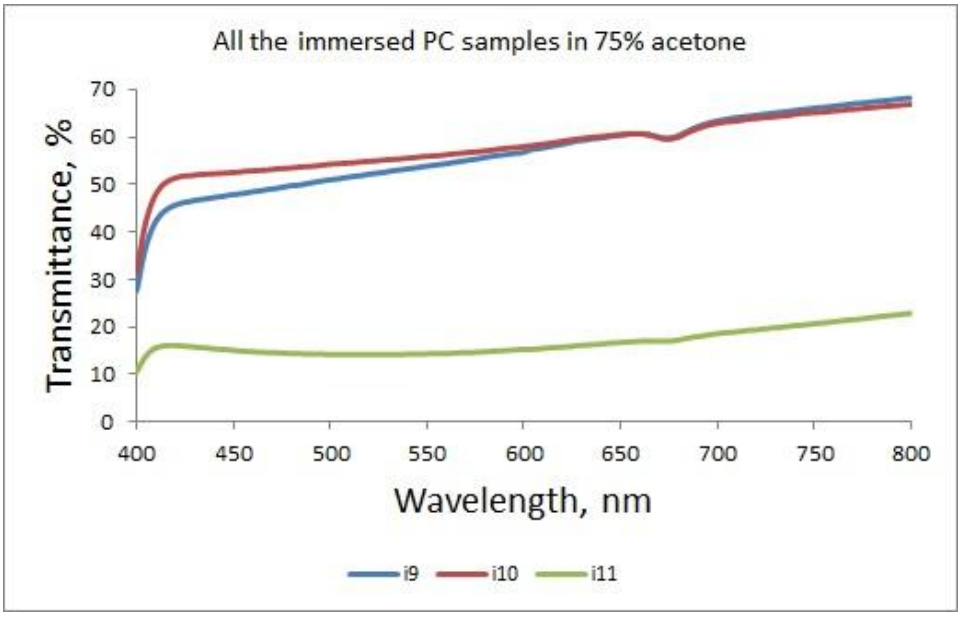

Figure5.13: Visible spectra of all the textured polycarbonate by immersion in pure liquid acetone for different durations.

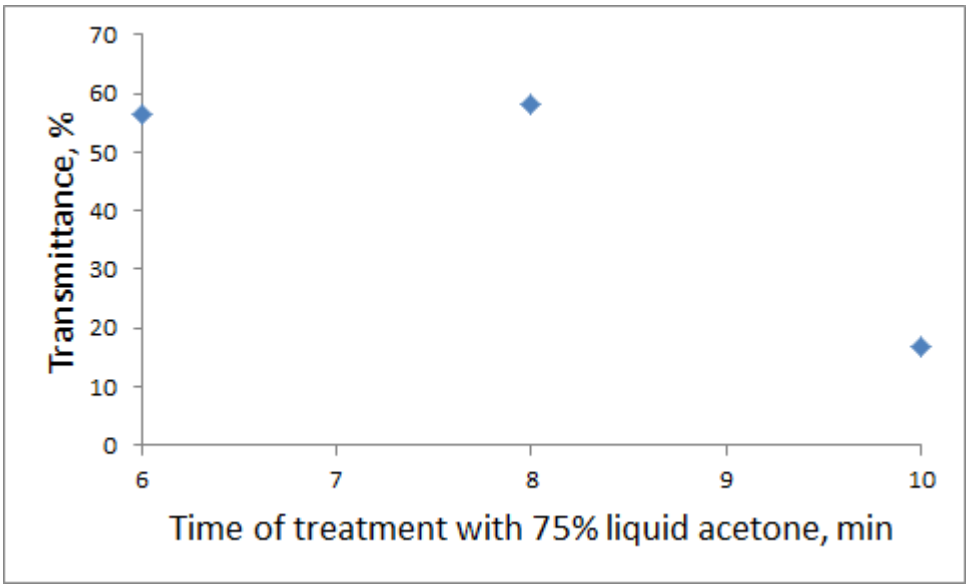

Figure5.14: The effect of the immersion duration of polycarbonate in liquid acetone on the average transmittance value.

5.2.4. Contact angle measurements:

CA of the patterned polycarbonate surface is measured by dropping a deionized water droplet over the textured surface and measured by using the goniometer's camera. Different areas of the surface are taken in to consideration during the measurements.

Immersion of polycarbonate sheet in pure liquid acetone for a period of one minute, denoted as i1, the contact angles of the three different areas over the surface are 107.9, 108.2 and 100.6^{o}, figures 5.15-A, B and C, respectively. The average contact angle for this sample is 105.57^{o}. For the i2 sample, immersed for a period of two minutes, the contact angles of the three different areas over the surface are 141.8, 140.9 and 114.4^{o}, figures 5.15-D, E and F, respectively. The average contact angle for this sample is 132.37^{o}. For the i3 sample, immersed for three minutes, the contact angles of the three different areas over the surface are 141.1, 139.9 and 139.0^{o}, figures 5.15-G, H and I, respectively. The average contact angle for this sample is 139.90^{o}. For the i4 sample, immersed for four minutes, the contact angles of the three different areas over the surface are 133.8, 134.7 and 134.1^{o}, figures 5.15-J, K and L, respectively. The average contact angle for this sample is 134.20^{o}. For the i5 sample, immersed for five minutes, the contact angles of the three different areas over the surface are 138.0, 144.1 and 138.0^{o}, figures 5.15-M, N and O, respectively. The average contact angle for this sample is 140.03^{o}. For the i6 sample, immersed for ten minutes, the contact angles of the three different areas over the surface are 138.3, 137.3 and 130.7^{o}, figures 5.15-P, Q and R, respectively. The

average contact angle for this sample is 135.57^{o}. Table 5.2 summarizes the immersion durations in minutes, the contact angle values of all the areas for all the samples and their average values per single sample. Figure 5.15 illustrates the values of the contact angles of the immersed, textured polycarbonate samples, the photos are taken by the goniometer's camera.

Table5.1: It illustrates the sample name, duration of immersion in liquid acetone, CA of each area over the same sample's surface and the average CA value for each sample.

Sample	Treatment time, min	C.A.(deg)	Average CA
i1 (area1)	1	107.9	105.5666667
i1 (area3)		108.2	
i1 (area2)		100.6	
i2 (area1)	2	141.8	132.3666667
i2 (area2)		140.9	
i2 (area3)		114.4	
i3 (area1)	3	141.1	139.9
i3 (area2)		139.6	
i3 (area3)		139	
i4 (area1)	4	133.8	134.2
i4 (area2)		134.7	
i4 (area3)		134.1	
i5 (area1)	5	138	140.0333333
i5 (area2)		144.1	
i5 (area3)		138	
i6 (area1)	10	138.3	135.5666667
i6 (area2)		137.7	
i6 (area3)		130.7	

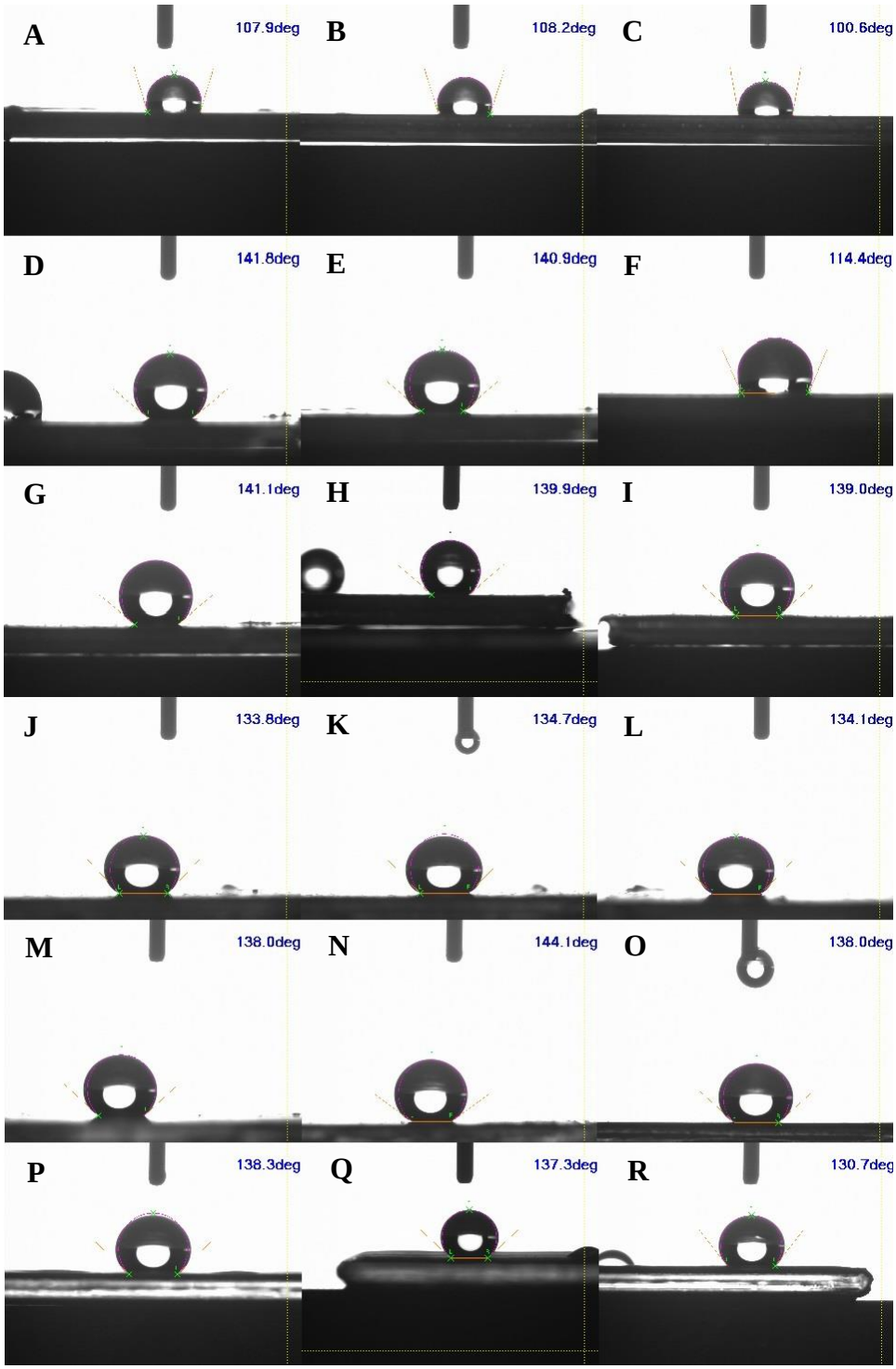

Figure5.15: CA of a textured polycarbonate sample by immersion in pure liquid acetone for: A, B & C: 1 minute. D, E & F: 2 minutes. G, H & I: 3 minutes. J, K & L: 4 minutes. M, N & O: 5 minutes. P, Q & R: 10 minutes.

From the tabulated data, interesting observations can be made. First, by increasing the immersion duration of the polycarbonate sample in the acetone, the contact angle increases. Second, a large jump in contact angle is observed, between the pure liquid acetone immersed sample for one min with an average contact angle of 105.57^{o}, and that immersed in liquid acetone for two min and has an average contact angle of 132.37^{o} (the difference between the two values is about 27^{o}). The average values of the contact angles of the remaining sample, immersed in pure liquid acetone for 3, 4, 5 and 10 minutes, fluctuate between 132.2^{o} to 140.03^{o}. Figure 5.16 illustrates the relationship between the duration of polycarbonate surface immersed in liquid acetone and the resulting, apparent contact angle. Finally, for the samples i1 and i2, it can be noted that each sample exhibited a relatively low contact angle. It can be observed visually that, the samples i1 and i2 have longitudinal lines after removing it out of the acetone liquid and drying it in the air. One of these lines has a bright white color, while the other has a pale white color and they are present alternatively. The contact angles at the two lines are examined; it is found that the bright white line has the higher contact angle; however, the pale white color has the lower contact angle. This is related to that the rate of the crystallization process is not homogenous over surface, so some areas are crystallized more than the others. These line structures maybe due to **i**) industrial processing and/or **ii**) the adhesive material used between the polycarbonate surface and the cover which maybe not homogenously spread. These lines disappeared in the rest of the sample and the contact angle values over the surface are nearly unified and that may be related to the extended

duration of immersion of the polycarbonate surface with the liquid acetone, so all the areas over the polycarbonate surface reached a maximum crystallization.

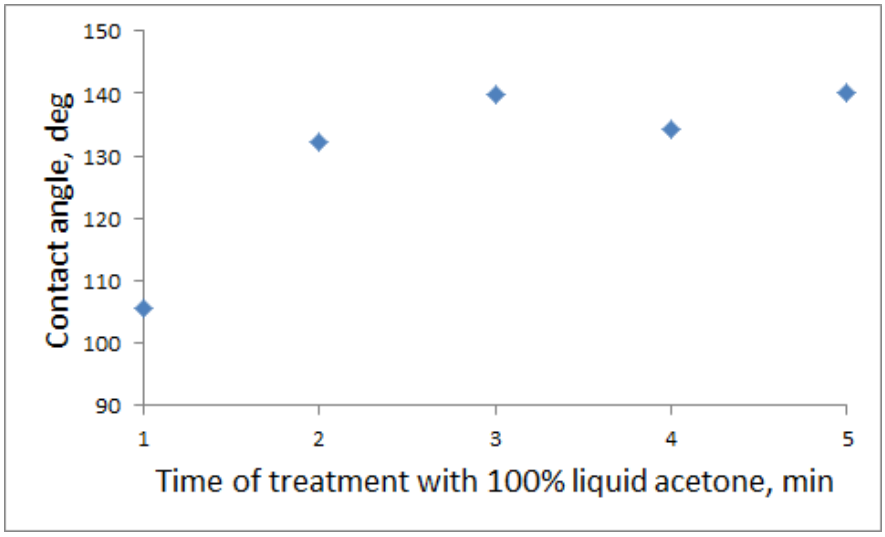

Figure5.16: The effect of the immersion duration of polycarbonate in liquid acetone on the CA.

Polycarbonate samples that are immersed in 75% liquid acetone, for the sample i9, and immersed in 75% liquid acetone for 6 min, the contact angles of three different areas over the surface are 80.4, 83.1 and 84.8^{o}, figures 5.17-A, B and C respectively. The average contact angle for this sample is 82.77^{o}. For the i10 sample, immersed for eight minutes, the contact angles of three different areas over the surface are 83.1, 82.6 and 83.6^{o}, figures 5.17-D, E and F, respectively. The average contact angle for this sample is 83.10^{o}. For the i11 sample, immersed for ten minutes, the contact angles of three different areas over the surface are 89.70, 91.70 and 87.60^{o}, figures 5.17-G, H and I, respectively. The average contact angle for this sample is 89.67^{o}. Table 5.3 summarizes the immersion durations in minutes, the contact angle values of all the areas for all of the samples and their average values per single sample. Figure 5.17 illustrates the values of the contact angles of the immersed, textured polycarbonate samples, the photos are taken by the goniometer's camera.

Table5.2: It illustrates the sample name, duration of immersion in liquid acetone, CA of each area over the same sample's surface and the average CA value for each sample.

Sample	Treatment time, min	C.A.(deg)	Average CA
i9 (area 1)	6	80.4	82.76666667
i9 (area 2)		83.1	
i9 (area 3)		84.8	
i10 (area 1)	8	83.1	83.1
i10 (area 2)		82.6	
i10 (area 3)		83.6	
i11 (area1)	10	92.6	93.1
i11 (area2)		91.7	
i11 (area3)		95	

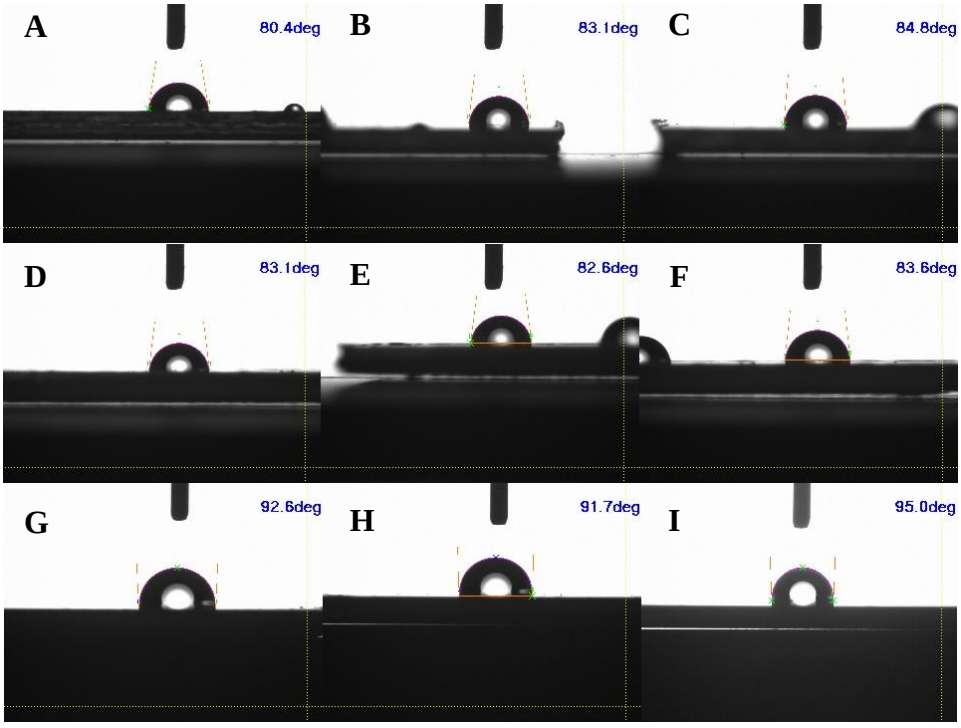

Figure5.17: CA of a textured polycarbonate sample by immersion in 75% liquid acetone for: A, B & C: 6 minute. D, E & F: 8 minutes. G, H & I: 10 minutes.

The tabulated data further proves that the texture generated at different immersion durations of polycarbonate sheet with the liquid acetone is directly proportional to the resulting contact angle. Besides that, there is a significant increase of the contact angle values of the samples i10, with an average contact angle of 83.10^{o}, and the sample i11 which has an average contact angle of 93.1^{o}. Figure 5.18 illustrates the relationship between the polycarbonate surface immersion duration in liquid acetone and the resulted, resulting, apparent contact angle. By comparing the contact angle values of the polycarbonate sheet which is immersed in pure liquid acetone for 10 min, i6 of average contact angle of 135.57^{o}, and that which is immersed in 75% liquid acetone for the same period, i11 of average contact angle of 93.10^{o}, it can be found that the sample i6 possesses a far greater contact angle than the sample i11. Therefore, i6 is far more hydrophobic than i11. From this comparison, it can be inferred that the concentration of acetone is directly proportional to the hydrophobicity of the immersed sample.

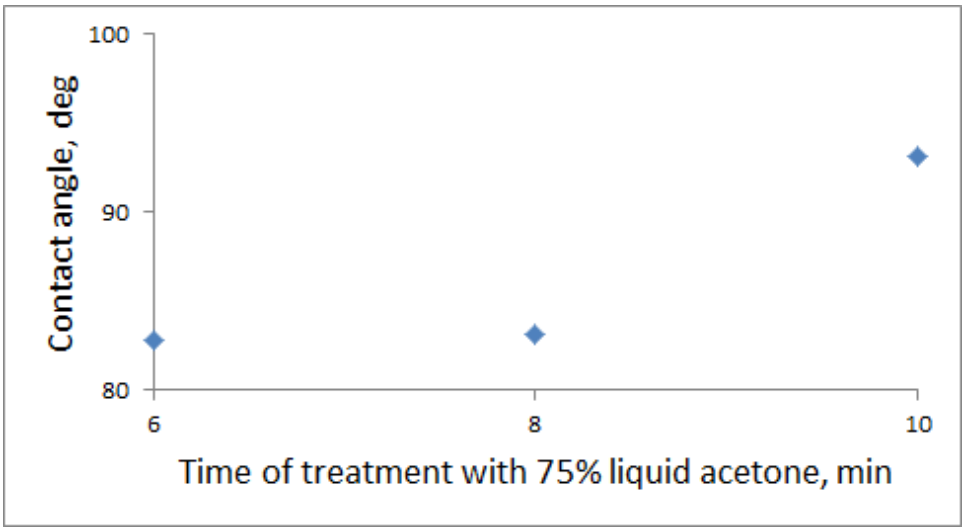

Figure5.18: The effect of the immersion duration of polycarbonate in acetone on the CA.

5.2.5. Optical microscope images:

An optical microscope is used to examine the morphology of the immersed polycarbonate surface. The first phase can be characterized and the shape and growth of the generated spherules due to the crystallization process can be tracked by examining a series of successive polycarbonate samples, immersed for successive durations in pure liquid acetone. Furthermore, the gaps or the distances between the spherules, where the crystallization process are absent to some extent, can be clearly viewed. The scale bar of most of the images is 100 μm.

Figure 5.19-A shows the startup of the spherules formation on the polycarbonate surface, in pure liquid acetone, for the sample i1, the spherules average width is about 10 μm. In the sample i2, the spherule's size increased and its width reached about 20 μm, figure 5.19-B. It can be noticed that some shallow heights started to appear within the gaps between the aggregations of the spherules, indicating that there are spherules which would grow through these areas. In the sample i3, figure 5.19-C, the spherules aggregations increased and spherules covered the most of the imaged areas. Through the sample i4, the spherules continue their growth and aggregations formation. It can be noticed that there is a fusion occurs between the adjacent grown spherules, figure 5.19-D. In sample i5, it's clear that the fusion occurred between some of the spherules and there are distinct lines separating those fused spherules. Furthermore, there are non-mature spherules growths within the gaps between the aggregates of the fused, mature spherules.

The non-mature spherules have also distinct lines separating between them, figure 5.19-E. The image is clear in the sample i6, figure 5.19-F, in which the fused, mature spherules can be well distinguished from the non-mature spherules, grow within the gaps.

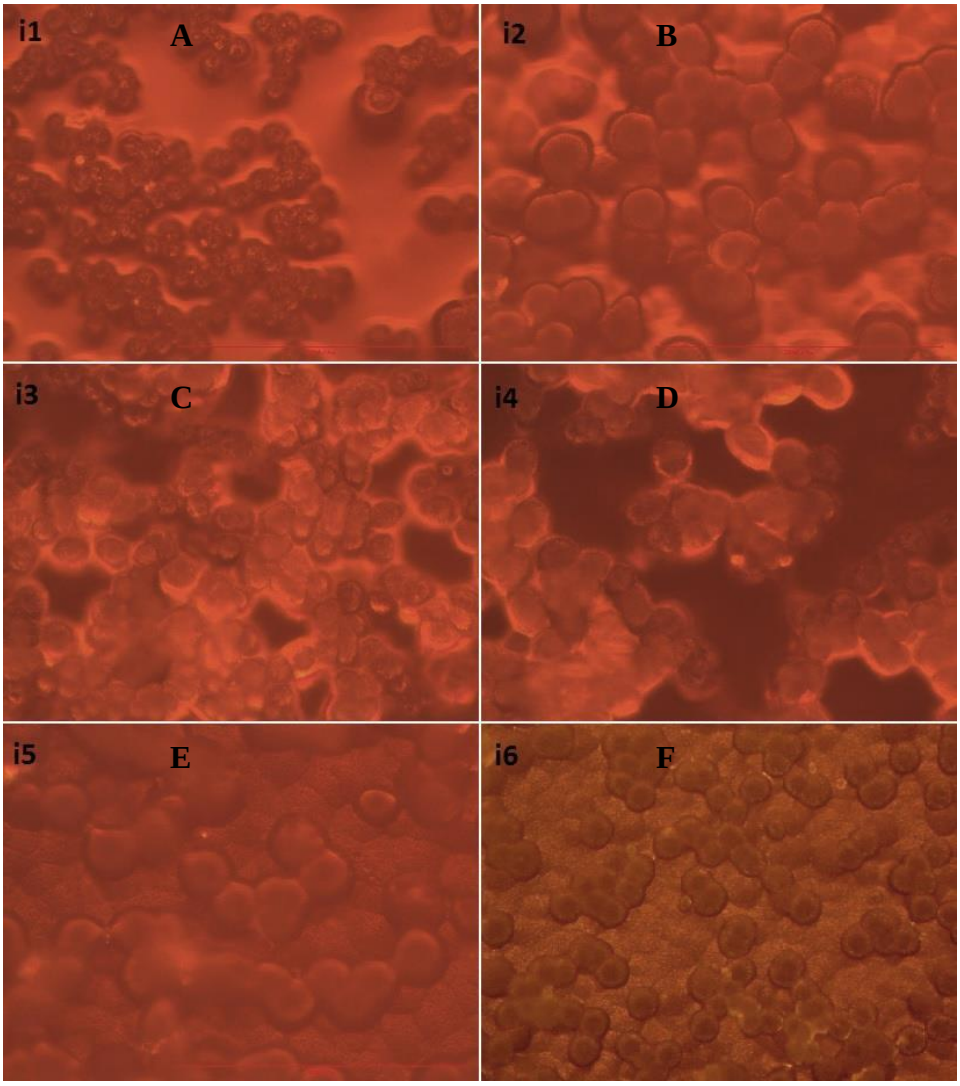

Figure5.19: Optical microscope image of a textured polycarbonate sample by immersion in pure liquid acetone for: A: 1 minute. B: 2 minutes. C: 3 minutes. D: 4 minutes. E: 5 minutes. F: 10 minutes.

5.2.6. FT-IR spectral analysis:

Fourier-transform Infrared technique is used for finding the presence of chemical groups, functional, side and terminal groups, within a certain chemical compound through the detection of the different stretching and bending modes of the bonds, present in these groups. A special tool is used to detect the chemical groups, present on the surface of the textured polycarbonate glass after the immersion process in liquid acetone.

In figure 5.20-A, FT-IR spectrum of textured polycarbonate surface, after immersion in pure liquid acetone for 3 minutes, is illustrated. The study focuses on the wavelength at which the peak of carbonyl, C=O, stretching mode appears. Before the exposure to acetone, the peak of carbonyl stretching mode appears at 1762 cm^{-1}, with absorbance value of 0.16. The peak of the phenyl stretching mode appears at 1499 cm^{-1}, with absorbance value of 0.08.

In figure 5.20-B, FT-IR spectrum of textured polycarbonate surface, after immersion in 75% liquid acetone for 6 minutes, is illustrated. The study focuses on the wavelength at which the peak of carbonyl, C=O, stretching mode appears. Before the exposure to acetone, the peak of carbonyl stretching mode appears at 1763 cm^{-1}, with absorbance value of 0.27. The peak of the phenyl stretching mode appears at 1499 cm^{-1}, with an absorbance value of 0.19.

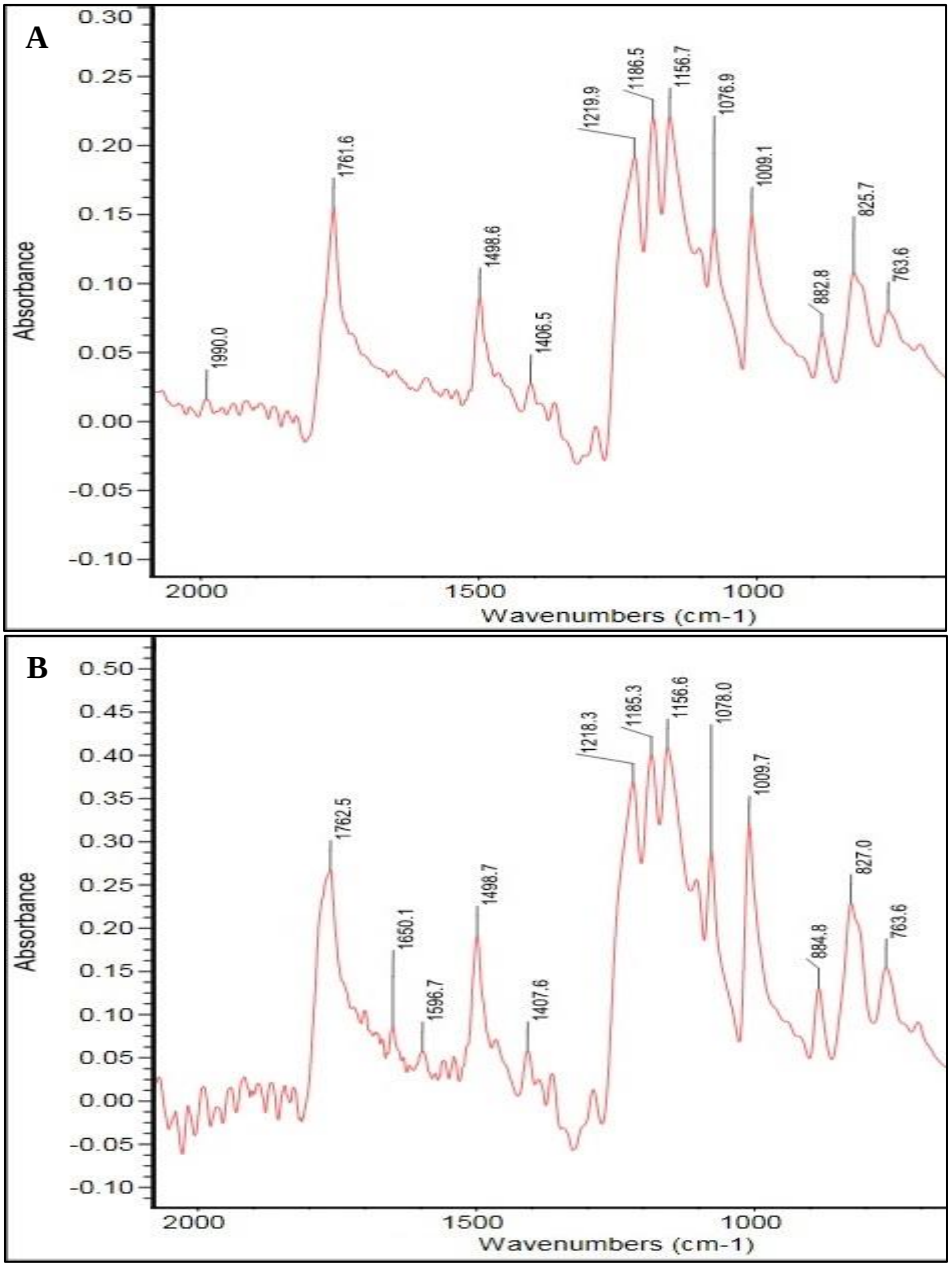

Figure5.20: A: FT-IR spectrum of a textured polycarbonate surface by immersion in pure liquid acetone for 4 minutes. B: FT-IR spectrum of a textured polycarbonate surface by immersion in 75% liquid acetone for 6 minutes.

5.3. The solid-vapor interface, polycarbonate- acetone vapor:

Polycarbonate sheets are exposed to acetone vapor for different durations, using different amounts of liquid acetone amounts, different distances between the polycarbonate glass surface and the liquid acetone surface and with and without heating. In this arrangement, the effect of the amount of acetone vapor, the distance between the liquid phase and solid phase surfaces, heating and the exposure duration to the acetone vapor on the developed texture is studied. Texture profile micrographs, from Atomic Force Microscope, give detailed images illustrating the distances between the pillars within the textured surfaces. Roughness mean square and roughness average values, from AFM, are the parameters which give insight into the surface texture and provide information to enhance the hydrophobicity of the surface. All the former characterizations have enriched this study with information which aided in measuring the contact angles of water droplets over the different textured surfaces as a tool for deducing the surfaces hydrophobicity.

5.3.1. Atomic force microscope (AFM) micrographs for a textured polycarbonate glass sample, exposed to acetone vapor for 24 hours:

5.3.1.1. Surface topology micrographs:

Several AFM micrographs are scanned at different areas on the textured polycarbonate glass surface, at different scales (500 nm, 1, 5, 10, 20 and 40 μm). The micrographs show clearly that there is a texture over the surface of the polycarbonate after exposure to the acetone vapor. In figure 5.21-A, with a scanning scale of 40 μm, well-detailed spherules appear over the surface after the exposure of the smooth polycarbonate sample to the acetone vapor. The average size of the spherules, appearing in the figure, is nearly 8 μm in width. The lines appearing as tails to the spherules are present due to AFM-tip slipping on sharp edges during the scanning process. In figure 5.21-B and at a scale of about 20 μm, the spherules appear more obviously and it can be noticed that there are some spherules fused together in adjacent aggregates. By zooming and reducing the scanning scale, the surface of the spherule appears with more details. Figure 5.21-C illustrates that there is a texture over the spherule's surface. The three-dimensional micrograph shows clearly the presence and size of that texture. One of the spherules appears to have a 1 μm width; another appears to have 2 μm width and two relatively bigger spherules of about 6 μm in width. By further reduction of the scanning

scale, the surface of the spherule becomes more obvious and the texture on top of it can be easily detected. It can be noticed that the surface of the spherule is rough, in other words, the spherule's surface becomes hilly; this hilly surface is a grass-like one, and this can be inferred from the three-dimensional micrograph, figure 5.21-D. In figure 5.21-E, at a scanning scale of 1 μm, two fused-spherules and two separate spherules appear; between them a relatively large gap is present, while between the two separate spherules, there is a relatively small gap. The larger gap width is about 100 nm and the smaller gap width is about 50 nm. For the figure 5.21-F, scanning scale of 500 nm, the noise-like surface of the spherule appears clearly.

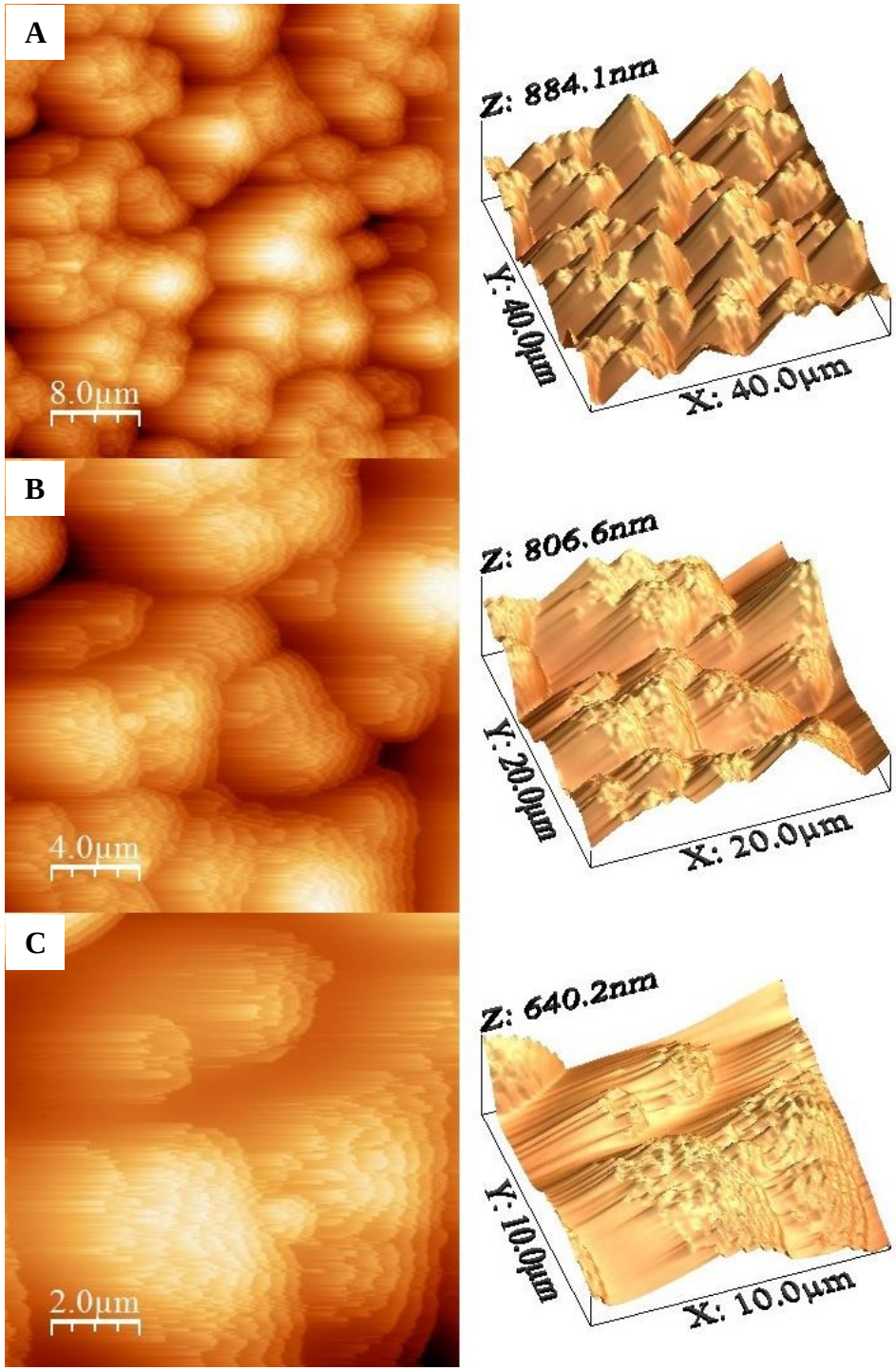
A
8.0µm
Z: 884.1nm
Y: 40.0µm
X: 40.0µm
B
4.0µm
Z: 806.6nm
Y: 20.0µm
X: 20.0µm
C
2.0µm
Z: 640.2nm
Y: 10.0µm
X: 10.0µm

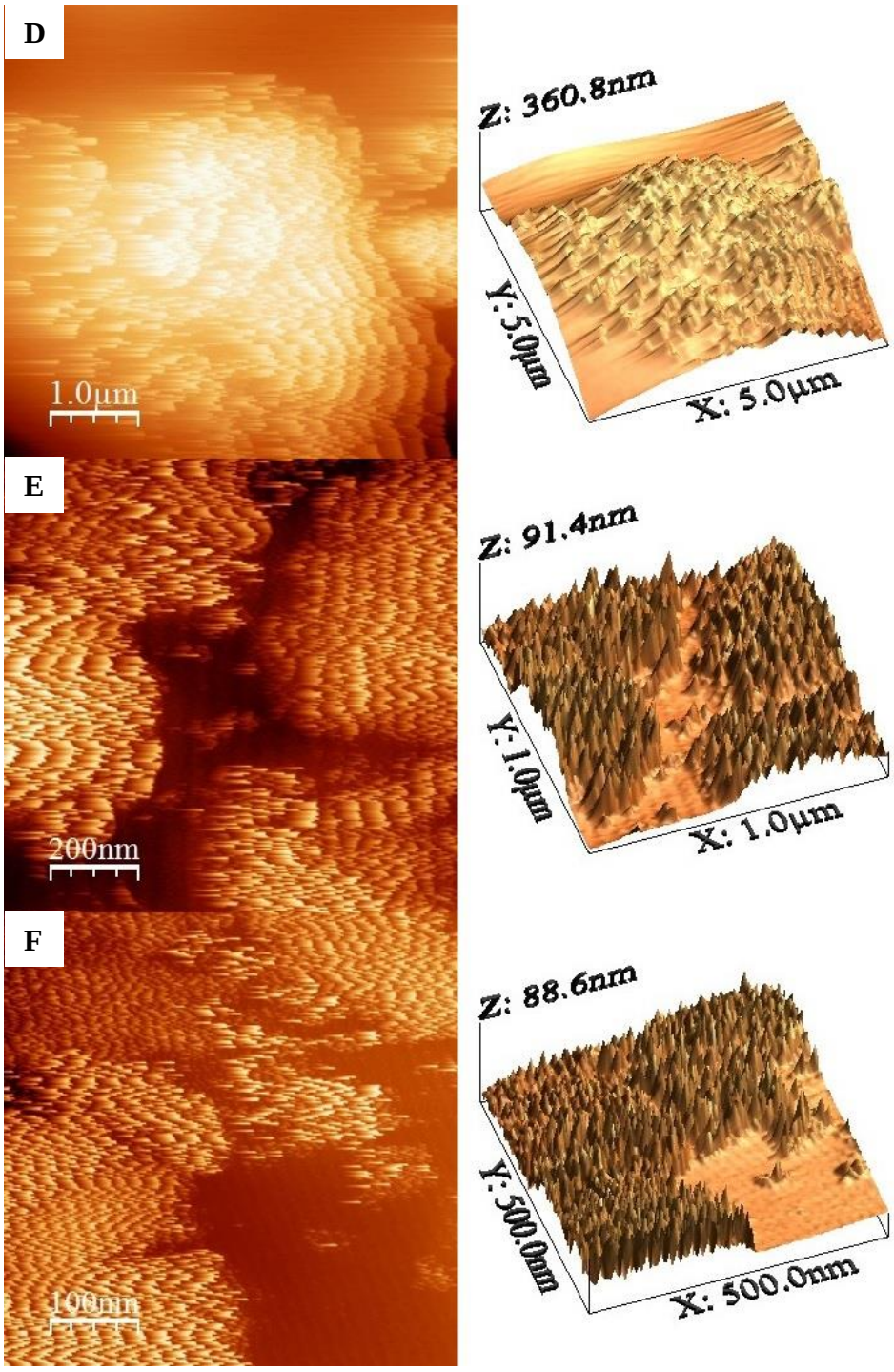

Figure5.21: 2D and 3D AFM micrographs at: A: 40 µm scale. B: 20 µm scale. C: 10 µm scale. D: 5 µm scale. E: 1 µm scale. F: 500 nm scale, for a textured polycarbonate surface by exposure to pure acetone vapor for 24 hours.

5.3.1.2. Texture profile micrographs:

This study involves investigating the structure of the textured surface in order to follow up the effect of acetone vapor on the polycarbonate surface. It can be noticed that at the various scales, from 40 μm to 500 nm, the surface texture does not exceed 450 nm in height. This indicates the degree of roughness of the patterned polycarbonate surface. In figure 5.22-A, the height of the spherules can be easily measured, it's about 375 nm. The width of the left spherule is about 13.5 μm. Figure 5.22-B illustrates a single and small spherule of 425 nm in height and nearly 12 μm in width. The texture over the spherule is evident in the figure. For further examination to the surface of the spherule, scanning scale is reduced and so the texture over the spherule's surface appears in more details, in figure 5.22-C. In figure 5.22-D, a distinctive profile micrograph of a single spherule's surface appears. The spherule contains grass-like shapes over its surface; this grass resembles the surface texture. In figure 5.22-E, the texture (noise-like) appears clearly and it looks like adjacent spikes. The width of the single spike is about 80 nm and its height is 37 nm. For further investigation the texture, the scanning scale is reduced down to 500 nm, figure 5.22-F. In this figure, the sharp texture (grass-like) is obvious; it's homogenous in height to some extent.

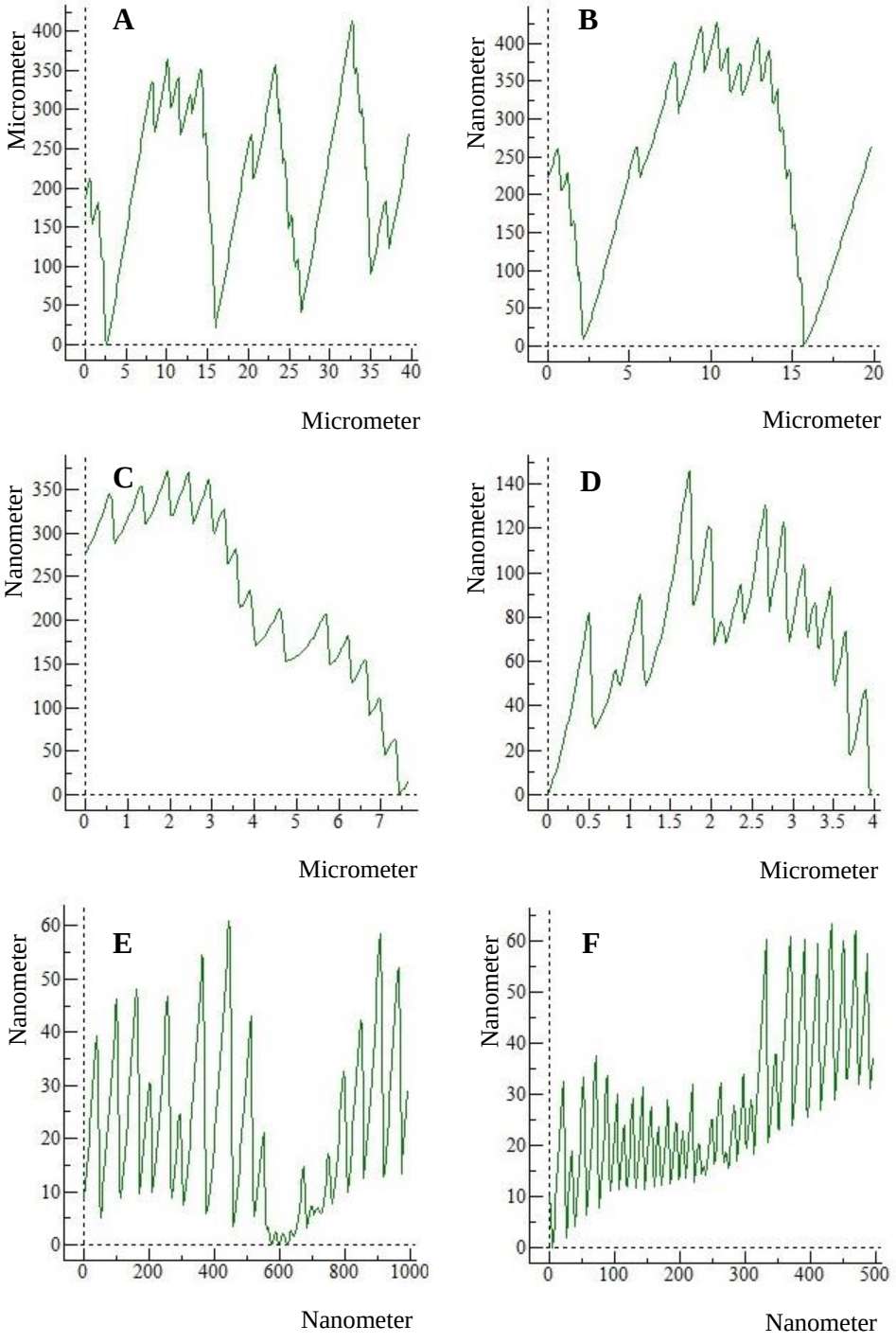

Figure5.22: AFM texture profile micrographs at: A: 40 µm scale. B: 20 µm scale. C: 10 µm scale. D: 5 µm scale. E: 1 µm scale. F: 500 nm scale, for a textured polycarbonate surface by exposure to pure acetone vapor for 24 hours.

5.3.2. Transmittance:

The Transmittance examination is performed to all the textured polycarbonate surfaces by acetone vapor at 18^{o}C and 33^{o}C. The resulted data are discussed separately according to the performed method.

5.3.2.1. Transmittance of the textured polycarbonate after exposure to acetone vapor at 18^{o}C, without heating:

Textured, rough polycarbonate sheets, due to exposure to acetone vapor, were scanned in UV-Vis spectrophotometer model between 400 nm to 800 nm to measure the transmittance. We are interested in the visible region. The transmittance values of the different samples under investigation are examined by placing each sample vertically perpendicular to the light path from the light source to the detector inside the chamber of the UV-Vis spectrophotometer. The instrument is set to give readings every 4 nm, with medium scan speed and scanning rate of 100 nm/ min. The untreated polycarbonate sample is used as a reference.

In figure 5.23-A, the sample, denoted s1, is exposed to pure acetone vapor for five min. The average transmittance in the visible region is 87.63%. In figure 5.23-B, the sample s2 is exposed to pure acetone vapor for 15 min. The average transmittance of this sample is 86.79%. In figure 5.23-C, the sample s4 is exposed to pure acetone vapor for twenty min. The average transmittance of this sample is 88.43%. The sample s5, figure

5.23-D, is exposed to pure acetone vapor for 25 min. The average transmittance of this sample is 80.44%. The sample s3, figure 5.23-E, is exposed to pure acetone vapor for 30 min. The average transmittance of this sample is 69.42%.

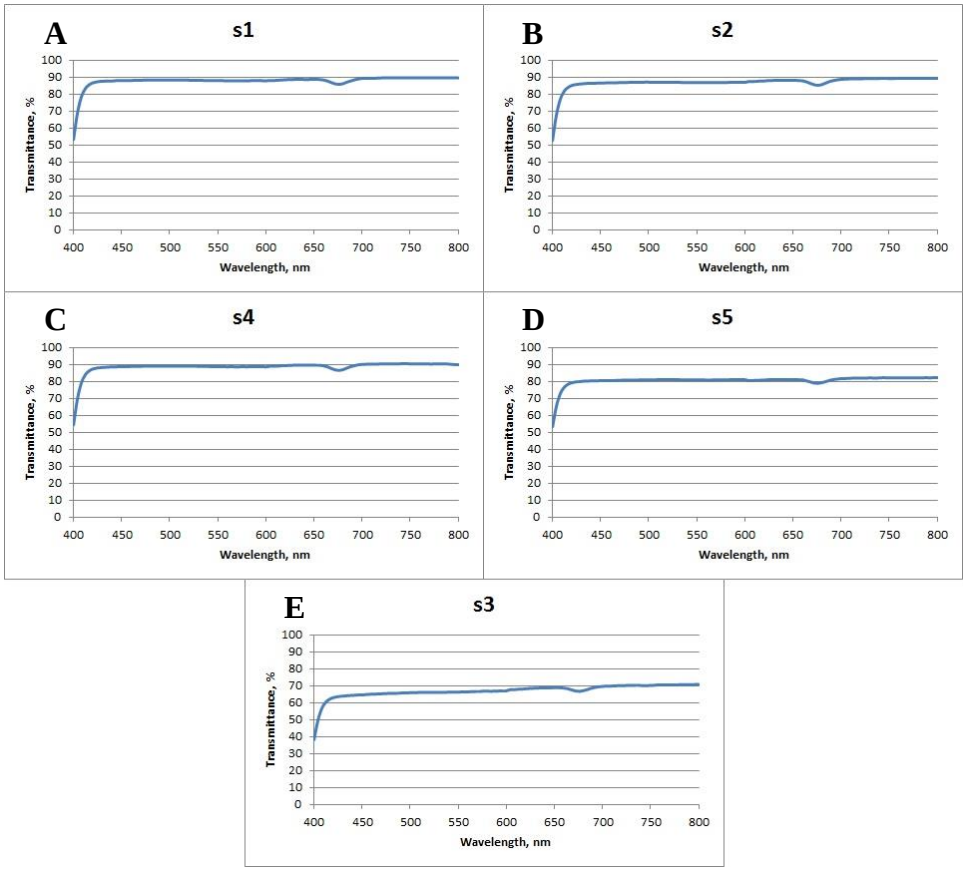

Figure5.23: Visible spectrum of a textured polycarbonate sample by exposure to pure acetone vapor for: A: 5 minutes. B: 15 minutes. C: 20 minutes. D: 25 minutes. E: 30 minutes.

Figure 5.24 includes all the transmittance curves for the 5 samples. The descending arrangement of the samples according to exposure duration to the acetone vapor is s3 > s5 > s4 > s2 > s1. The descending arrangement of the transmittance values for the samples are s1 > s2 > s4 > s5 > s3. It can be inferred that the transmittance value is inversely proportional to the exposure duration to acetone vapor. So that, by increasing the exposure duration to the acetone vapor, at constant acetone concentration, the transmittance of the patterned surface decreases. Figure 5.25 illustrates the relation between the exposure duration to acetone vapor and the average transmittance of each sample.

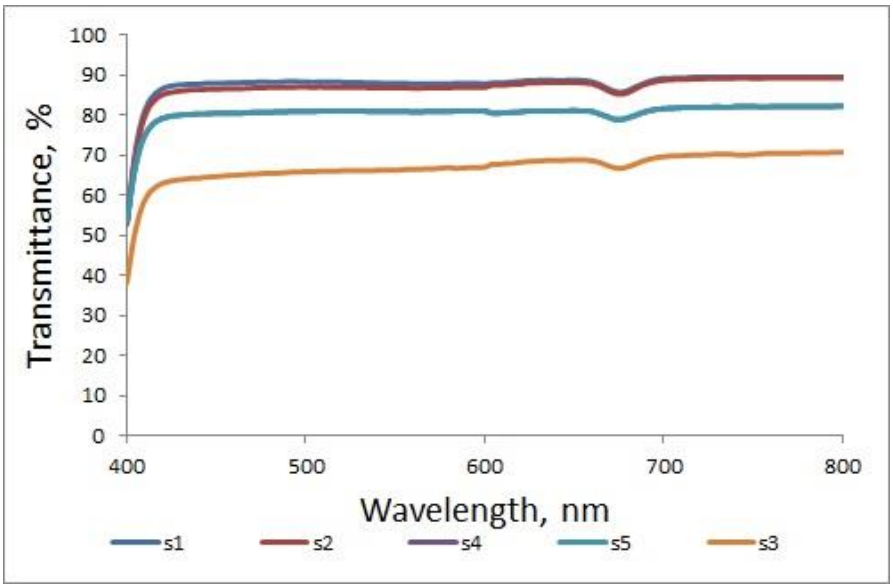

Figure5.24: Visible spectra of all the textured polycarbonate by exposure to pure acetone vapor for different durations.

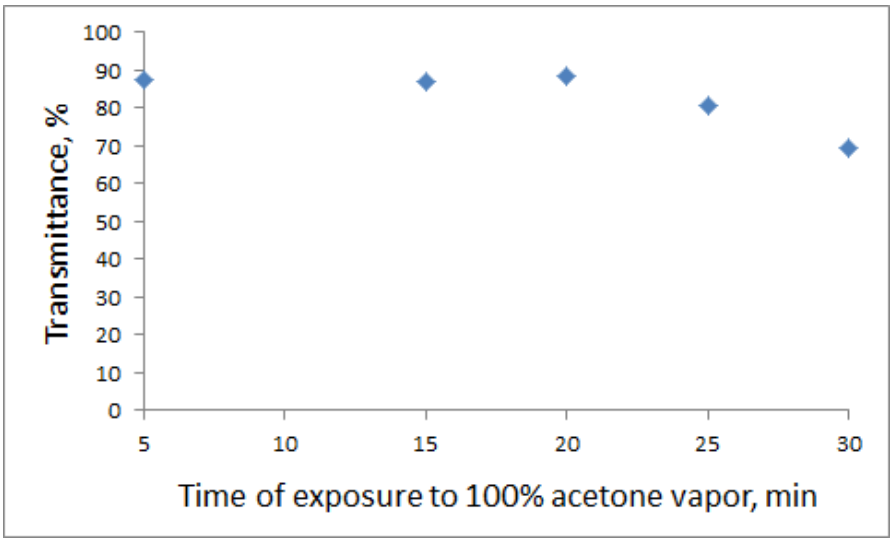

Figure5.25: Transmittance values of different polycarbonate samples.

5.3.2.2. Transmittance of the textured polycarbonate after exposure to acetone vapor at 33^{o}C:

In figure 5.26-A, the sample, denoted c4, is exposed to pure acetone vapor for one min at 18^{o}C. The average transmittance in the visible region is 87.34%. In figure 5.26-B, the sample c5 is exposed to pure acetone vapor with heating for two min. The average transmittance of this sample is 73.55%. In figure 5.26-C, the sample c6 is exposed to pure acetone vapor with heating for three min. The average transmittance of this sample is 63.64%. The sample c7, figure 5.26-D, is exposed to pure acetone vapor with heating for four min. The average transmittance of this sample is 49.63%. The sample c8, figure 5.26-E, is exposed to pure acetone vapor with heating for six min. The average transmittance of this sample is 51.46%. The sample c9, figure 5.26-F, is exposed to pure acetone vapor with heating for seven min. The average transmittance of this sample is 43.80%. The sample c10, figure 5.26-G, is exposed to pure acetone vapor with heating for 8 min. The average transmittance of this sample is 48.10%. The sample c11, figure 5.26-H, is exposed to pure acetone vapor with heating for 9 min. The average transmittance of this sample is 45.70%.

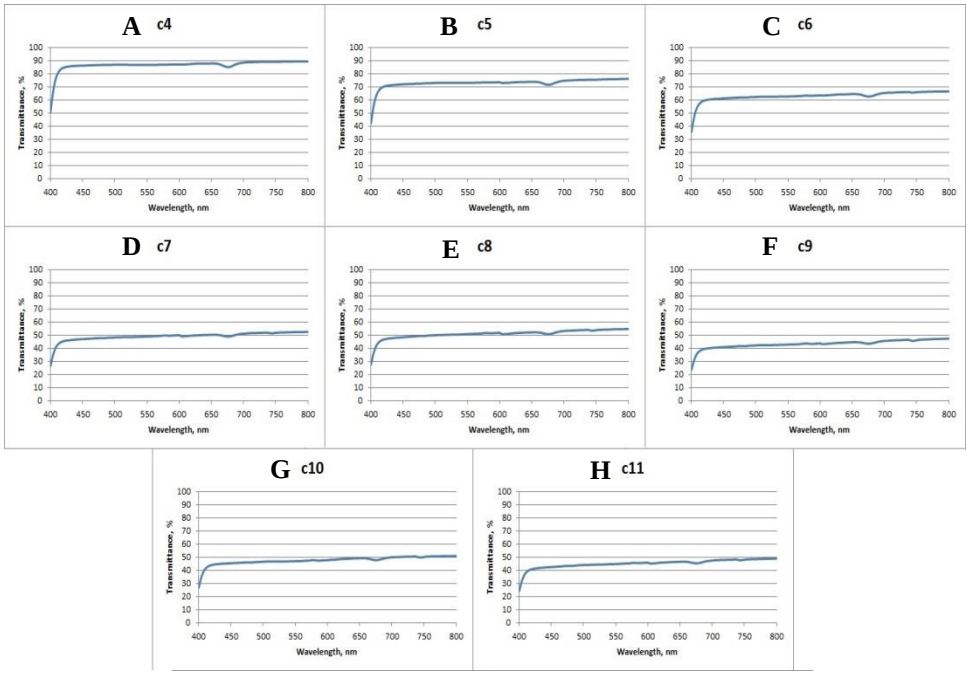

Figure5.26: Visible spectrum of a textured polycarbonate sample by exposure to pure acetone vapor for: A: 1 minute. B: 2 minutes. C: 3 minutes. D: 4 minutes. E: 6 minutes. F: 7 minutes. G: 8 minutes. H: 9 minutes.

Figure 5.27 includes all the transmittance curves for the 8 samples. The descending transmittance values of the samples according to exposure duration to the acetone vapor are arranged as the following: c11 > c10 > c9 > c8 > c7 > c6 > c5 > c4. The descending arrangement of the transmittance values for the samples are c4 > c5 > c6 > c8 > c7 > c10 > c11 > c9. It can be inferred that the transmittance value is inversely proportional to the exposure duration to acetone vapor and the decrease in the transmittance is exponential. So that, by increasing the exposure duration to the acetone vapor, at constant acetone concentration, the transmittance of the patterned surface decreases exponentially. There are some waviness or fluctuations present in the curve, however, the values change within this range still in a narrow area with a standard deviation of 3.05 not clear. Figure 5.28 illustrates the relation between the exposure duration to acetone vapor versus the average transmittance of each sample.

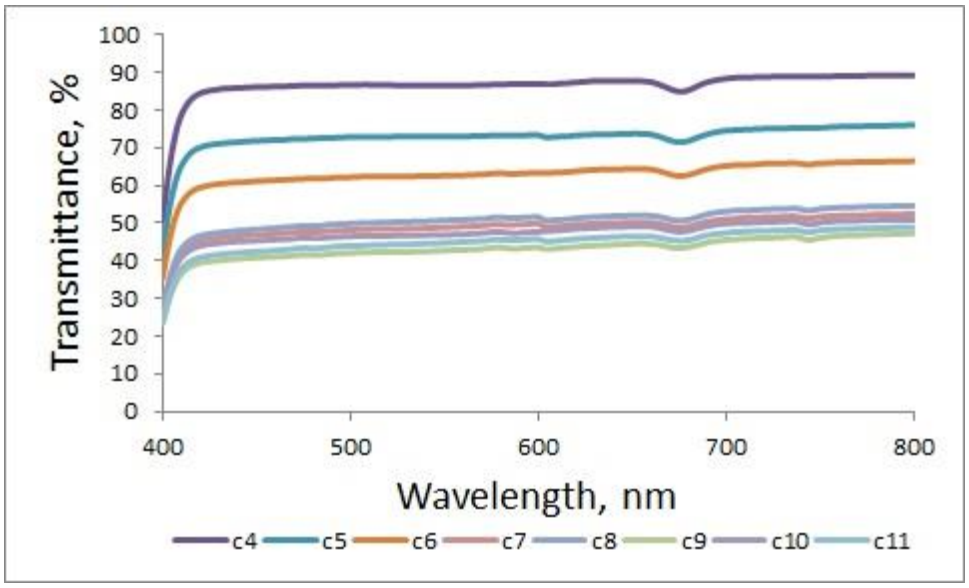

Figure5.27: Visible spectra of all the textured polycarbonate by exposure to pure acetone vapor for different durations.

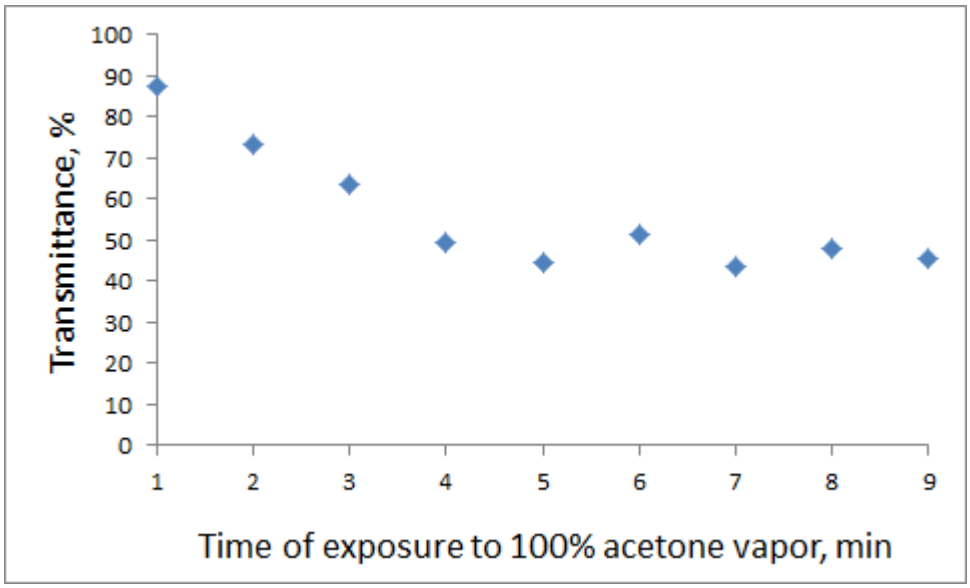

Figure5.28: The effect of the exposure duration of polycarbonate to acetone vapor on the average transmittance value.

5.3.2.3. Transmittance of the textured polycarbonate after exposure to acetone vapor through at 33°C, holed vapor-outlet:

In figure 5.29-A, the sample, denoted cr2, is exposed to pure acetone vapor change for 2 min. The average transmittance in the visible region is 88.86%. In figure 5.29-B, the sample cr4 is exposed to pure acetone vapor with heating for 4 min. The average transmittance of this sample is 84.45%. In figure 5.29-C, the sample cr6 is exposed to pure acetone vapor with heating for 6 min. The average transmittance of this sample is 77.52%. The sample cr8, figure 5.29-D, is exposed to pure acetone vapor with heating for 8 min. The average transmittance of this sample is 75.04%. The sample cr10, figure 5.29-E, is exposed to pure acetone vapor with heating for 10 min. The average transmittance of this sample is 56.92%.

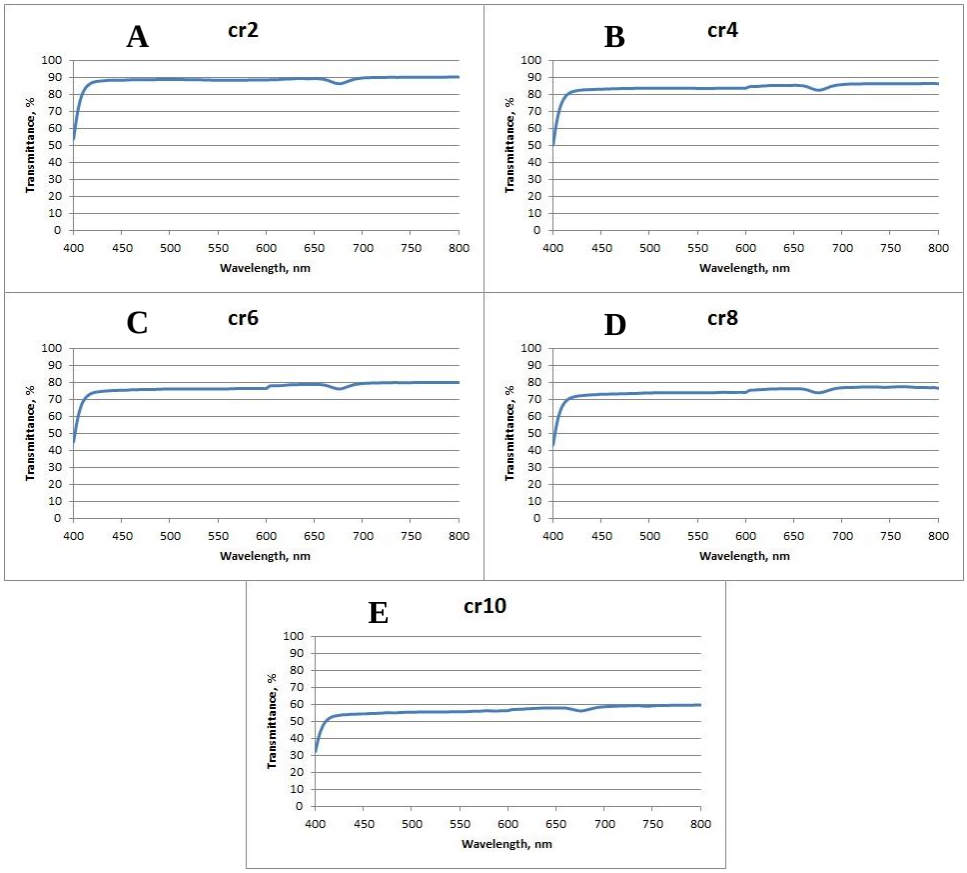

Figure5.29: Visible spectrum of a textured polycarbonate sample by exposure to pure acetone vapor for: A: 2 minutes. B: 4 minutes. C: 6 minutes. D: 8 minutes. E: 10 minutes.

Figure 5.30 includes all the transmittance curves for the 5 samples. The descending arrangement of the samples according to exposure duration to the acetone vapor is cr2 > cr4 > cr6 > cr8 > cr10. The descending arrangement of the transmittance values for the samples are cr10 > cr8 > cr6 > cr4 > cr2. It can be inferred that the transmittance value is inversely proportional to the exposure duration to acetone vapor. So that, by increasing the exposure duration to the acetone vapor, at constant acetone concentration, the transmittance of the patterned surface decreases. Figure 5.31 illustrates the relation between exposure duration to acetone vapor and the average transmittance of each sample.

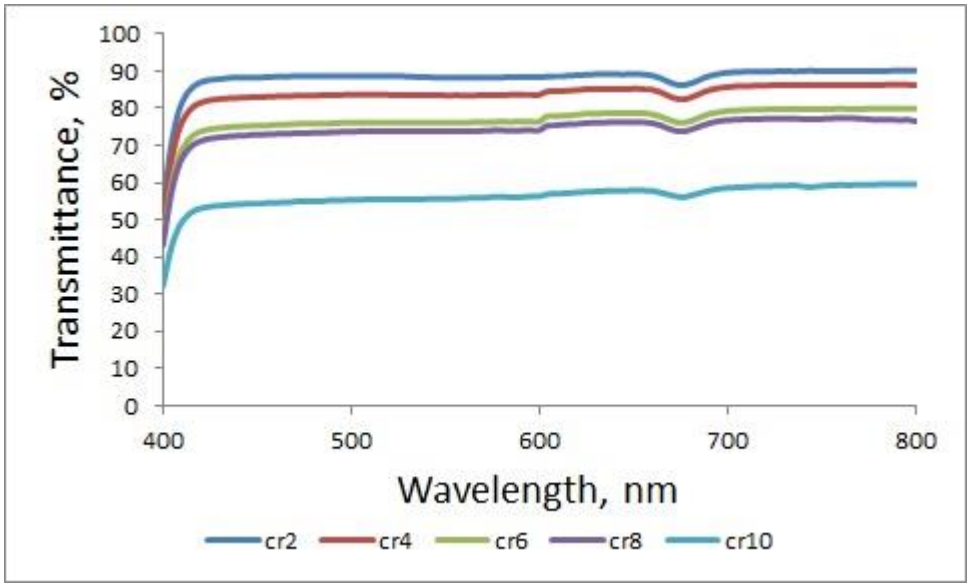

Figure5.30: Visible spectra of all the textured polycarbonate by exposure to pure acetone vapor for different durations.

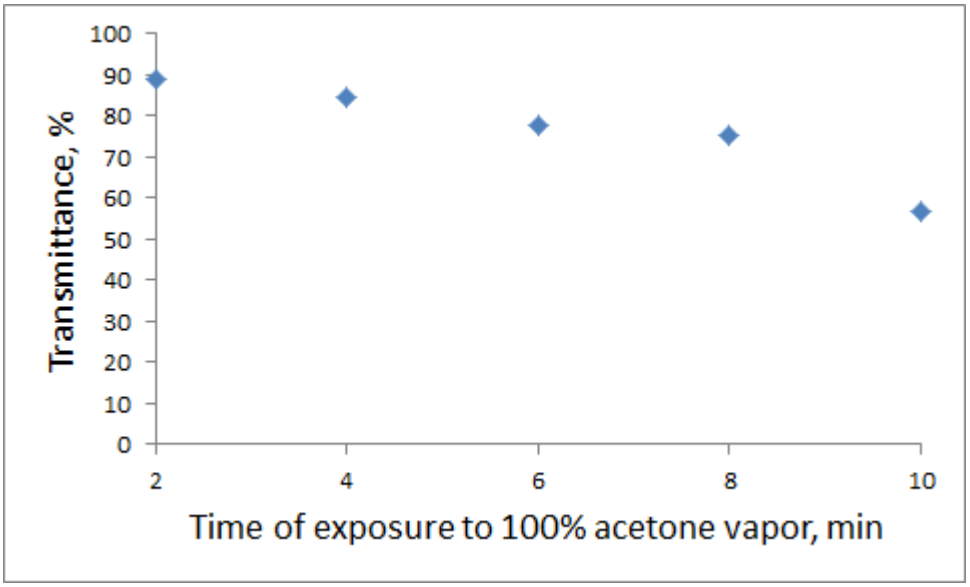

Figure5.31: The effect of the exposure duration of polycarbonate to acetone vapor on the average transmittance value.

5.3.3. Contact angle measurements:

The contact angle of the patterned polycarbonate surface is detected by dropping a deionized water droplet over the textured surface and measured by using the goniometer's camera. Different areas of the surface are taken in to consideration during the measurements.

5.3.3.1. Contact angle measurements of the textured polycarbonate by the exposure to acetone vapor at 18^{o}C:

For polycarbonate sheet exposed to pure acetone vapor for 25 minutes, denoted as s5, the contact angles of two different areas over the surface are 81.9 and 82.1^{o}, figures 5.32-A and B, respectively. The average contact angle for this sample is 82^{o}. For the s3 sample, exposed to acetone vapor for 30 minutes, the contact angles of three different areas over the surface are 95.5, 85.3 and 86.9^{o}, figures 5.32-C, D and E, respectively. The average contact angle for this sample is 89.23^{o}. Figure 5.31 illustrates the values of the contact angles of the textured polycarbonate samples after the exposure to acetone vapor, the photos are taken by the goniometer's camera. From the mentioned data, it can be noticed that by increasing the exposure duration of the polycarbonate surface to the acetone vapor, the contact angle increases.

Table5.3: It illustrates the sample name, exposure duration to acetone vapor, CA of each area over the same sample's surface and the average CA value for each sample.

Sample	Exposure time, min	C.A.(deg)	Average CA
s5 (area1)	25	81.9	82
s5 (area2)		82.1	
s3 (area1)	30	95.5	89.23333333
s3 (area2)		85.3	
s3 (area3)		86.9	

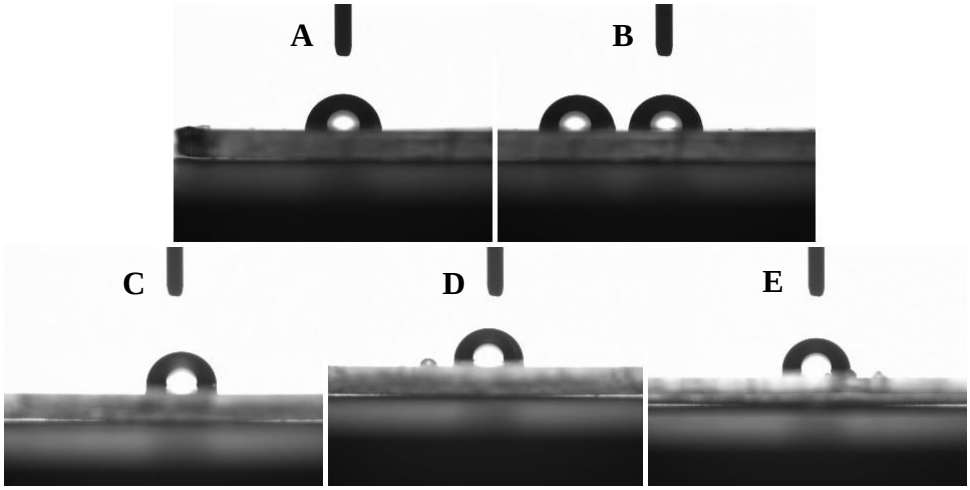

Figure5.32: CA of a textured polycarbonate sample by exposure to pure acetone vapor for: A & B: 25 minutes. C, D & E: 30 minutes.

5.3.3.2. For the textured polycarbonate by the exposure to acetone vapor at 33°C:

For polycarbonate sheet exposed to pure acetone vapor for 1 minute with heating, denoted as c4, the contact angles of two different areas over the surface are 81.2 and 77.9°, figures 5.33-A and B, respectively. The average contact angle for this sample is 79.55°. For the c5 sample, exposed to acetone vapor for 2 minutes with heating, the contact angles of two different areas over the surface are 79.2 and 79.9°, figures 5.33-C and D, respectively. The average contact angle for this sample is 79.55°. For the c6 sample, exposed to acetone vapor for 3 minutes with heating, the contact angles of two different areas over the surface are 83.2 and 71°, figures 5.33-E and F, respectively. The average contact angle for this sample is 77.1°. For the c7 sample, exposed to acetone vapor for 4 minutes with heating, the contact angles of three different areas over the surface are 74.8, 71.9 and 76.4°, figures 5.33-G, H and I, respectively. The average contact angle for this sample is 74.37°. For the c8 sample, exposed to acetone vapor for 6 minutes with heating, the contact angles of three different areas over the surface are 75.3, 73.4 and 74.6°, figures 5.33-J, K and L, respectively. The average contact angle for this sample is 74.43°. For the c9 sample, exposed to acetone vapor for 7 minutes with heating, the contact angles of three different areas over the surface are 73.6, 74.1 and 75.1°, figures 5.33-M, N and O, respectively. The average contact angle for this sample is 72.27°. For the c10 sample, exposed to acetone vapor for 8 minutes with heating, the

contact angles of three different areas over the surface are 72, 73.4 and 71.2^{o}, figures 5.33-P, Q and R, respectively. The average contact angle for this sample is 72.2^{o}. For the c11 sample, exposed to acetone vapor for 9 minutes with heating, the contact angles of three different areas over the surface are 71.3, 73.5 and 73.1^{o}, figures 5.33-S, T and U, respectively. The average contact angle for this sample is 72.63^{o}. Figure 5.33 illustrates the photos of the contact angles of the textured polycarbonate samples after the exposure to acetone vapor, these photos are taken by the goniometer's camera. From the mentioned data, it can be deduced that by increasing the exposure duration of the polycarbonate surface to the acetone vapor, the contact angle decreases.

Table5.4: It illustrates the sample name, exposure duration to acetone vapor, CA of each area over the same sample's surface and the average CA value for each sample.

Sample	Exposure time, min	C.A.(deg)	Average CA
c4 (area1)	1	81.2	79.55
c4 (area2)		77.9	
c5 (area1)	2	79.2	79.55
c5 (area2)		79.9	
c6 (area1)	3	83.2	77.1
c6 (area2)		71	
c7 (area1)	4	74.8	74.36666667
c7 (area2)		71.9	
c7 (area3)		76.4	
c8 (area1)	6	75.3	74.43333333
c8 (area2)		73.4	
c8 (area3)		74.6	
c9 (area1)	7	73.6	74.26666667
c9 (area2)		74.1	
c9 (area3)		75.1	
c10 (area1)	8	72	72.2
c10 (area2)		73.4	
c10 (area3)		71.2	
c11 (area1)	9	71.3	72.63333333
c11 (area2)		73.5	
c11 (area3)		73.1	

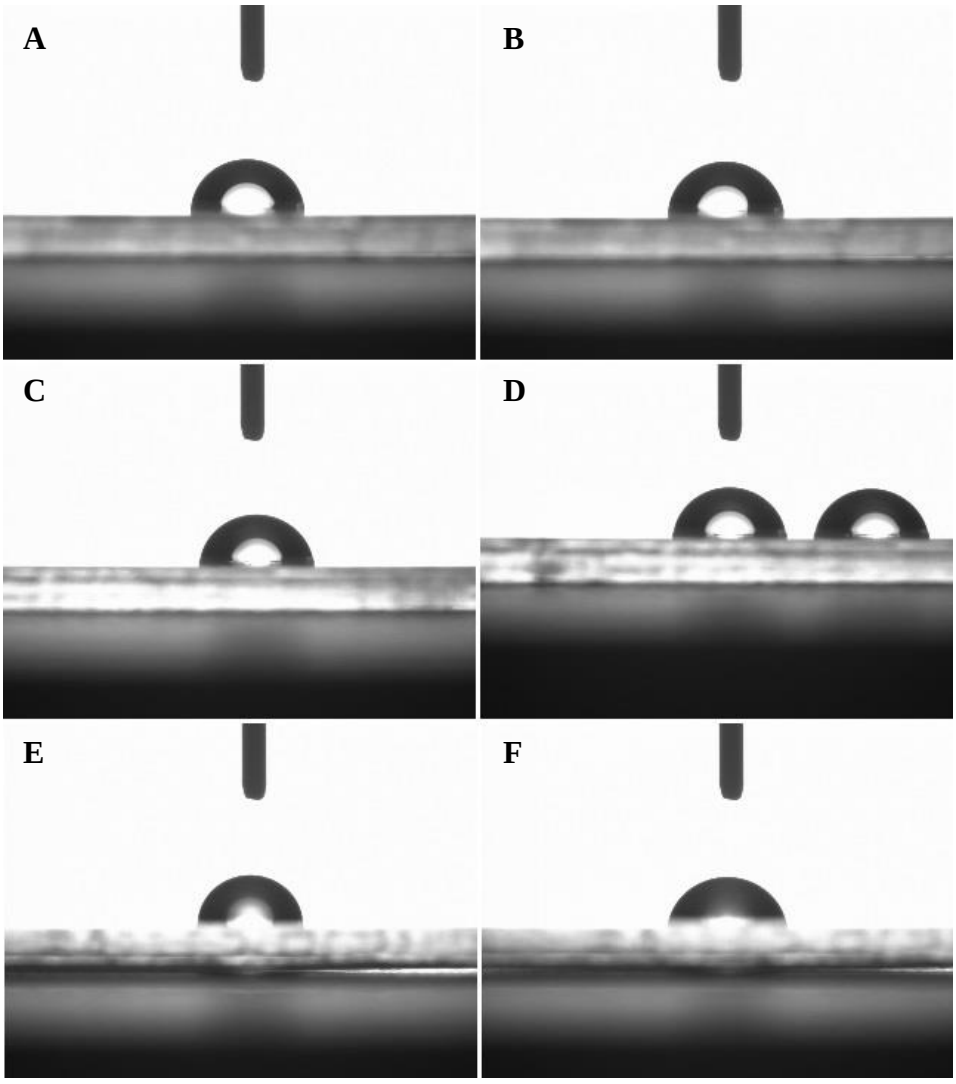
A
B
C
D
E
F

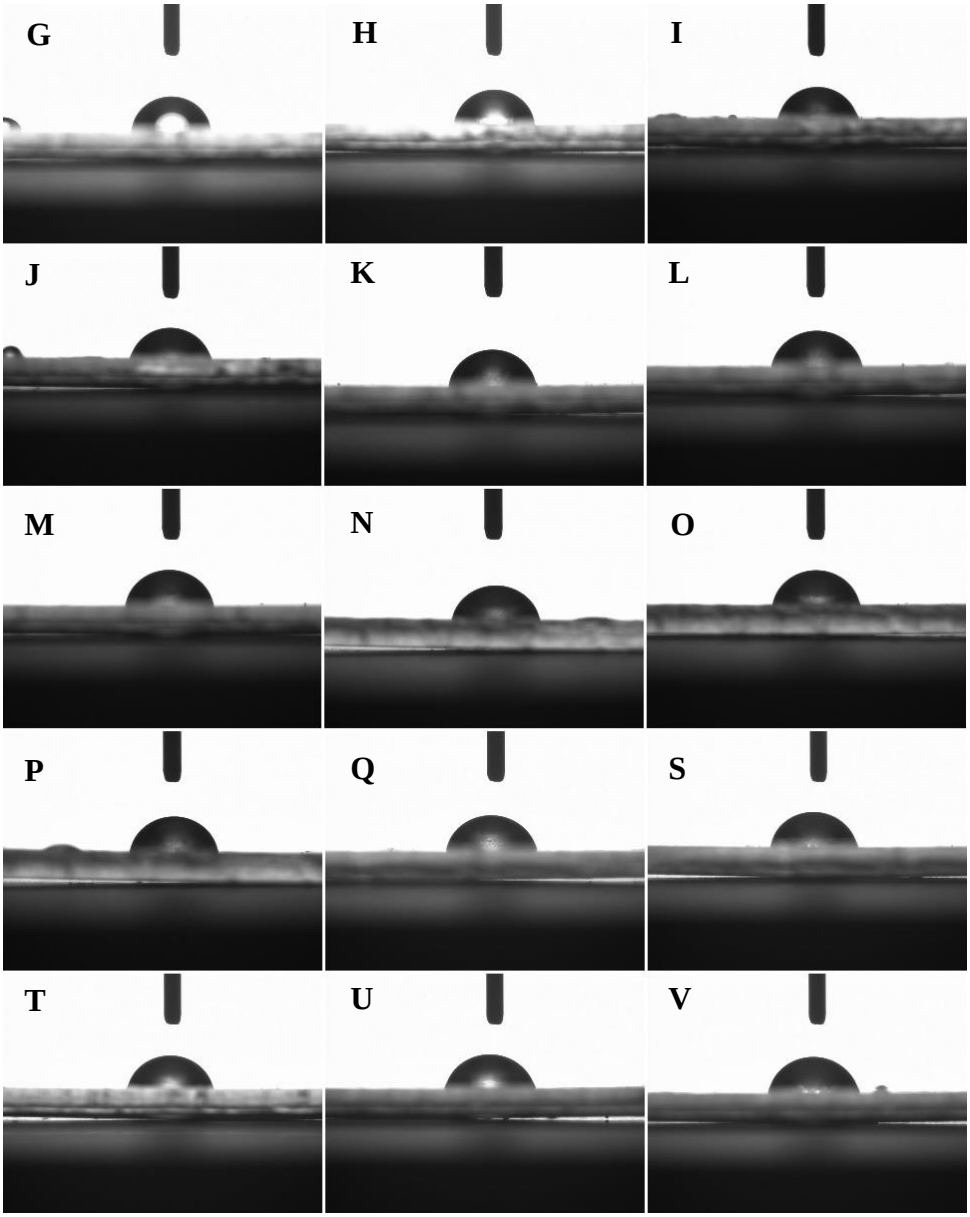

Figure5.33: CA of a textured polycarbonate sample by exposure to pure acetone vapor for: A & B: 1 minute. C & D: 2 minutes. E & F: 3 minutes. G, H & I: 4 minutes. J, K & L: 6 minutes. M, N & O: 7 minutes. P, Q & R: 8 minutes. S, T & U: 9 minutes.

From the above mentioned data, many observations can be deduced. Firstly, by increasing the exposure duration of the polycarbonate sample to the acetone vapor, the contact angle decreases. Secondly, the decrement in the contact angle value is resembled by a jump from the polycarbonate sheet, exposed to the pure acetone vapor for 2 minutes and has an average contact angle of 79.55^{o}, to that exposed to acetone vapor for 4 minutes and has an average contact angle of 74.43^{o} (the difference between the two values is about 5^{o}). Then, another relatively small jump happens between the sample which is exposed to the acetone vapor for 7 minutes and has an average contact angle of 74.27^{o} and that exposed to acetone vapor for 8 minutes and has an average contact angle of 72.2^{o} (the difference between the two values is about 2^{o}). Figure 5.34 illustrates the relationship between the exposure duration of polycarbonate surfaces to the acetone vapor and the resulted, apparent contact angle. Finally, for the samples c4 and c5, it can be noted that they have nearly the same contact angles values and so, they are represented by a horizontal line in the plot, figure 5.33. The same notice can be considered for the samples c7, c8 and c9 with the samples c10 and c11. Therefore, the curve appears to have three relaxation durations, the first is between minutes 1 and 2, the second is from the 4^{th} minute to the 7^{th} minute and the third one is within the 8^{th} and 9^{th} minutes.

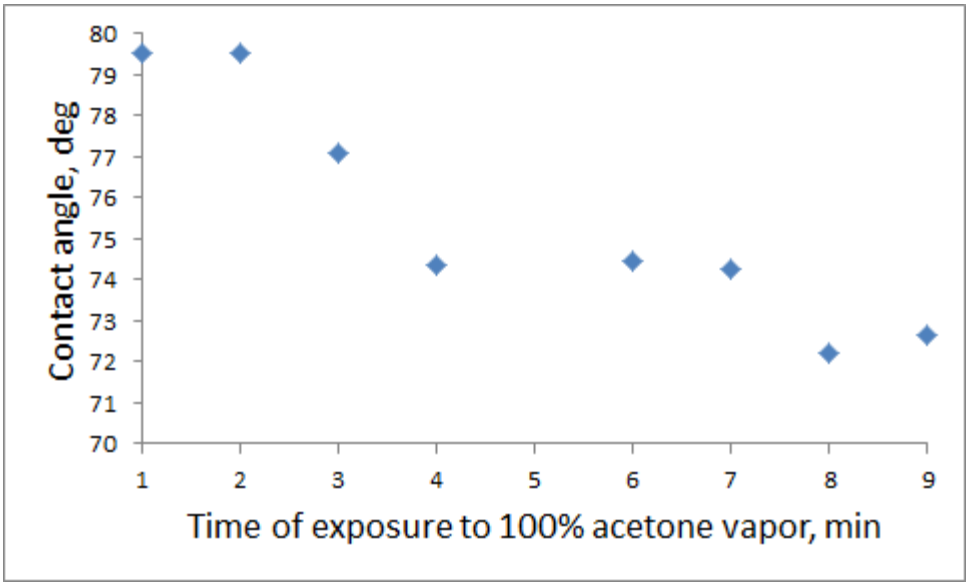

Figure5.34: The effect of the exposure duration of polycarbonate to acetone vapor on the CA.

5.3.3.3. For the textured polycarbonate by the exposure to acetone vapor at 33°C, holed vapor-outlet:

For polycarbonate sheet exposed to pure acetone vapor for 2 minutes with heating, denoted as cr2, the contact angles of two different areas over the surface are 78.5 and 78.2°, figures 5.35-A and B, respectively. The average contact angle for this sample is 78.35°. For the cr4 sample, exposed to acetone vapor for 4 minutes with heating, the contact angles of three different areas over the surface are 78.9, 79.7 and 75.9°, figures 5.35-C, D and E, respectively. The average contact angle for this sample is 78.17°. For the cr6 sample, exposed to acetone vapor for 6 minutes with heating, the contact angles of three different areas over the surface are 75.3, 77 and 74°, figures 5.35-F, G and H, respectively. The average contact angle for this sample is 75.43°. For the cr8 sample, exposed to acetone vapor for 8 minutes with heating, the contact angles of two different areas over the surface are 78.7 and 76.4°, figures 5.35-I and J, respectively. The average contact angle for this sample is 77.55°. For the cr10 sample, exposed to acetone vapor for 10 minutes with heating, the contact angles of three different areas over the surface are 74.1, 74 and 75°, figures 5.35-K, L and M, respectively. The average contact angle for this sample is 74.36°.

Table5.5: It illustrates the sample name, exposure duration to acetone vapor, CA of each area over the same sample's surface and the average CA value for each sample.

Sample	Exposure time, min	C.A.(deg)	Average CA
cr2 (area1)	2	78.5	78.35
cr2 (area3)		78.2	
cr4 (area1)	4	78.9	78.16666667
cr4 (area2)		79.7	
cr4 (area3)		75.9	
cr6 (area1)	6	75.3	75.43333333
cr6 (area2)		77	
cr6 (area3)		74	
cr8 (area1)	8	78.7	77.55
cr8 (area2)		76.4	
cr10 (area1)	10	74.1	74.36666667
cr10 (area2)		74	
cr10 (area3)		75	

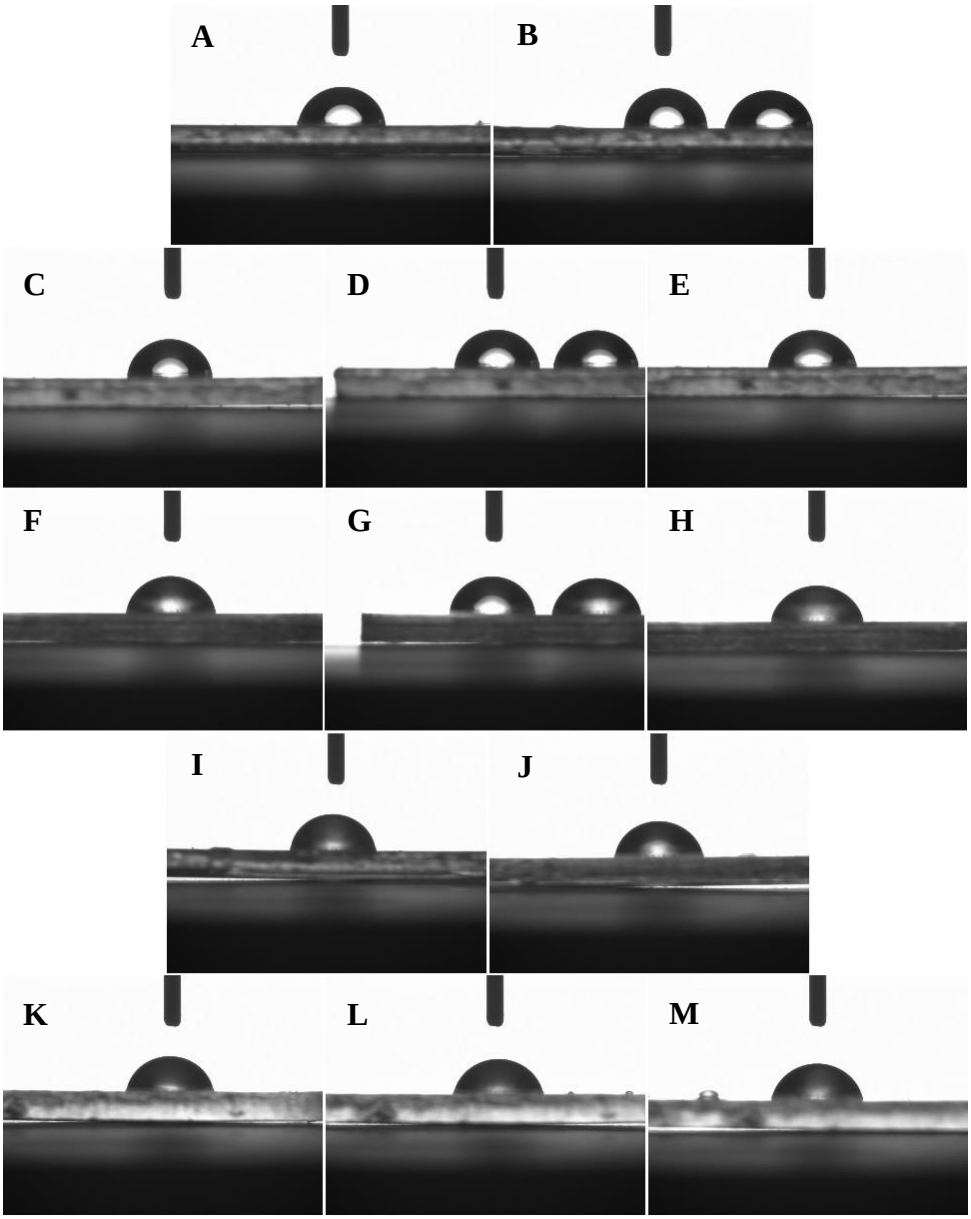

Figure5.35: CA of a textured polycarbonate sample by exposure to pure acetone vapor for: A & B: 2 minutes. C, D & E: 4 minutes. F, G & H: 6 minutes. I & J: 8 minutes. K, L & M: 10 minutes.

From the previous data, the following observations are concluded. Firstly, by increasing the exposure duration of the polycarbonate sample to the acetone vapor, the contact angle decreases. Secondly, the decrement in the contact angle value is not resembled by a straight line; instead, it's represented by a wavy line. The average contact angle value remains almost constant within the first 4 minutes, 78 35 to 78.17^{o}, then a decrease occurs down to 75.43^{o} on average at the minute 6, followed by a slight increase in the average contact angle by 2^{o} to become 77.55^{o} at the 8th minute, however it remains below the starting average contact angle value at the 2nd minute, and, finally, the average contact angle value decreases down to be 74.37^{o} at the 10th minute, figure 5.36.

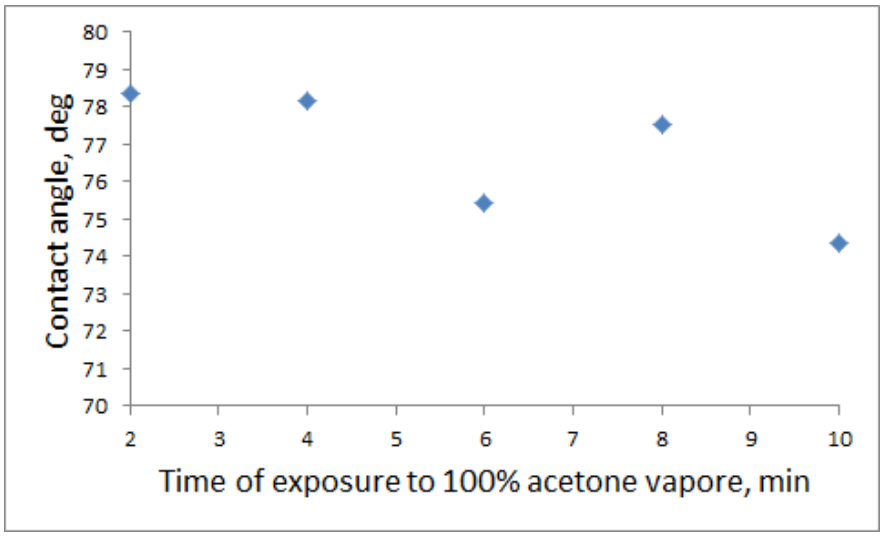

Figure5.36: The effect of the exposure duration of polycarbonate to acetone vapor on the CA.

5.3.4. Optical microscope images:

Optical microscope is used in order to examine the topology of the treated polycarbonate surface. The first phase can be characterized and the shape and growth of the formed spherules due to the crystallization process can be tracked. Furthermore, the gaps or the distances between the spherules, where the crystallization process are absent to some extent, can be clearly viewed. The scale bar, included within the most of the images is 100 μm.

5.3.4.1. For the textured polycarbonate by the exposure to acetone vapor at 18°C, without heating:

For the polycarbonate sheets, exposed to pure acetone vapor, figure 5.37-A, in the sample s2, the formation of spherules has started. The spherules average width is about or slightly less than 1 μm. In the sample s4, the spherule's size remained almost constant and its width remained 1 μm on average, figure 5.37-B. In the sample s5, figure 5.37-C, the spherules start to increase in size and form aggregations. For the sample s3, the spherules continue their growth and aggregations formation. Not only that, but also it can be noticed that there is a fusion occurring between the adjacent grown spherules, figure 5.37-D. The width of the single spherule is about 5 μm. The image further illustrates the arrangement of some spherules in straight lines.

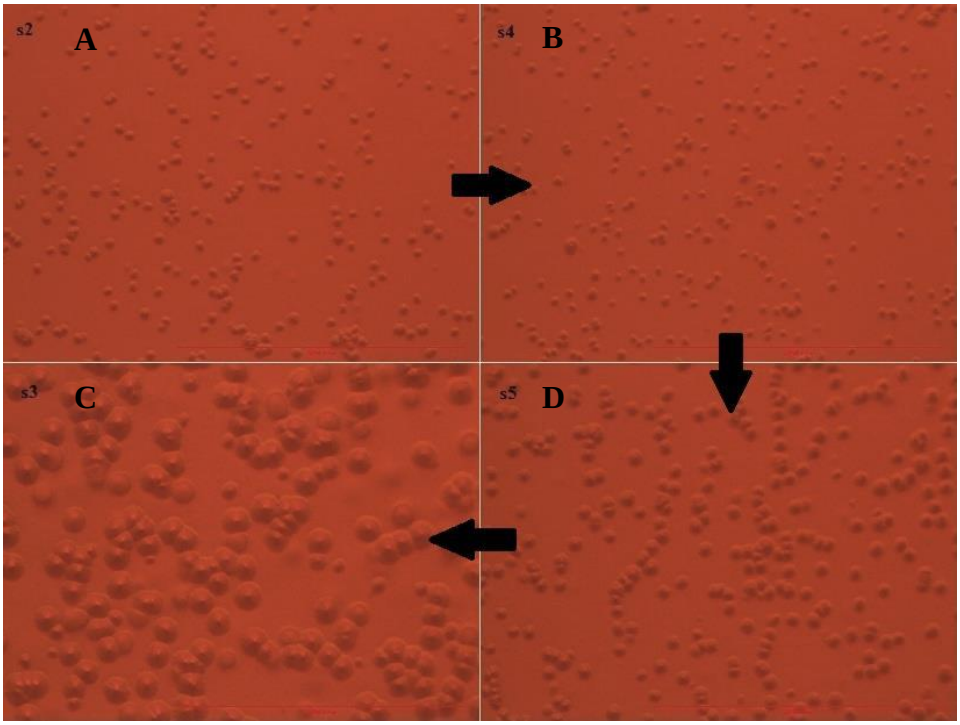

Figure5.37: Optical microscope image of a textured polycarbonate sample by exposure to pure acetone vapor for: A: 15 minutes. B: 20 minutes. C: 25 minutes. D: 30 minutes.

5.3.4.2. For the textured polycarbonate by the exposure to acetone vapor at $33^{o}C$:

For the polycarbonate sheets, exposed to pure acetone vapor, figure 5.38-A, in the sample c4, the formation of spherules has started. The spherules average width is less than 1 μm. In the sample c5, the spherule's size slightly increases to be about 1 μm on average, figure 5.38-B. The gaps between the spherules are too wide. In the sample c6, figure 5.38-C, the spherules' sizes increased tremendously and aggregations of spherules starts to form. Lines of fused spherules can be noticed among this image. Not only the lines, but also shiny tips can be noticed over the growing spherules. For the samples c7 and c8, the spherules continue their growth and aggregations formation and the gaps between the spherules aggregations decreases, figures 5.38-D and E, respectively. In figure 5.38-F, sample c9, the spherules occupy most of the areas and fused spherules increased in number. Not only the single spherules fuse, however, the aggregations themselves fuse and the gaps between them decrease dramatically. New spherules, which start to appear, can be noticed within the gaps. In the samples c10 and c11, the gaps completely disappear and they are replaced by non-mature spherules instead. The spherules that grow from the early beginning of the exposure to the acetone vapor can be termed as mature spherules, figures 5.38-G and H, respectively.

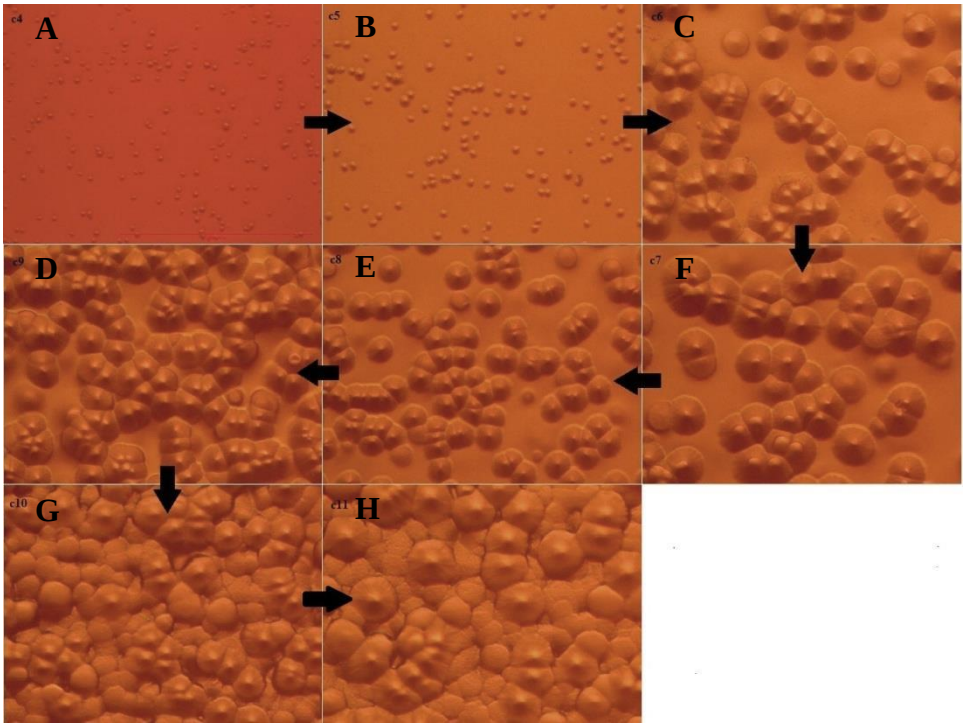

Figure5.38: Optical microscope image of a textured polycarbonate sample by exposure to pure acetone vapor for: A: 1 minute. B: 2 minutes. C: 3 minutes. D: 4 minutes. E: 6 minutes. F: 7 minutes. D: 8 minutes. D: 9 minutes.

5.3.4.3. For the textured polycarbonate by the exposure to acetone vapor at 33°C, holed vapor-outlet:

For the polycarbonate sheets, exposed to pure acetone vapor, figure 5.39-A, in the sample cr4, the formation of spherules has started. The spherules average width is about 5 μm. In the sample cr6, the spherule's size increases dramatically, aggregations of spherules form, spherules fuse and gaps decrease, figure 5.39-B. In the sample cr8, figure 5.39-C, the spherules continue fusing and aggregating. New spherules start to appear within the gaps. For the sample cr10, the gaps completely disappear and they are replaced by non-mature spherules instead. Groves appear surrounding the mature spherules, figure 5.39-D.

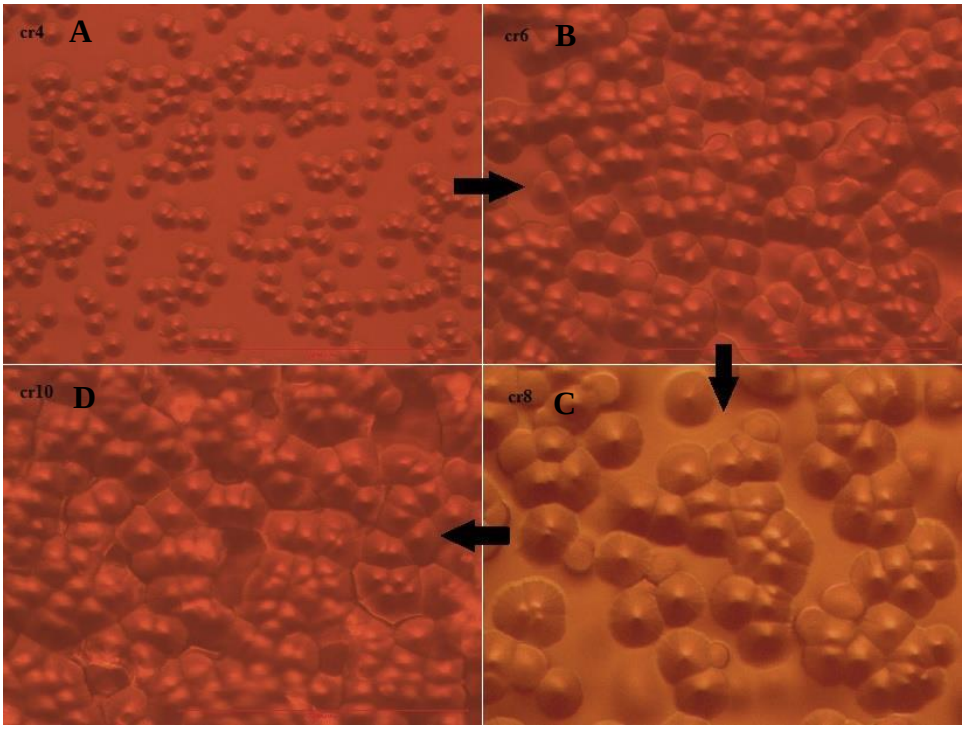

Figure5.39: Optical microscope image of a textured polycarbonate sample by exposure to pure acetone vapor for: A: 4 minute. B: 6 minutes. C: 8 minutes. D: 10 minutes.

5.3.5. FT-IR spectra:

Fourier-transform Infrared technique is used to verify the presence of chemical groups, functional, side and terminal groups, within a certain chemical compound through the detection of the different stretching and bending modes of the bonds, present in these groups. A special tool is used to detect the chemical groups, present on the surface of the textured polycarbonate glass after the exposure to the acetone vapor process.

5.3.5.1. For the textured polycarbonate by the exposure to acetone vapor at 18°C, without heating:

In figure 5.40, FT-IR spectrum is illustrated. The study focuses on the wavelength at which the peak of carbonyl, C=O, stretching mode appears. Before the exposure to acetone, the peak of carbonyl stretching mode appears at 1762 cm^{-1}, with absorbance value of 0.24. The peak of the phenyl stretching mode appears at 1499 cm^{-1}, with absorbance value of 0.18.

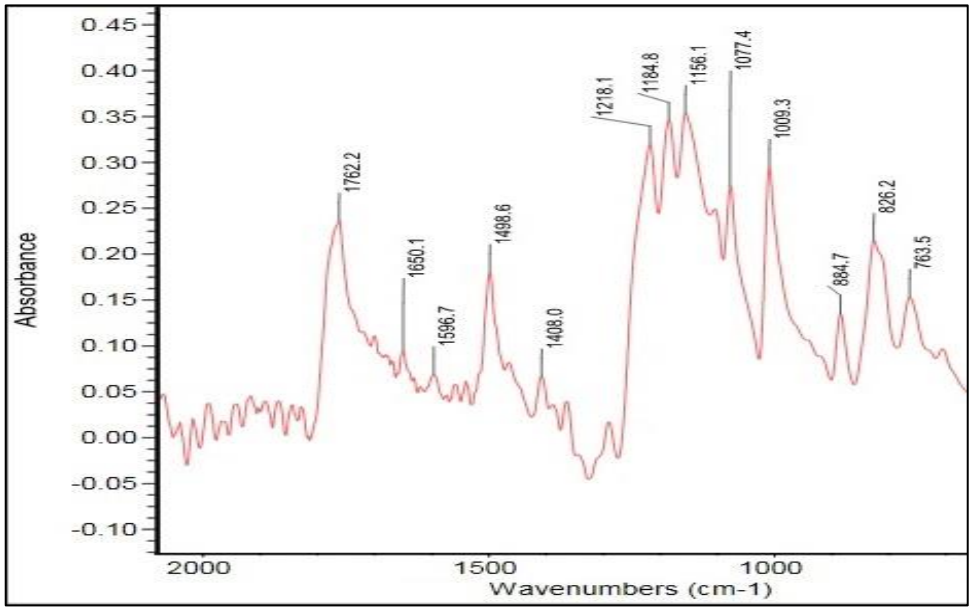

Figure5.40: FT-IR spectrum of a textured polycarbonate surface by exposure to pure acetone vapor for 25 minutes.

5.3.5.2. For the textured polycarbonate by the exposure to acetone vapor at 33^{o}C:

In figure 5.41, FT-IR spectrum is illustrated. The study focuses on the wavelength at which the peak of carbonyl, C=O, stretching mode appears. Before the exposure to acetone, the peak of carbonyl stretching mode appears at 1762 cm^{-1}, with absorbance value of 0.22. The peak of the phenyl stretching mode appears at 1499 cm^{-1}, with absorbance value of 0.17.

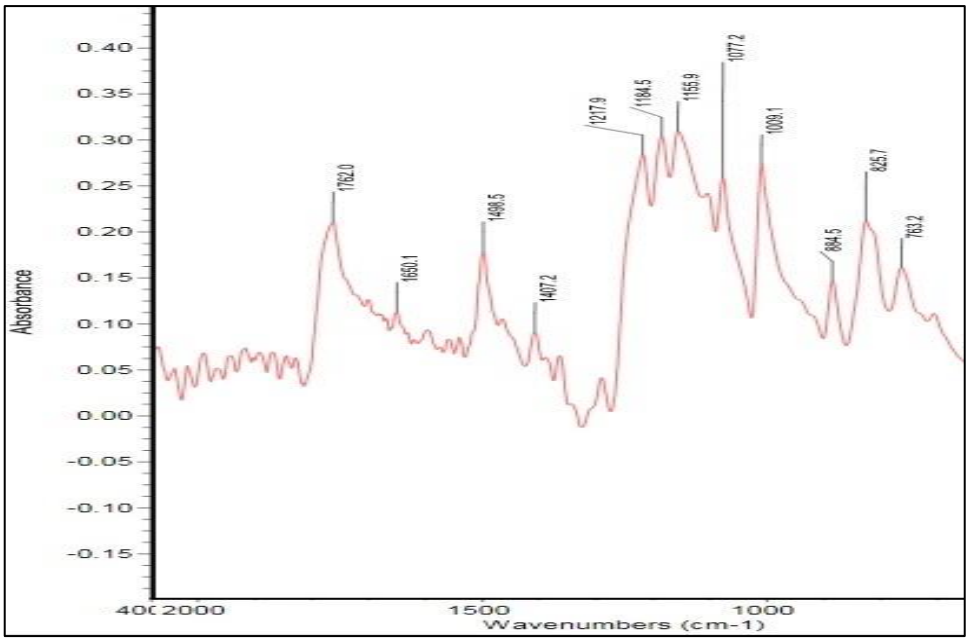

Figure5.41: FT-IR spectrum of a textured polycarbonate surface by exposure to pure acetone vapor for 7 minutes.

5.3.5.3. For the textured polycarbonate by the exposure to acetone vapor at $33^{o}C$, holed vapor-outlet:

In figure 5.42, FT-IR spectrum is illustrated. The study focuses on the wavelength at which the peak of carbonyl, C=O, stretching mode appears. Before the exposure to acetone, the peak of carbonyl stretching mode appears at 1762 cm^{-1}, with absorbance value of 0.24. The peak of the phenyl stretching mode appears at 1499 cm^{-1}, with absorbance value of 0.17.

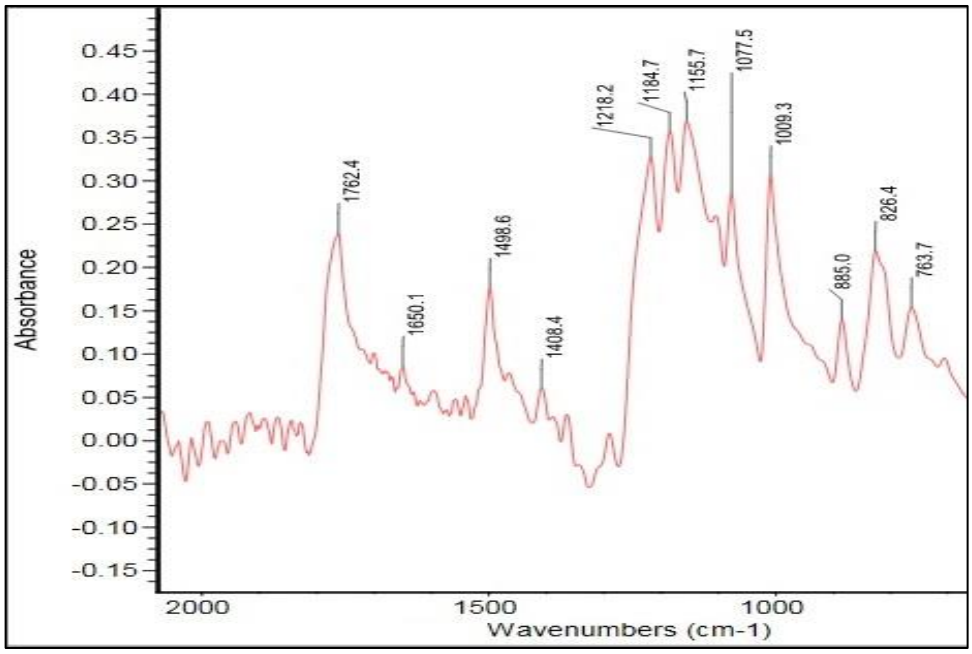

Figure5.42: FT-IR spectrum of a textured polycarbonate surface by exposure to pure acetone vapor for 8 minutes.

CHAPTER 6

DISCUSSION

6.1. The mechanism of the polycarbonate surface crystallization:

Crystallization is a kinetic process, in which molecular or atomic rearrangement process takes place in order to achieve stable orientations. Semi-crystalline polymers have many industrial applications, so scientists have directed their attentions along the last sixty years on studying this category of polymers. The crystallization process involves three main steps: **i**) Initiation of crystallization, **ii**) Primary crystallization and **iii**) Secondary crystallization [53].

The crystallization process starts with a crystalline nucleation from an amorphous phase. Because polymer chains attain stability upon their orientations to form favorable conformations, the nucleation process is kinetically-controlled. The factor that manages the nucleation rate is the gap between the melting and crystallization temperatures. According to the classical (homogenous) nucleation theory, the polymer chains form identical conformations by aligning in a parallel way, emerging a fetus. By the time, additional chains are added to the newly formed fetus, leading to an increment in the free energy till the fetus reaches a critical size; at this level, the system free energy decreases

with the continuous chains addition, so the nucleus growth process becomes spontaneous [53], figure 6.1 [54].

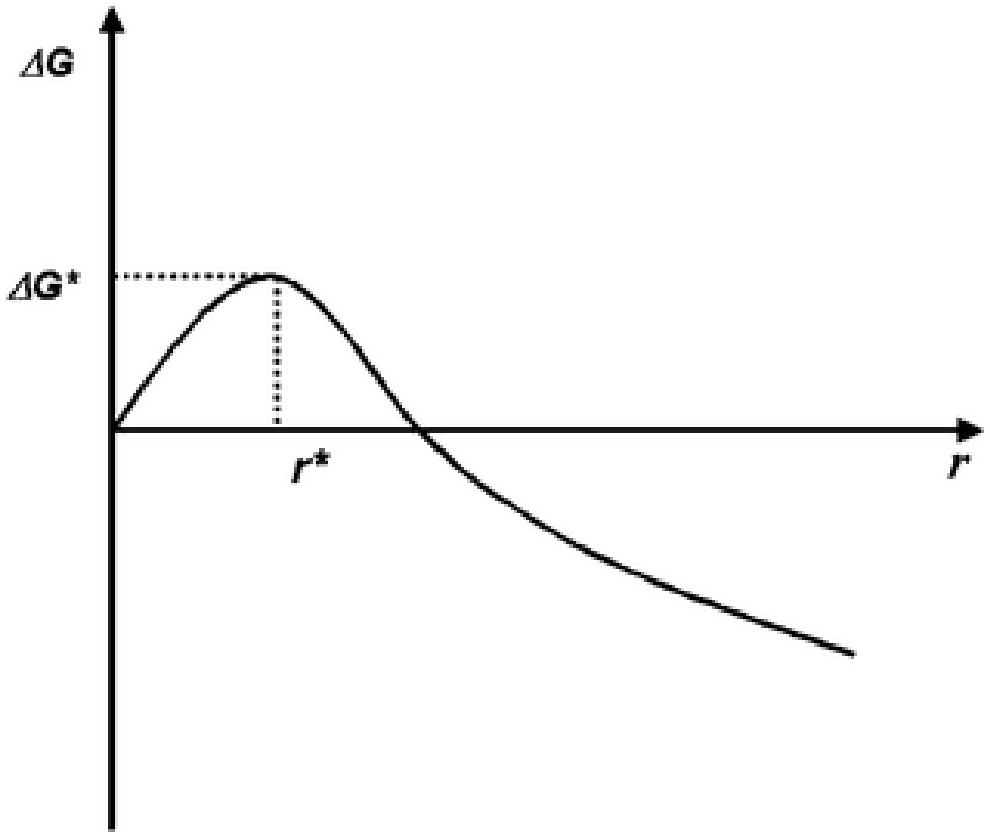

Figure6.1: Change of the free energy with changing the fetus radius. r^* represents the critical radius at which the free energy value is maximum, ΔG^* [54].

By assuming that the nucleus has a spherical shape with radius r, therefore the free energy is [55], **equation 6.1**:

$$\Delta G = \frac{4\pi r^3}{3}\,\Delta G_c + 4\pi\sigma r^2$$

, where ΔG_c: the crystallization free energy, σ: the crystal/amorphous interfacial free energy, and r: the radius of the spherical nucleus. The latent heat of fusion and undercooling ($T_m - T_c$) can be related to the free energy [55] , **equation 6.2**:

$$\Delta G_c = \frac{-\Delta H_m\,(T_m - T_c)}{T_m}$$

, where ΔG_c: the crystallization free energy, ΔH_m: the enthalpy change during melting process, T_m: the melting temperature, and T_c: the crystallization temperature. The crystallization free energy has a negative value if the crystallization temperature, T_c, is lower than the melting temperature, T_m, and it is positive if T_c is larger than T_m. The free energy value is controlled by the second term, equation 6.1, if the r value is small. However, in case of large r value, the crystallization free energy term dominates. r^* represents the critical radius at which the free energy value is maximum. The value of the critical radius, r^*, can be obtained by equating the first derivative of free energy to zero in equation 6.1, therefore [55] ,

$$\frac{\delta\Delta G}{\delta r} = 4\pi r^2\Delta G_c + 8\pi\sigma r$$

, where ($\delta\Delta G/\delta r$): the first derivative of free energy with respect to the spherical nucleus radius, r: the radius of the spherical nucleus, ΔG_c: the crystallization free energy, and σ: the crystal/amorphous interfacial free energy.

So, **equation 6.3** is:

$$r^* = \frac{2T_m\sigma}{\Delta H_m\,(T_m - T_c)}$$

, where r^*: the critical radius, T_m: the melting temperature, σ: the crystal/amorphous interfacial free energy, ΔH_m: the enthalpy change during melting process, and T_c: the crystallization temperature. So, the free energy of critical nucleus formation becomes [55] , **equation 6.4**:

$$\Delta G^* = \frac{16\pi {T_m}^2\sigma^3}{3{\Delta H_m}^2(T_m - T_c)^2}$$

, where ΔG^*: the maximum free energy, T_m: the melting temperature, σ: the crystal/amorphous interfacial free energy, ΔH_m: the enthalpy change during melting process, and T_c: the crystallization temperature. Therefore, it's required for transforming a material from its amorphous state to crystalline state to pass exceed the barrier of the free energy ΔG^*.

The rate of the homogenous nucleation is, **equation 6.5**:

$$I = \frac{k_B T_c}{h} J(T_c) \exp\left(\frac{-\Delta G^*}{rT_c}\right)$$

, where I: the rate of nucleation, k_B: the Boltzmann's constant T_c: the crystallization temperature, h: the Planck's constant and $J(T_c)$: a temperature-dependent term that is related to the polymer segments mobility at the amorphous-crystal interface, ΔG^*: the maximum free energy, and r: the radius of the spherical nucleus [55].

The crystallization process of the polycarbonate material, by using acetone, lies under the solvent-induced crystallization category. The Hildebrand solubility parameters of both the polycarbonate and the acetone are almost the same, 20.1 and 20.3 H respectively [56, 57], so that they are completely miscible [58]. Upon exposure to the solvent, acetone diffuses through the polymer sheet's layers, so creates a molten, turgid surface. In case of crystallizing the polycarbonate surface by treatment with liquid acetone [6], the hydrostatic pressure plays a role in the diffusion process, while in the vapor crystallization of polycarbonate, gas pressure and condensation process that occurs over the surface are the key factors that control the acetone diffusion. The acetone diffusion process within the polycarbonate glass does not obey Fick's equation [8, 57]; instead, it's related to Case II sorption[57]. In this case, the acetone liquid diffuses between the molten layer and the glassy polymer with a constant speed and a sharp front. Due to the migration of the organic solvent through the layers of the glassy polymer, the glass transition temperature (T_g) decreases down to become below the room temperature, so the turgid layers of polycarbonate plasticizes [57, 59]. After taking it out of the acetone bath, polycarbonate surface crystallizes due to the acetone evaporation process. The crystallization process follows the same mechanism of thermal quenching-induced

crystallization of a gelated polymer. Owing to the acetone evaporation, the glass transition temperature rises, therefore super-cooling state takes place, as a result, and the swollen polycarbonate surface crystallizes, following that, are the nucleation and growth of the spherules. The continuous growth of the spherule size with increasing the treatment duration takes place owing to the increase in the depth to which the acetone diffuses. In case of the layer depths are less than the spherule size, so that results in incomplete spherule coverage, while, if the depths are larger than the size of the spherule, this leads to pores formation. Spherule grows due to the presence of impurities, which act as nucleation sites. Spike-like nano-fibers can be noticed over the top surface of the spherule.

6.2. Potentials and effects of using two methods for crystallizations:

Two methods are used to treat the polycarbonate surface with acetone: **i**) The solid-liquid interface method for crystallization of polycarbonate glass and **ii**) The solid-vapor interface crystallization of polycarbonate glass. The crystallization of polycarbonate surface process, by immersing it in liquid acetone, leads to creating a textured surface of high roughness. This can be related to the hydrostatic pressure that is applied on the immersed polycarbonate surface in the liquid acetone. The hydrostatic (P_{hyd}) pressure can be identified as the pressure at a certain depth inside a static liquid and it's represented by

the summation of the weight of the liquid, acting on a unit area at that depth, and the atmospheric pressure (P_{atm}), **equation 6.6**:

$$P_{hyd} = P_{atm} + \rho g h$$

, where P_{atm}: the atmospheric pressure ρ: the density of the liquid, g: the gravitational acceleration and h: the distance between the liquid and the object surfaces. In this study, the polycarbonate sheets are immersed under acetone height of 1.5 cm. The sheet's thickness is 0.3 cm, so h value equals 1.2 cm. The acetone density is 791 kg/m^3, g equals 9.8 m/s^2 and the experiment is performed under the atmospheric pressure, 1.01325×10^5 Pa, so the hydrostatic pressure value is:

$$P_{hyd} = (1.01325 \times 10^5) + (791 \times 9.8 \times 0.012) = 1.01418 \times 10^5\ Pa$$

However, in case of texturing the polycarbonate surface by using the acetone in its vapor state, the gas pressure term dominates. The gas pressure is a kinetic term, which is temperature-dependent. It can be represented by [60] , **equation 6.7**:

$$P = \frac{2N}{3V}\left(\frac{1}{2}mv^2\right) = \frac{2N}{3V}K.E$$

, where P: the total pressure applied over the polycarbonate surface, N: the number of gas molecules, V: the volume of the gas, m: the mass of the gas, v: the gas speed, and K.E.: the kinetic energy. According to the ideal gas law [61], **equation 6.8**:

$$PV = nRT = Nk_BT$$

, where P: the total pressure applied over the polycarbonate surface, V: the volume of the gas, N: the number of gas molecules, n: the number of moles of the gas, R: the universal gas constant, k_B: the Boltzmann's constant, and T: the absolute temperature. Therefore, the temperature can be related to the kinetic energy of the gas, **equation 6.9**:

$$T = \frac{2}{3}\frac{N}{nR}K.E = \frac{2}{3k_B}K.E$$

, where T: the absolute temperature, N: the number of gas molecules, n: the number of moles of the gas, R: the universal gas constant, k_B: the Boltzmann's constant, and K.E.: the kinetic energy. From the previous equation, the kinetic energy can be calculated at the room temperature, 292 K:

$$K.E = \frac{3 \times 1.3806 \times 10^{-23} \times 292}{2} = 6.047 \times 10^{-21} J$$

Because 1.5 mL of acetone evaporated to texture the polycarbonate surface, therefore, assuming 0.0204 mole of acetone is evaporated, so N equals the number of moles multiplied by the Avogadro's number, $n.N_A$, and the gas volume equals to the volume of the space between the acetone liquid surface and the polycarbonate surface [62], **equation 6.10**:

$$number\ of\ moles, n = \frac{mass}{molar\ mass} = \frac{density \times volume}{molar\ mass} = \frac{791000 \times 1.5 \times 10^{-6}}{58.08}$$

$$= 0.0204\ mole$$

$$P_{total} = \frac{2 \times 0.0204 \times 6.0221 \times 10^{23}}{3\pi \times (0.08)^2 \times 0.014} \times 6.047 \times 10^{-21} = 1.7594 \times 10^5\ Pa$$

Because the experiment is done under the atmospheric pressure, so the gas partial pressure that is applied to the polycarbonate surface is, **equation 6.11**:

$$P_{gas} = P_{total} - P_{atm}$$

$$P_{gas} = 1.7594 \times 10^5 - 1.0133 \times 10^5 = 7.461 \times 10^4\ Pa$$

So, from the calculated data, the hydrostatic pressure, which is applied on the immersed polycarbonate surface in liquid acetone, equals P_{hyd} = 1.01418×10^5 Pa. However, the gas pressure, which is applied on the exposed polycarbonate surface to acetone vapor, equals P_{gas} = 7.461×10^4 Pa. The value of the P_{hyd} is larger than the P_{gas}, so this answers why the texture of the immersed polycarbonate surface in liquid acetone is heavier than that of the exposed polycarbonate surface to acetone vapor. The high hydrostatic pressure applied on the polycarbonate surface, which is immersed in liquid acetone, allows deep diffusion of acetone in the polymer layer. The spherule growth takes place according to how deep the acetone diffuses. Furthermore, pores formation is done if the layer depth is larger than the size of the spherule; however, incomplete spherule coverage results in case of less layer depth than the spherule size. Therefore, the hydrostatic pressure enhances the diffusion of the acetone within the polycarbonate, leading to high diffusion depth. For the gas pressure, which is applied on the exposed

polycarbonate surface to acetone vapor, due to its low value, incomplete coverage of crystals takes place, leading to semi-crystallized polymer.

In addition, for the solid-vapor method of polymer crystallization, the acetone vapor condenses over the polycarbonate surface. Therefore, the polycarbonate becomes in contact with, only, 1 mL of acetone on average. So, the mass transfer in this case will be far lower than that in case of immersing the surface in liquid acetone. Mass transfer, which is a driving-force dependent, affects the diffusion process dramatically. The mass transfer equation between two phases is [63], **equation 6.12**:

$$N_A = k\ a\ \Delta C_A$$

, where N_A: the mass transfer rate of component A, k: the mass transfer coefficient, a: the transfer area, and ΔC_A: the concentration driving force. The driving force is the result of the difference between the concentration of the liquid in the bulk and the concentration of the liquid in the formed boundary-film interface. So, the concentration of the liquid in the bulk is far higher, in case of the immersion in liquid acetone, than that in case of exposing the polymer surface to acetone vapor. Consequently, deeper diffusion and larger crystals take place in the former case. Also, the gravitational force has an effect in reducing the diffusion extent, in case of exposing the polycarbonate surface to the acetone vapor, but its effect is neglected.

6.3. Roughness values:

Roughness of the different surfaces can be calculated, using the atomic force microscope. The study gives the roughness of the polycarbonate surfaces (smooth, textured by immersion in liquid acetone and textured by exposure to acetone vapor) much concentration because it's one of the parameters that are responsible for the hydrophilicity or the hydrophobicity of the surface. Roughness values are taken for three different polycarbonate samples for the comparison purpose: **i**) Smooth, untreated polycarbonate surface, **ii**) Textured polycarbonate surface due to immersion in pure liquid acetone for 10 minutes and **iii**) Textured polycarbonate surface due to exposure to pure acetone vapor for 24 hours. Two values of roughness can be given by the AFM for the single sample's surface, roughness root mean square (RMS) value and roughness average (Ra) value. Table 6.1-A illustrates the RMS and table 6.1-B illustrates the Ra values of different polycarbonate samples.

Table6.1: A: RMS- and B: Ra-values of the smooth (untreated), solid-vapor interface textured and solid-liquid interface textured polycarbonate glass surfaces.

A scale, µm	RMS values, nm		
	smooth PCG	Solid-Vapor PCG	Solid-Liquid PCG
40	23.99	131.19	610
20	11.52	135.61	543.1
10	5.26	97.65	250
5	2.44	65.83	108.44
1	0.81	18.36	31.1
0.5	0.73	15.21	27.6843
B scale, µm	Ra values, nm		
	smooth PCG	Solid-Vapor PCG	Solid-Liquid PCG
40	18.85	104.27	460
20	9.27	109.57	407
10	4.19	76.78	210
5	1.9	55.12	87.61
1	0.64	15.02	25.01
0.5	0.58	11.39	22.7432

It’s clear from the values of both the RMS and Ra that the textured polycarbonate surface by immersion in pure liquid acetone for 10 minutes has the highest roughness, even far higher than the roughness of the textured polycarbonate surface by exposure to pure acetone vapor for 24 hours, at 18^{o}C. This promotes the strong effect of the applied high hydrostatic pressure, 10^{5} Pa magnitude, on the treated polycarbonate surface, which allows deep diffusion of the acetone liquid within the polymer layer, leading to complete-crystals coverage, pores formation and as a consequence, high roughness in a very short duration. Although, the weak gas pressure, 10^{4} Pa, leads to a relatively shallow diffusion of acetone, so as a result, incomplete coverage of crystals and low roughness values, despite the long treatment duration. Figure 6.2 includes two-dimensional and surface profile micrographs of two different textured polycarbonate surfaces, one with immersion in pure liquid acetone for 10 min, while the other by exposure to pure acetone vapor for 24 hours. Table 6.2 summarizes the two dimensions of the texture of the two different textured polycarbonate samples.

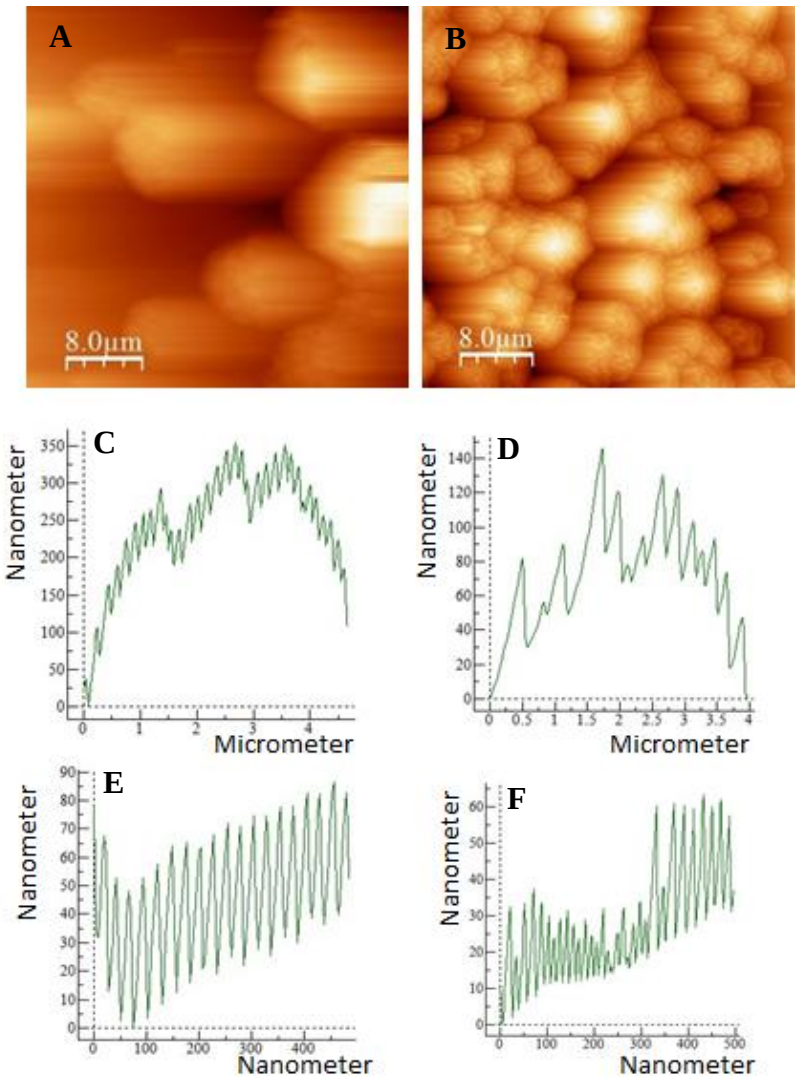

Figure6.2: 40 µm scale 2D-AFM micrograph of a textured PCG sample by: A: immersion in pure liquid acetone for 10 minutes, taken at. B: exposure to pure acetone vapor for 24 hours. Surface profile micrographs of a textured PCG sample by: C & E: immersion in pure liquid acetone for 10 minutes, taken at 5 µm and 500 nm scales respectively. D & F: exposure to pure acetone vapor for 24 hours, taken at 5 µm and 500 nm scales respectively.

Table6.2: Heights and widths measurements of spherules, hills and spikes that are present over the textured PCG surfaces by solid-liquid interface and solid-vapor interface method s of crystallization

40 µm scale		
Object	**Solid-Liquid**	**Solid-Vapor**
Spherule's width, nm	13000	4000
Spherule's height, nm	1750	375
5 µm scale		
Spherule's width, nm	> 5000	4000
Spherule's height, nm	350	140
Hill's width, nm	1500	1500
Hill's height, nm	150	70
500 nm scale		
Spike's width, nm	25	80
Spike's height, nm	48	37

6.4. Application of heating during the crystallization process by acetone vapor:

The effect of heating during the crystallization process is studied through this work. Polycarbonate surface exposes to acetone vapor with: **i**) room temperature, ~18^{o}C and **ii**) mild heating, ~33^{o}C. Changing the liquid temperature affects its vapor pressure, according to Clausius-Calpeyron equation [64], **equation 6.13**:

$$\ln\left(\frac{P_2}{P_1}\right) = \frac{\Delta H_{vap}}{R}\left(\frac{1}{T_1} - \frac{1}{T_2}\right)$$

, where P_1: the vapor pressure of the liquid at T_1, P_2: the vapor pressure of the liquid at T_2, ΔH_{vap}: the enthalpy change of vaporization, and R: universal gas constant. Clausius-Calpeyron equation gives the relation between T and P in a two-phase pure substance system. Vapor pressure can be defined as the pressure, applied by the vapor which is in a thermodynamic equilibrium with its condensed phases, at a given temperature in a closed system. Acetone has a ΔH_{vap} of 31300 J/mole and P_1 of 175 mmHg at 20^{o}C [65]. To determine the vapor pressure of the acetone at 33^{o}C, simply, apply the ΔH_{vap} and P_1 values in the former equation to get the value of P_2, which equals to 302 mmHg. So, the aim of increasing the acetone temperature from 18 to 33^{o}C is to establish a new thermodynamic equilibrium between the acetone vapor and acetone liquid at a higher vapor pressure value.

Increasing the temperature, not only affects the vapor pressure, however, in addition it affects the diffusivity of the acetone molecules through the molten polymer layers. According to Stokes-Einstein equation for the spherical particles diffusion through liquids [66], **equation 6.14**:

$$D = \frac{RT}{N_A}\frac{1}{6\pi\eta r}$$

, where D: the diffusion constant, T: the temperature, R: the universal gas constant, N_A: the Avogadro's number, η: the viscosity of the medium, and r: the radius of the spherical particles. From the equation, the direct proportionality between the diffusion constant and the temperature is clear. Therefore, increasing the temperature leads to the diffusivity increment.

This can be translated in getting textured surfaces after exposing polycarbonate to the acetone vapor for 1 minute when heating is applied, at 33^{o}C, figure 6.3-A. However, in case of working at room temperature, 18^{o}C, there no texture appeared before 15 min exposure to acetone vapor, figure 6.3-B. Both the higher vapor pressure and the higher diffusion constant, owing to the temperature increment, lead to texturing the polycarbonate by surface crystallization in shorter durations.

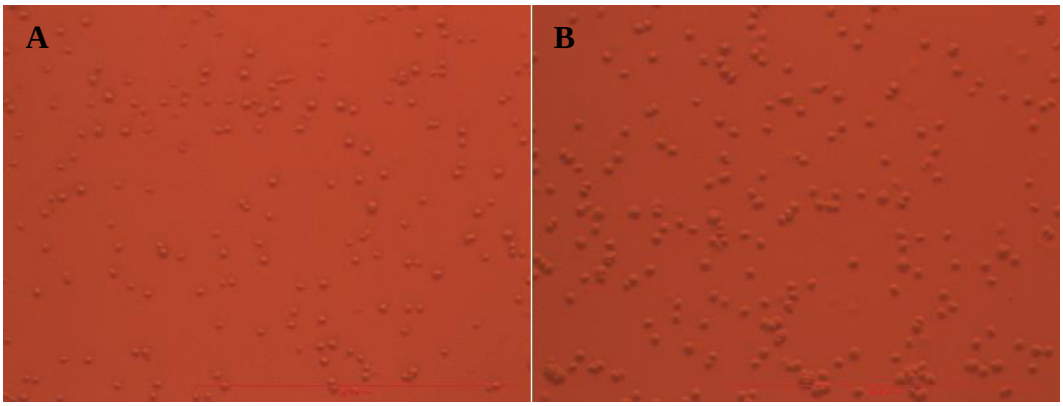

Figure6.3: A: Optical microscope image of a textured PCG surface by exposure to pure acetone vapor for 1 min at 33^{o}C. B: Optical microscope image of a textured PCG surface by exposure to pure acetone vapor for 15 min at 18^{o}C.

6.5. The change of average transmittance values with changing the texturing method:

Because one of the most important applications of these textured surfaces is in the protection of the PV cells, the research gives much concern to studying the effect of the texturing process on the surfaces transmittances. According to the results, polycarbonate surfaces textured by immersion in pure liquid acetone for different durations have very low transmittance values, ranging from 17.9% down to 0.58% with increasing the immersion duration from 1 to 10 minutes. For those textured surfaces by immersion in 75% acetone liquid, transmittances enhance, ranging from 56.6% down to 16.7% with increasing the immersion duration from 6 to 10 minutes. However, for the generally textured samples due to exposure to pure acetone vapor, greater enhancement in the transmittance of the textured surfaces takes place; it ranges from about 88% down to 57% with increasing the exposure duration from 1 to 30 minutes, on average.

From the optical microscope photos outcomes, it can be generally inferred that the average spherules sizes of the textured surfaces by the solid-liquid interface method of crystallization are totally larger than the sizes of the spherules present over the textured surfaces by the solid-vapor interface method of crystallization, figure 5.46. Furthermore, according to the surface profile micrographs, figures 5.44-C and D, the gaps within the texture in the textured polycarbonate samples by the solid-liquid interface method of

crystallization are smaller in width than those present over the textured surfaces by the solid-vapor interface method of crystallization.

Transmittance drop occurs due to the reflection process of the incident radiation. The reflection process is a certain result of the light scattering from the textured polycarbonate surface. Light scattering from a surface is caused by the deflection of the light beam from its straight path due to the irregularity of that surface. Rayleigh scattering theory defines the light scattering as an elastic collision between the light and surface particles. Therefore, Rayleigh theory is applied on the vapor textured surfaces because the spherules sizes are slightly smaller or almost equal to the wavelengths of the incident light, visible light 400-800 nm. According to Rayleigh theory [67]:

$$\frac{I}{I_o} \alpha \left(\frac{1}{R^2}\right)\left(\frac{d^6}{\lambda^4}\right)$$

, where I: the intensity of scattered light, I_o: the initial light intensity, R: the distance between the surface and the detector, d: the particle diameter, and λ: the wavelength of the incident radiation. Assuming that, the distance between the surface and the detector (R) and the wavelength of the incident radiation (λ), which lies within the visible light range, are constants. Therefore, the intensity of the scattered light is directly proportional to the diameter of the surface texture to the sixth power.

$$I \alpha d^6$$

This relationship illustrates how sensitive the diameter of the texture is, in case of the presence of smaller texture than the incident light wavelength. Any small change in the diameter value results in magnifying the intensity of the scattered light by 6 times. This explains the drop in the average transmittance values which accompanies the increase in the spherule width due to either long exposure duration to the acetone vapor or immersing the sample in the liquid acetone under the high hydrostatic pressure [8]. In extension, the presence of deep grooves within the texture of the treated polycarbonate surfaces further decrease the light transmittance because of their responsibility for making internal reflections. Scientists indicated that the crystallization process of polymers can be confirmed by the transmittance loss [6,7, 68].

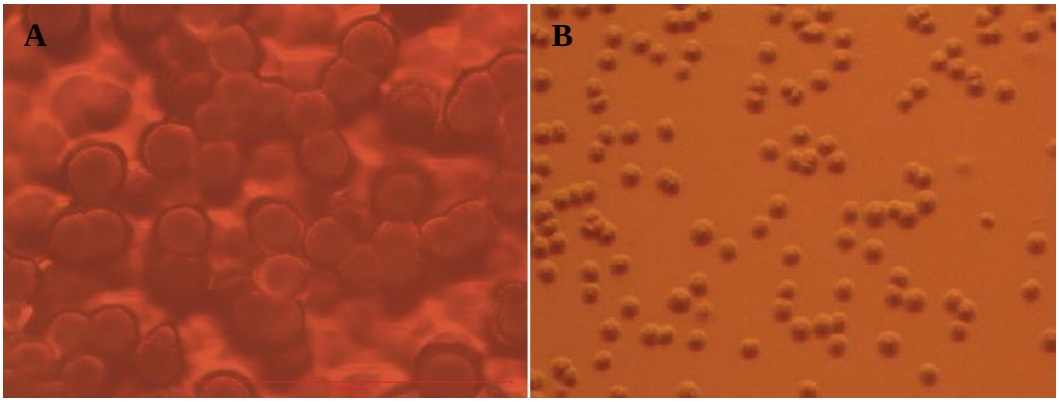

Figure6.4: A: Optical microscope image of a textured PCG surface by immersion in pure liquid acetone liquid for 2 min. B: Optical microscope image of a textured PCG surface by exposure to pure acetone vapor for 2 min.

6.6. The surface wettability according to Cassie-Baxter's and Wenzel's equations:

The research focuses on studying the effect of textured surface tribology on the apparent contact angle of the water droplet with that surface. Two states can describe the behavior of the textured surface towards the water droplet, with which it is in contact: **i**) Cassie-Baxter's state and **ii**) Wenzel's state.

For the hydrophobic surfaces (contact angle $\theta > 90^o$), Cassie-Baxter state is applied, whose equation is [26, 69] , **equation 6.15**:

$$\cos\theta_{cb} = \varphi_s(\cos\theta_y + 1) - 1$$

, where θ_{cb}: the Cassie's (apparent) contact angle, $\theta_{cb} > 90^o$, θ_y: the Young's contact angle (contact angle of the corresponding smooth surface) and ϕ_s: the solid fraction which is in contact with the water droplet. For calculating the value of ϕ_s for the single textured hydrophobic surface, **equation 6.16**:

$$\varphi_s = \frac{\cos\theta_{cb} + 1}{\cos\theta_y + 1}$$

Because the apparent contact angles of the textured surfaces, due to immersion in pure liquid acetone for different durations, are larger than 90^o, so as a consequence,

Cassie-Baxter's state is applicable. Calculations of ϕ_s values for the 6 different textured surfaces are illustrated in table 6.3.

Table6.3: Calculations of solid fraction values (φ_s) of the textured PCG samples by immersion in pure liquid acetone.

Sample	Time, min	Apparent CA, deg	cos θcb	cos θcb +1	Young's CA	cos θ	cos θ+1	Solid fraction, ϕs
i1	1	105.57	-0.2684	0.7316	84.3	0.0993	1.0993	0.665514418
i2	2	132.37	-0.6739	0.3261	84.3	0.0993	1.0993	0.296643318
i3	3	139.9	-0.7649	0.2351	84.3	0.0993	1.0993	0.213863368
i4	4	134.2	-0.6972	0.3028	84.3	0.0993	1.0993	0.275448012
i5	5	140.03	-0.7664	0.2336	84.3	0.0993	1.0993	0.212498863
i6	10	135.57	-0.7141	0.2859	84.3	0.0993	1.0993	0.260074593
Right angle		90	0	1	84.3	0.0993	1.0993	**0.90966979**
180 angle		180	-1	0	84.3	0.0993	1.0993	**0**

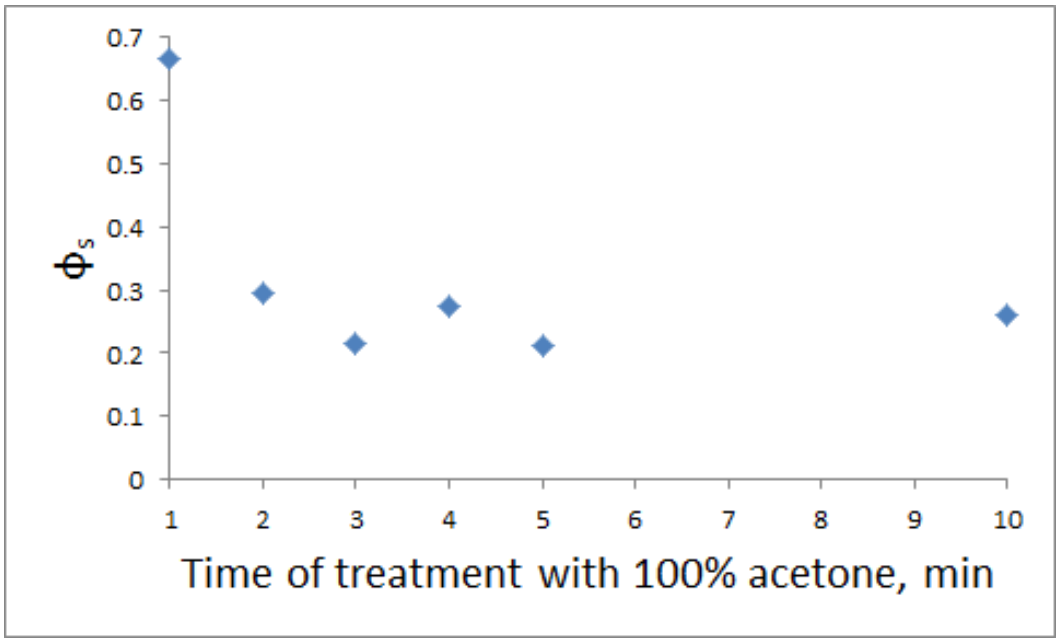

Figure6.5: The effect of the immersion duration of polycarbonate in pure acetone liquid on the φ_s value.

From the table, the solid fraction values lie in the range between 0.67 and 0.26 for the immersion durations from 1 to 10 minutes, respectively. The solid fraction value for a sample with a right apparent contact angle (i.e. the down limit CA of a hydrophobic surface) is 0.91. Thus, by increasing the immersion duration in acetone, the polycarbonate surface gets more crystallized, pores form with high depth, air-pockets compose within the formed pores, the solid-fraction that in contact with the water droplet decreases, the contact area between the surface and the droplet decreases and the hydrophobicity increases. Approaching zero solid-fraction value, it means that the contact angle increases, consequently, hydrophobicity increases. Figure 5.47 illustrates the change in the solid-fraction value (ϕ_s) with changing the immersion duration of polycarbonate in pure liquid acetone.

Wenzel's state is applicable for the hydrophilic textured surfaces, whose apparent contact angles are lower than the right angle ($\theta < 90^o$). Wenzel's equation is as the following [24, 69] , equation 5.15:

$$\cos\theta_w = r\cos\theta_y$$

, where θ_w: the Wenzel's (apparent) contact angle, $\theta_w < 90^o$, θ_y: the Young's contact angle (contact angle of the corresponding smooth surface) and r: the roughness ratio factor of the textured surface. For calculating the value of r for the single textured hydrophobic surface, equation 5.16:

$$r = \frac{\cos \theta_w}{\cos \theta_y}$$

Because the apparent contact angles of the textured surfaces, due to either immersion in 75% liquid acetone or exposure to pure acetone vapor for different durations, are less than 90^o, so as a consequence, Wenzel's state is applicable. Calculations of r values for the different textured surfaces are illustrated in table 6.4.

Table6.4: Calculations of roughness ratio values (r) of both the textured PCG samples by immersion in 75% liquid acetone liquid and the textured PCG samples by exposure to 75% acetone vapor with, without heating and with crevice corrosion.

Sample	Time, min	Apparent CA, deg	cos θw	Young's CA	cos θy	roughness ratio, r
i9	6	82.77	0.1258	84.3	0.0993	1.266868077
i10	8	83.1	0.1201	84.3	0.0993	1.209466264
i11	10	89.67	0.0058	84.3	0.0993	0.058408862
s5	25	82	0.1392	84.3	0.0993	1.401812689
s3	30	89.23	0.0134	84.3	0.0993	0.134944612
c4	1	79.55	0.1814	84.3	0.0993	1.826787513
c5	2	79.55	0.1814	84.3	0.0993	1.826787513
c6	3	77.1	0.2233	84.3	0.0993	2.248741188
c7	4	74.37	0.2694	84.3	0.0993	2.712990937
c8	6	74.43	0.2684	84.3	0.0993	2.702920443
c9	7	74.27	0.2711	84.3	0.0993	2.730110775
c10	8	72.2	0.3057	84.3	0.0993	3.078549849
c11	9	72.63	0.2985	84.3	0.0993	3.006042296
cr2	2	78.35	0.2019	84.3	0.0993	2.033232628
cr4	4	78.17	0.205	84.3	0.0993	2.064451158
cr6	6	75.43	0.2516	84.3	0.0993	2.533736153
cr8	8	77.55	0.2156	84.3	0.0993	2.171198389
cr10	10	74.37	0.2694	84.3	0.0993	2.712990937
0 angle		0	1	84.3	0.0993	10.07049345
Right angle		90	0	84.3	0.0993	0

From the table, the roughness ratio values lie in the range between 1.27 and 0.05 for the immersion duration from 6 to 10 minutes, respectively. For the textured polycarbonate surfaces by exposure to pure acetone vapor at 18^{o}C, the roughness ratio values are 1.40 and 0.13 for the exposure duration of 25 to 30 minutes, respectively. For the textured polycarbonate surfaces by exposure to pure acetone vapor at 33^{o}C, the roughness ratio values lie in the range between 1.83 and 3.01 for the exposure duration from 1 to 9 minutes, respectively. For the textured polycarbonate surfaces by exposure to pure acetone vapor at 33^{o}C with crevice formation, the roughness ratio values lie in the range between 2.03 and 2.71 for the exposure duration from 2 to 10 minutes, respectively. The roughness ratio value for a sample with a right apparent contact angle (i.e. the down limit CA of a hydrophilic surface) is 0, while the r value for a sample with complete wettability (i.e. zero apparent contact angle) equals to 10.07. Thus, by increasing the immersion duration in 75% liquid acetone, the polycarbonate surface gets more crystallized, pores depths increase, the composition of the air-pockets start, the roughness ratio value decreases and the hydrophilicity decreases. While in vapor-crystallized polycarbonate surfaces, generally, the roughness ratio factor increases with increasing the exposure duration to the acetone vapors. Shallow texturing, with wide gaps and high solid-liquid contact area with high surface energy all lead to increase the hydrophilicity of the textured samples. Figure 5.48

illustrates the change in the roughness ratio value (r) with changing the exposure duration of polycarbonate to acetone.

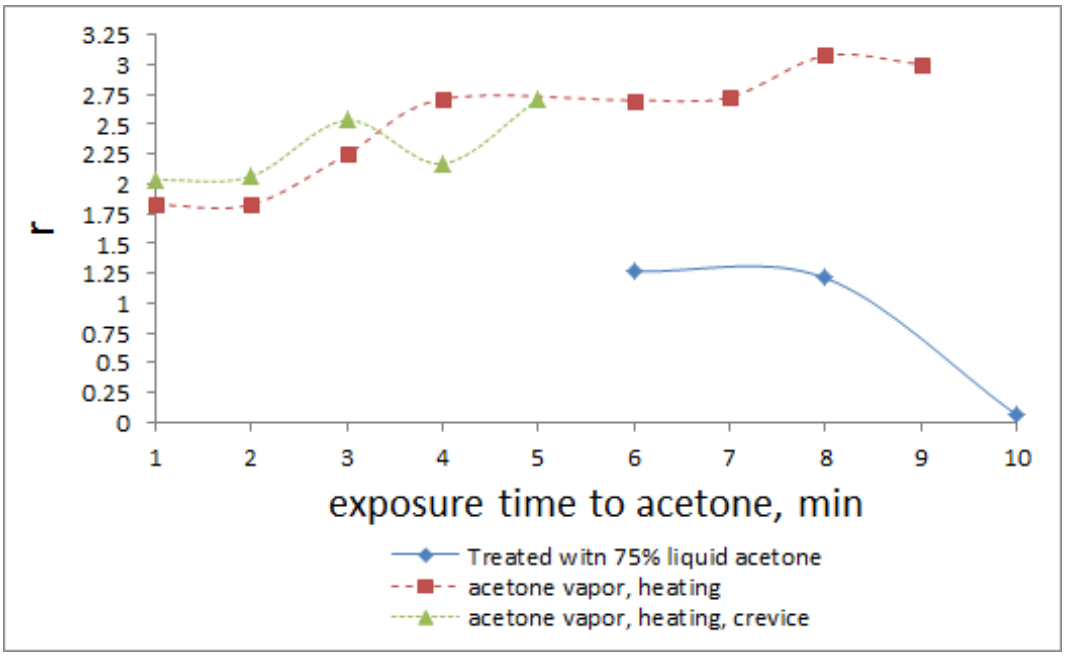

Figure6.6: The effect of the exposure duration of different polycarbonate samples to acetone on the r value.

6.7. FT-IR data analysis:

Fourier-Transform Infrared (FT-IR) technique is used to study the chemical structure of the polycarbonate surface before and after the treatment process. In addition, the technique gives an indication on the degree of crystallization of the surface after the treatment process through the peaks intensities values. Amorphous form of polymer gives a relatively higher degree of freedom to the polymers tail motion [7]. This permits the absorption of lager amounts of energy, and consequently, the performance of stronger vibrations, in case of molecules or groups that have a dipole moment (asymmetric chemical structure) [70].

Dybal et al. [71] noticed a shift in the carbonyl peak from 1770 to 1756 cm^{-1} with a tremendous decrease in the peak's intensity. Liu et al. [46] related this shift to the material-phase transformation from the amorphous state to the crystalline state. In addition, The decrease in the peak's intensity is related to the phase transformation of the polymer from the amorphous phase, which allows a higher degree of freedom to the chains motion and bonds vibrations, to the crystalline phase, in which the molecules are tightly packed and consequently, the vibrations and motions are restricted [7, 72]. It's indicated also that the acetone interaction with the polycarbonate is a physical process because there is no new peak emerged after the treatment process [46].

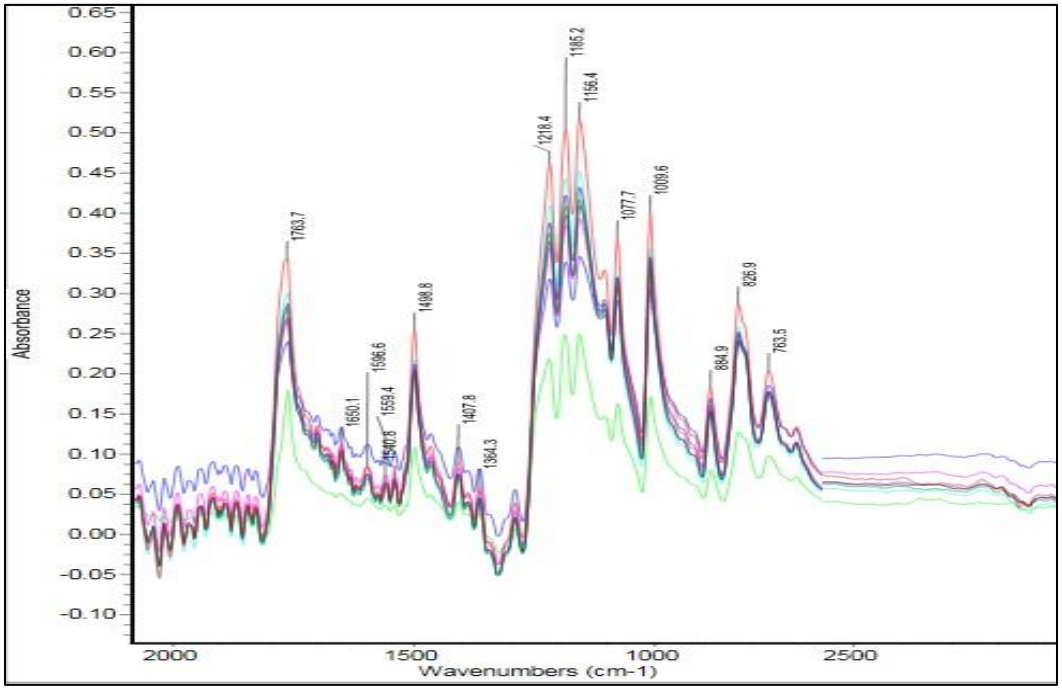

Figure6.7: FT-IR spectra of all the textured polycarbonate surfaces.

CHAPTER 7

CONCLUSION AND FUTURE WORK

Two methods, with a simply designed setup, are investigated for the solvent-induced crystallization process of a polycarbonate surface, by using acetone liquid and acetone vapor as an organic solvent, in order to design a hierarchically structured surface. By immersing the surface in pure liquid acetone for 5 minutes, the highest apparent contact angle is 144^{o}; while the highest apparent contact angle value is 95^{o}, after 10 minutes surface-immersion in 75% liquid acetone. The transmittance values of the immersed samples in liquid acetone are low, in general; this is related back to big-size crystals, formed due to the deep diffusion of the acetone through the polycarbonate surface sheets, which takes place by the strong hydrostatic pressure and the very high mass transfer. Cassie-Baxter state is applicable and the resulted solid fraction values, φ_s, lie within the range of 0.7 - 0.3 for the immersed samples in pure liquid acetone. However, for the immersed polymer surfaces in 75% liquid acetone, Wenzel state is applied, because the surfaces are hydrophilic, and the roughness ratio, r, values lie within the range of 1.3 – 0.1. FT-IR data indicated the strong crystallization, induced with pure liquid acetone, by the tremendous decrease in the chart peaks intensities.

The induced polycarbonate-crystallization by using acetone vapor is investigated at two different temperatures, 18^{o}C and 33^{o}C. At 18^{o}C, the highest apparent contact angle is 96^{o} after exposing the surface to acetone vapor for 30 minutes. At 33^{o}C, the highest apparent contact angle is 81^{o} after exposure to acetone vapor, evolving from a squared outlet, for 1 minute and the highest apparent contact angle is 79^{o} after exposure to acetone vapor, evolving from a holed outlet, for 2 minute. In contrast to all the former texturing processes, the CA value decreases with increasing the exposure duration to acetone vapor at 33^{o}C. The least required exposure duration to get crystals over the polycarbonate surface is 15 minutes at 18^{o}C, while only 1 minute is enough to see crystals over the polymer surface at 33^{o}C; this can be related to the increase in the vapor pressure due to the temperature increase, which consequently raises the gas pressure over the surface. Generally, transmittance values of the textured polycarbonate surfaces by using acetone vapor are high, this is related to the shallow diffusion of the condensed acetone droplets through the polymer surface layers due to the weak gas pressure, low mass transfer and effective gravitational forces. The surfaces are wettable, so Wenzel state is applied; at 18^{o}C, roughness ratio, r, values lie in the range of 1.4 - 0.1, and at 33^{o}C, the range is 1.8 – 3.0, indicating the hydrophilicity of the designed surfaces. FT-IR data indicated the weak crystallization, induced with the acetone vapor, by the slight decrease in the chart peaks intensities.

It’s recommended for future to use tetraethoxysilane, after processing it by Sol-Gel method, as a coating material in order to get proper contact angle values for the acetone

vapor-induced crystallized polycarbonate surfaces. For enhancing the transmittance of the textured polycarbonate surfaces by pure liquid acetone, the textured surfaces can be impregnated with specific oils to match the refractive index of the polycarbonate and recover the high transmittance of its surface before the texturing process.

REFERENCES

1. Verma, L.K., et al., *Self-cleaning and antireflective packaging glass for solar modules.* Renewable Energy, 2011. **36**(9): p. 2489-2493.

2. Gao, L. and T.J. McCarthy, *A perfectly hydrophobic surface (θA/θR= 180/180).* Journal of the American Chemical Society, 2006. **128**(28): p. 9052-9053.

3. Adamson A. W., G.A.P., *Physical Chemistry of Surfaces*. Wiley Blackwell. 1997.

4. Wang, R., et al., *Light-induced amphiphilic surfaces.* Nature, 1997. **388**: p. 431-432.

5. Takeuchi, K., *Polycarbonates. Chemistry and Technology of Polycondensates*, in *Elsevier B.V.* 2012. p. 363-376.

6. Cui, Y., et al., *Hierarchical polymeric textures via solvent-induced phase transformation: A single-step production of large-area superhydrophobic surfaces.* Colloids and Surfaces A: Physicochemical and Engineering Aspects, 2012. **394**: p. 8-13.

7. de Oliveira, F.L.O., et al., *Study on bisphenol-A polycarbonates samples crystallized by acetone vapor induction.* Polymer bulletin, 2011. **67**(6): p. 1045-1057.

8. Fan, Z., et al., *Vapor-induced crystallization behavior of bisphenol-A polycarbonate.* Polymer Engineering & Science, 2006. **46**(6): p. 729-734.

9. Aharoni, S.M. and N.S. Murthy, *Effects of Solvent-induced Crystallization on the Amorphous Phase of Polycarbonate of bisphenol A).* International Journal of Polymeric Materials, 1998. **42**(3-4): p. 275-283.

10. Sheldon, R. and P. Blakey, *Liquid-induced crystallization in polymers.* 1962.

11. Liang, G.G., et al., *Diallyl orthophthalate as a reactive plasticizer for polycarbonate. Part 1: Uncured system.* European Polymer Journal, 2008. **44**(2): p. 366-375.

12. Turska, E., P. W, and M. M. *CRYSTALLIZATION KINETICS OF POLYCARBONATES. I.* in *JOURNAL OF POLYMER SCIENCE PART C-POLYMER SYMPOSIUM*. 1968. JOHN WILEY & SONS INC 605 THIRD AVE, NEW YORK, NY 10158-0012.

13. Mercier, J., G. Groeninckx, and M. Lesne. *Some aspects of vapor-induced crystallization of polycarbonate of bisphenol A.* in *Journal of Polymer Science Part C: Polymer Symposia*. 1967. Wiley Online Library.

14. Turska, E. and H. Janeczek, *Liquid-induced crystallization of a bisphenol-A polycarbonate.* Polymer, 1979. **20**(7): p. 855-858.

15. Nakajima, A., et al., *Transparent superhydrophobic thin films with self-cleaning properties.* Langmuir, 2000. **16**(17): p. 7044-7047.

16. Shirtcliffe, N.J., et al., *An introduction to superhydrophobicity.* Advances in colloid and interface science, 2010. **161**(1): p. 124-138.

17. He, G., C. Zhou, and Z. Li, *Review of self-cleaning method for solar cell array.* Procedia Engineering, 2011. **16**: p. 640-645.

18. Bruynooghe, S., et al., *Realization of High Performance AR-coatings with Dust- and Water-Repellent Properties.* Vakuum in Forschung Und Praxis, 2008. **20**(5): p. 25-29.

19. Ganbavle, V.V., et al., *Self-cleaning silica coatings on glass by single step sol–gel route.* Surface and Coatings Technology, 2011. **205**(23): p. 5338-5344.

20. Lai, Y., et al., *Transparent superhydrophobic/superhydrophilic TiO2-based coatings for self-cleaning and anti-fogging.* Journal of Materials Chemistry, 2012. **22**(15): p. 7420-7426.

21. Chen, Y., et al., *Transparent superhydrophobic/superhydrophilic coatings for self-cleaning and anti-fogging.* Applied Physics Letters, 2012. **101**(3): p. 033701.

22. De Gennes, P.-G., F. Brochard-Wyart, and D. Quéré, *Capillarity and wetting phenomena: drops, bubbles, pearls, waves*. 2004: Springer.

23. Young, T., *An essay on the cohesion of fluids.* Philosophical Transactions of the Royal Society of London, 1805: p. 65-87.

24. Wenzel, R.N., *Resistance of solid surfaces to wetting by water.* Industrial & Engineering Chemistry, 1936. **28**(8): p. 988-994.

25. Wenzel, R.N., *Surface roughness and contact angle.* The Journal of Physical Chemistry, 1949. **53**(9): p. 1466-1467.

26. Cassie, A. and S. Baxter, *Wettability of porous surfaces.* Transactions of the Faraday Society, 1944. **40**: p. 546-551.

27. Lafuma, A. and D. Quéré, *Superhydrophobic states.* Nature materials, 2003. **2**(7): p. 457-460.

28. Wong, T.-S., et al., *Bioinspired self-repairing slippery surfaces with pressure-stable omniphobicity*. Nature, 2011. **477**(7365): p. 443-447.

29. Dorrer, C. and J. Rühe, *Some thoughts on superhydrophobic wetting.* Soft Matter, 2009. **5**(1): p. 51-61.

30. Miwa, M., et al., *Effects of the surface roughness on sliding angles of water droplets on superhydrophobic surfaces.* Langmuir, 2000. **16**(13): p. 5754-5760.

31. Quéré, D., *Non-sticking drops.* Reports on Progress in Physics, 2005. **68**(11): p. 2495.

32. Smyth, K., et al. *Dynamic wetting on superhydrophobic surfaces: Droplet impact and wetting hysteresis*. in *Thermal and Thermomechanical Phenomena in Electronic Systems (ITherm), 2010 12th IEEE Intersociety Conference on*. 2010. IEEE.

33. Lafuma, A. and D. Quéré, *Slippery pre-suffused surfaces.* EPL (Europhysics Letters), 2011. **96**(5): p. 56001.

34. Smith, J.D., et al., *Droplet mobility on lubricant-impregnated surfaces.* Soft Matter, 2013. **9**(6): p. 1772-1780.

35. Boinovich, L.B. and A.M. Emelyanenko, *Hydrophobic materials and coatings: principles of design, properties and applications.* Russian Chemical Reviews, 2008. **77**(7): p. 583.

36. Yan, Y., N. Gao, and W. Barthlott, *Mimicking natural superhydrophobic surfaces and grasping the wetting process: A review on recent progress in preparing superhydrophobic surfaces.* Advances in colloid and interface science, 2011. **169**(2): p. 80-105.

37. Zhang, X., et al., *Superhydrophobic surfaces: from structural control to functional application.* Journal of Materials Chemistry, 2008. **18**(6): p. 621-633.

38. Park, Y.-B., et al., *Self-cleaning effect of highly water-repellent microshell structures for solar cell applications.* Journal of Materials Chemistry, 2011. **21**(3): p. 633-636.

39. Hee, J.Y., et al., *The Effect of Dust on Transmission and Self-cleaning Property of Solar Panels.* Energy Procedia, 2012. **15**: p. 421-427.

40. Liu, H., et al., *Organogel-based Thin Films for Self-Cleaning on Various Surfaces.* Advanced Materials, 2013. **25**(32): p. 4477-4481.

41. Kim, P., et al., *Liquid-infused nanostructured surfaces with extreme anti-ice and anti-frost performance.* ACS nano, 2012. **6**(8): p. 6569-6577.

42. Rykaczewski, K., et al., *Mechanism of frost formation on lubricant-impregnated surfaces.* Langmuir, 2013. **29**(17): p. 5230-5238.

43. Anand, S., et al., *Enhanced condensation on lubricant-impregnated nanotextured surfaces.* Acs Nano, 2012. **6**(11): p. 10122-10129.

44. Xiao, R., et al., *Immersion Condensation on Oil-Infused Heterogeneous Surfaces for Enhanced Heat Transfer.* Scientific reports, 2013. **3**.

45. Kappl, M., *Surface and interfacial forces*. 2009: John Wiley & Sons.

46. Liu, C.K., C.T. Hu, and S. Lee, *Effect of compression and thickness on acetone transport in polycarbonate.* Polymer Engineering & Science, 2005. **45**(5): p. 687-693.

47. Cui, Y., et al. *Superhydrophobic polymer surface via solvent-induced crystallization*. in *Thermal and Thermomechanical Phenomena in Electronic Systems (ITherm), 2012 13th IEEE Intersociety Conference on*. 2012. IEEE.

48. Varanasi, K.K., et al., *Hierarchical thermoplastic surface textures formed by phase transformation and methods of making*. 2010, Google Patents.

49. Bhushan, B. and Y.C. Jung, *Natural and biomimetic artificial surfaces for superhydrophobicity, self-cleaning, low adhesion, and drag reduction.* Progress in Materials Science, 2011. **56**(1): p. 1-108.

50. Erbil, H.Y., et al., *Transformation of a simple plastic into a superhydrophobic surface.* Science, 2003. **299**(5611): p. 1377-1380.

51. Bico, J., U. Thiele, and D. Quéré, *Wetting of textured surfaces.* Colloids and Surfaces A: Physicochemical and Engineering Aspects, 2002. **206**(1): p. 41-46.

52. Blossey, R., *Self-cleaning surfaces—virtual realities.* Nature materials, 2003. **2**(5): p. 301-306.

53. Farmer, R., *A study of crystallization in Bisphenol A polycarbonate*. 2001, Virginia Polytechnic Institute and State University.

54. Zhang, Q., S.-J. Liu, and S.-H. Yu, *Recent advances in oriented attachment growth and synthesis of functional materials: concept, evidence, mechanism, and future.* Journal of Materials Chemistry, 2009. **19**(2): p. 191-207.

55. Bassett, D.C., *Principles of polymer morphology*. 1981: CUP Archive.

56. Brandrup, J., et al., *Polymer handbook*. Vol. 1999. 1999: Wiley New York.

57. Paxson, A., *Condensation heat transfer on nanoengineered surfaces*, in *Mechanical Engineering*. 2009, Massachusetts Institute of Technology.

58. Sperling, L.H., *Introduction to physical polymer science*. 2005: John Wiley & Sons.

59. Van Krevelen, D.W. and K. Te Nijenhuis, *Properties of polymers: their correlation with chemical structure; their numerical estimation and prediction from additive group contributions*. 2009: Elsevier.

60. Bhasin, S., *Pharmaceutical Physical Chemistry: Theory and Practices*. 2012: Pearson Education India.

61. Prigogine, I., R. Defay, and D.H. Everett, *Chemical thermodynamics*. 1962: Longmans New York.

62. Vogel, A.I., *text-book of quantitative inorganic analysis including elementary instrumental analysis.* 1961.

63. Sinha, A. and P. De, *Mass Transfer: Principles and Operations*. 2012: PHI Learning Pvt. Ltd.

64. Jenkins, H.D.B., *Chemical thermodynamics at a glance*. 2008: John Wiley & Sons.

65. Lide, D.R., *CRC Handbook of Chemistry and Physics*. 44 ed. 2005, Internet Version: CRC Press.

66. Einstein, A., *The Photoelectric Effect.* Ann. Phys, 1905. **17**: p. 132.

67. Pandis, S.a., *Atmospheric Chemistry and Physics*. 2 ed. 2006: John Wiley and Sons.

68. Daniels, C.A., *Polymers: structure and properties*. 1989: CRC Press.

69. Banerjee, S., *Simple derivation of Young, Wenzel and Cassie-Baxter equations and its interpretations.* arXiv preprint arXiv:0808.1460, 2008.

70. Atkins, P., *Paula J. Atkins' physical chemistry*. 2012, Oxford, New York: Oxford University Press.

71. Dybal, J., et al., *Ordered structures in polycarbonate studied by infrared and Raman spectroscopy, wide-angle X-ray scattering, and differential scanning calorimetry.* Macromolecules, 1998. **31**(19): p. 6611-6619.

72. Paragkumar N, T., D. Edith, and J.-L. Six, *Surface characteristics of PLA and PLGA films.* Applied Surface Science, 2006. **253**(5): p. 2758-2764.

VITAE

Name: Ahmed Owais Mohamed Ahmed

Nationality: Egyptian

Date of Birth: Aug. 21, 1988

Email: ahmed-owais@hotmail.com

Address: King Fahd University of Petroleum and Minerals, Box No. 8227, Dhahran 31261, Saudi Arabia

Academic Background:

Ahmed is a graduate of Faculty of Science at Beni-Suef University. He was awarded his BSc degree in Chemistry and Biochemistry with a Very Good grade with honor, awarded the Pre-MS Certificate (graduate courses in Physical, Analytical and Inorganic Chemistry) from the same institution and MS in Chemistry from King Fahd University of Petroleum and Minerals. His research work was in collaboration with Varanasi group in Manufacturing and Productivity lab at Massachusetts Institute of Technology, and he joined the group during the summer semester of 2013. Ahmed accomplished his thesis work by Feb. 27, 2014. He submitted two papers for publishing and has one accepted in CIMTEC 2014 conference, Italy.